CANADIAN THESES

THÈSES CANADIENNES

NOTICE

The quality of this microfiche is heavily dependent upon the quality of the original thesis submitted for microfilming. Every effort has been made to ensure the highest quality of reproduction possible.

If pages are missing, contact the university which granted the degree.

Some pages may have indistinct print especially if the original pages were typed with a poor typewriter ribbon or if the university sent us an inferior photocopy.

Previously copyrighted materials (journal articles, published tests, etc.) are not filmed.

Reproduction in full or in part of this film is governed by the Canadian Copyright Act, R.S.C. 1970, c. C-30.

AVIS

La qualité de cette microfiche dépend grandement de la qualité de la thèse soumise au microfilmage. Nous avons tout fait pour assurer une qualité supérieure de reproduction.

S'il manque des pages, veuillez communiquer avec l'université qui a conféré le grade.

La qualité d'impression de certaines pages peut laisser à désirer, surtout si les pages originales ont été dactylographiées à l'aide d'un ruban usé ou si l'université nous a fait parvenir une photocopie de qualité inférieure.

Les documents qui font déjà l'objet d'un droit d'auteur (articles de revue, examens publiés, etc.) ne sont pas microfilmés.

La reproduction, même partielle, de ce microfilm est soumise à la Loi canadienne sur le droit d'auteur, SRC 1970, c. C-30.

THIS DISSERTATION HAS BEEN MICROFILMED EXACTLY AS RECEIVED

LA THÈSE A ÉTÉ MICROFILMÉE TELLE QUE NOUS L'AVONS REÇUE

Canada

THE UNIVERSITY OF ALBERTA

EXPERIMENTAL BRAIN EDEMA STUDIED WITH PROTON NMR

by

MANUEL EDUARDO CASTRO

A THESIS

SUBMITTED TO THE FACULTY OF GRADUATE STUDIES AND RESEARCH IN PARTIAL

FULFILMENT OF THE REQUIRMENTS FOR THE DEGREE OF

DOCTOR OF PHILOSOPHY

IN EXPERIMENTAL SURGERY

DEPARTMENT OF SURGERY
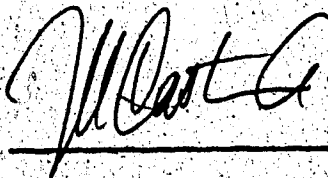
EDMONTON, ALBERTA

FALL, 1986

THE UNIVERSITY OF ALBERTA

RELEASE FORM

NAME OF AUTHOR: MANUEL EDUARDO CASTRO

TITLE OF THESIS: EXPERIMENTAL BRAIN EDEMA STUDIED WITH

PROTON NMR

DEGREE: Ph.D.

YEAR THIS DEGREE GRANTED: 1986

Permission is hereby granted to THE UNIVERSITY OF ALBERTA

LIBRARY to reproduce single copies of this thesis and to lend or sell

such copies for private, scholarly or scientific research purposes

only.

The author reserves other publication rights, and neither the

thesis nor extensive extracts from it may be printed or otherwise

reproduced without the author's written permission.
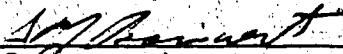
302, 10015 - 85th Avenue,
Edmonton, Alberta
T6E 2J9

Date: SEPTEMBER 1986

THE UNIVERSITY OF ALBERTA

FACULTY OF GRADUATE STUDIES AND RESEARCH

The undersigned certify that they have read, and recommend to
the Faculty of Graduate Studies and Research for acceptance, a thesis
entitled "EXPERIMENTAL BRAIN EDEMA STUDIED WITH PROTON NMR",
submitted by MANUEL EDUARDO CASTRO in partial fulfilment of the
requirements for the degree of Doctor of Philosophy/in EXPERIMENTAL
SURGERY.

_____
(Supervisor)

_____

_____

_____

_____
(External Examiner)

Date: 10 June 1986

dedicated to

Rosy

ABSTRACT

It is now recognized that there are various forms of brain edema. The commonest two, vasogenic and cytotoxic, are the result of impaired cell membrane funct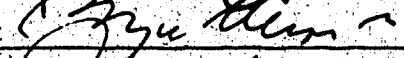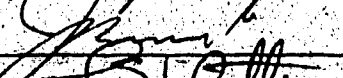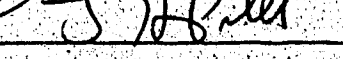ion at different anatomical locations and lead to a disturbance in fluid homeostasis within the brain. Advances in treatment of cerebral edema, however, have not developed as quickly as advances in the study of its pathophysiology. The lack of techniques for assessing the severity, extent, and functional alterations in patients with brain edema are, in part, responsible for the slow progress in therapy. The aim of this work was to evaluate some of the features of proton nuclear magnetic resonance (NMR) as they apply to the assessment of brain edema.

STUDY A:

To determine the effect of biochemical changes occurring in edema on the NMR relaxation of solvent protons, individual and pooled samples of cerebrospinal fluid (CSF) were used as a model of edema fluid. Concentrations of individual proteins and their mixtures, as well as concentrations of electrolytes and H^+ (i.e., pH) were varied and the proton NMR relaxation rates of water were measured. The results showed that the type and amount of protein were the main factors contributing to increases in relaxation efficiency of water protons. The effect of pH and electrolyte

concentration was very small. A model of proton relaxation involving two different environments for water molecules was employed to predict the observed relaxation rates. This model, although oversimplified, adequately described the gross characteristics of proton relaxation in edema fluid.

STUDY B:

To differentiate vasogenic from cytotoxic edema, normal values of relaxation rates, and water and protein content in brain tissues were established in a group of cats. The relaxation recovery or decay of brain tissues could be described by a single exponential within the time frame of the observations. Cerebral edema was induced in cats by xenotransplantation of brain tumors or injection of triethyltin (TET). Brain tumors were associated with vasogenic edema in white matter, whereas TET intoxication produced cytotoxic edema in the same structure. The tissue water-content was elevated in edematous white matter of both groups of animals and the corresponding rates of relaxation were lower than normal. Biexponential decay described the transverse relaxation (R_2) of edematous white matter in both groups of animals, of which the weighted average closely correlated with tissue water content. Unexpectedly the sensitivity of transverse relaxation rates to water content was similar in the two groups of cats. Because the tissue protein content did not correlate with the averaged transverse relaxation rates in peritumor white matter edema, We concluded that the averaged R_2 is not a sensitive index for.

detection of protein changes in vasogenic edema. On the other hand, the slow component of the biexponential decay, R_{2s}, was significantly different in vasogenic from cytotoxic edema. This component probably corresponds to the signal decay from extracellular fluid as judged by changes in its rate and its weighting with death. Such changes agree with shifts of fluid from the extracellular to the intracellular space as predicted by the Gibbs—Donnan equilibrium. We conclude that R_{2s} is a sensitive index for discriminating between vasogenic and cytotoxic edema.

The model of proton relaxation used to describe the relaxation of CSF-protein solutions was applied to the relaxation data from edematous tissue. It predicted that the increase in water is the main factor affecting relaxation rates observed in cytotoxic edema of the white matter. A hypothesis suggesting that impaired water homeostasis due to altered energy metabolism is responsible for the biexponential transverse relaxation decay of edematous white matter was developed.

The application of quantitative NMR techniques at high magnetic field strength enabled assessment of the severity, extent, and type of edema present in animal models.

PREFACE

Cerebral edema is probably the commonest cause of morbidity and mortality in patients with neurologic disorders. The brain, an organ whose composition renders it especially prone to develop edema, swells in response to nearly all forms of insult, and because it is encased in bone there is little space for expansion. Increases in volume lead to shifts and compression of nervous centers, impairing vital functions and altering tissue perfusion. The resultant regions of ischemia may be responsible for serious sequelae, and dysfunction of vital centers may lead to death. Therefore, the early diagnosis and treatment of cerebral edema are of great clinical importance.

The diagnosis of cerebral edema is hampered by lack of specific clinical signs and symptoms -- there is no 'edema syndrome' that can be separated from manifestations of the primary lesion. With the advent of computerized x-ray tomography, however, it is possible to diagnose the extent of edema and monitor its progression.

Until now the treatment of brain edema has remained largely empirical, due to the lack of objective measures to assess its nature, extent and severity, or response to therapy. Computerized tomography provides an index of tissue density, but this is a rather insensitive determinant of the severity of the edema. By contrast, proton nuclear magnetic resonance (NMR) gives

information on the amount and dynamic properties of water molecules in tissues. The recent development of NMR for imaging promises to provide very sensitive in-vivo indices that reflect both the extent and the severity of the edematous process and thus, an objective assessment of the effects of treatments or natural progression of the pathologic condition can be obtained.

NMR may also provide information about the pathophysiology of the process, specifically alterations in function that are associated with disordered water distribution in brain tissues. However, knowledge of the relationships between changes in brain tissue fluids and the in-vivo NMR indices, and between the latter and the in-vitro NMR parameters, is required to establish the value of NMR for assessment of brain edema. The present work was designed to clarify this issue, as well as, to determine the ability of NMR to show functional alterations that result in different forms of cerebral edema.

ACKNOWLEDGEMENTS

I wish to express my great appreciation to Marion and Allan

Martin and Janice and Robert Buker for making my stay in Canada a

most pleasant experience.

This study was supported by grants from the Alberta Heritage

Foundation for Medical Research (AHFMR) and the Alberta Heritage

Savings Trust Fund Applied Research - Cancer, Postdoctoral

Fellowship from the AHFMR, and the University of Alberta.

TABLE OF CONTENTS

Chaper II

I. Study A: EVALUATION OF THE CHARACTERISTICS OF PROTON NMR
RELAXATION IN A MODEL OF BRAIN EDEMA FLUID

Chapter III

MODELS DEVELOPED FROM THE PRESENT STUDIES

Chapter IV

CONCLUSIONS AND RECOMMENDATIONS

LIST OF TABLES

LIST OF FIGURES

CHAPTER ONE

Part I: THE PROBLEM OF CEREBRAL EDEMA

1. Definition

Cerebral edema is the response of nervous tissue to multifarious pathologic conditions, both local and systemic; the net result is an increase in the volume of brain tissue, from fluid accumulation in the interstitium, or within the cells, or both. Brain swelling is considered by some investigators as a separate entity representing the increase in tissue volume that results from expansion of the intravascular space. To avoid confusion, the term swelling is not used in this work. The increase in tissue water is due to impairment of the mechanisms responsible for fluid homeostasis within the cerebral parenchyma. Brain edema is, in most cases, an evoked response to an injurious stimulus and has several components (i.e., formation, spread, and resolution). The clinical presentation and course of brain edema varies, depending upon the location, type, severity, and duration of the lesion.

2. Common Causes of Edema

Cerebral edema develops most commonly after cerebrovascular disorders and trauma or in association with brain tumors and infections. It is also frequently observed with hydrocephalus. Less common causes of cerebral edema include intoxication, especially with lead, arsenic, and alcohol, severe hypertension, water intoxication,

heat stroke, severe burns, hypoglycemia, radiation, uremia, diabetic coma, hepatic failure, and anoxia.

3. Classification

Cerebral edema was recognized early in history. Hippocrates described increased fluid content of the brain caused by epileptic seizures (quoted in Garrison, 1929). However, it was not until the last century that the first attempts to classify edema into categories were made. Pathologist John Hughes Bennett distinguished two main classes of cerebral softening: (a) inflammatory, characterized by an exudate of red blood cells, and (b) non-inflammatory, with imbibition of serum in brain tissue (quoted in Bell, 1983). In 1905, Martin Reichardt, a German pathologist, divided brain edema into Hirnödem, in which the swollen brain is soft and water drips from the cut surface, and Hirnschwellung, in which the cerebral tissue is firm and the cut surface is dry (quoted in Klatzo, 1967). Reichardt speculated that the former was due to the accumulation of cerebrospinal fluid (CSF) within the brain's extracellular space, and in the latter to the accumulation of fluid within cells resulting in the apparently dry cut surface of the brain. In 1939, however, Stewart-Wallace -- after draining, suctioning, filtering, and squeezing in gauze and silk bags white matter that contained 12% more tissue water than in the contralateral side -- presented convincing evidence that fluid does not drip from edematous brain . Stewart-Wallace defined brain edema as increased water content of the tissues. This was a more accurate description

of edema, because the term 'swelling' used by Reichardt implied an increased brain volume relative to the normal brain volume in a given individual, and thus required knowledge of the capacity of that person's skull and the volume of his brain in the normal and pathologic states.

In 1967, Zulch used the same terms as Reichardt (i.e., brain swelling and brain edema) to classify cerebral edema. 'Swelling' was defined as the cellular imbibition of water in brain that had a dry, sticky, firm appearance. In 'edema', on the other hand, the brain appeared elastic and rubbery and the tissues were characterized by accumulations of protein-rich exudate containing mainly albumin and alpha globulin.

Klatzo (1967) recognized two types of brain edema based on anatomic and pathogenetic observations. Vasogenic edema, the commoner form, is characterized by the accumulation of protein-rich fluid in the extracellular space. This fluid comes from plasma released from the blood vessels by the disruption of normal transport across the blood--brain barrier (BBB). The second type, cytotoxic edema, is the abnormal accumulation of protein-poor fluid within the cells. The various mechanisms that lead to this form of edema usually have a common effect upon the metabolic properties of brain cells that are responsible for maintaining osmotic gradients inside and outside the cells. This classification has gained widespread acceptance and is the most commonly used today; however, as Manz (1974) noted, this classification describes the two ends of a spectrum, and most clinical cases fall somewhere in between. Both

Manz (1974) and Fishman (1975) proposed a third type: interstitial edema. This results from the periventricular accumulation of cerebrospinal fluid in the extracellular space, a result of increased pressure in the cerebral ventricles and reversal of the normal flow of extracellular fluid in the brain.

Commenting on Klatzo's observation (1967), Lee (1971) concluded that except for the intracellular edema-caused by autolysis, all types of brain edema are related to a breakdown of the BBB. He proposed two types of BBB breakdown which give rise to different types of edema. The first, which he called complete BBB breakdown, results in the exudation of proteinaceous material from localized, observable vascular lesions and its spread to distant regions, with sudden onset and early recovery. The second type -- partial BBB breakdown -- results in excess extravasation of water and electrolytes but not macromolecules from vascular lesions, which are slight, even under the electron microscope, and occur in several regions of the brain or even throughout it. This second type of edema is slow in onset and resolution and commonly fatal. The Joint Committee on Stroke and Brain Edema (Katzman et al., 1977), in agreement with Lee, concluded that the cerebral edema associated with cerebrovascular occlusion (i.e., autolysis) warrants a separate classification.

4. Volume Regulation within the Brain

To understand the mechanisms of brain edema, it is necessary to know the normal function of the BBB and its regulatory transport mechanisms as well as both the normal anatomy and biochemical composition of the brain's fluid compartments. This section describes the normal anatomy of brain capillaries and their function, and the fluid compartments within the brain.

4a. Role of the blood--brain barrier

The concept of a barrier between the intravascular compartment and the extracellular fluid of the brain arose from the work of Ehrlich in 1885, in which he observed that certain dyes crossed the capillaries of other organs but not those of the brain. This developed into the hypothesis of a cellular barrier between blood and the interstitial space of the cerebral parenchyma (Krogh, 1946). When electron microscopy was introduced the precise location of this barrier was revealed: in the endothelium of the cerebral capillaries. These endothelial cells restricted the passage of solutes of molecular weight ranging from 1800 daltons (Reese et al., 1971) to 900,000 daltons (Milhorat et al., 1973); however, lanthanum ions of 500 daltons freely crossed the BBB (Reese et al., 1971).

Several anatomical properties of endothelial cells are responsible for their low permeability to these substances: tight junctions, paucity of pinocytotic activity, lack of transendothelial channels, and lack of contractile proteins.

The interendothelial tight junction appears as a site of fusion of the outer plasma membranes of two neighboring endothelial cells. These junctions form continuous, interconnecting rings around the endothelial cell that are responsible for the very low permeability of the paracellular pathway (Shivers, 1979). Moreover, endothelial cells can form an uninterrupted cylinder around the capillary lumen that further reduces the paracellular transport of substances (Oldendorf et al., 1977).

If the passage of substances between endothelial cells, at least of macromolecules, is negligible, they may move by vesicular transport or passage across cells. In non-neural tissues, pinocytotic vesicles are common sites for the transfer of macromolecules out of peripheral vessels: the capillaries of muscle, for example, contain freely mobile pinocytotic vesicles within the cytoplasm and may even coalesce to form transcellular channels across the endothelial cell (Simionescu et al., 1978). By contrast, the brain capillaries have few, if any, pinocytotic vesicles in normal conditions (Reese and Karnovski, 1967) -- although their number can be increased by changes in local cyclic-AMP concentrations (Joo, 1972), indicating different degrees of vesicular transport accompanying different intracellular conditions. Westergaard and Brightman (1973) have described vesicular transport of horseradish peroxidase at certain segments of brain arterioles. Because vesicular transport is not selective, this may be a mechanism for moving serum proteins across the BBB. Under normal conditions vesicular transport is limited, which may account for the lower

levels of serum protein in the extracellular fluid in brain

(0.2--0.4 g/liter) than in other organs (e.g.; 18 g/liter in skeletal

muscle).

The permeability characteristics of cerebral endothelial cells

allow a similar passage of solutes to that across plasma membranes.

Rapoport et al. (1979), in extensive studies of the permeability of

brain capillaries, have found a direct proportion between

cerebrovascular permeability and the octanol/water partition

coefficient. There are two other types of transendothelial

transport: (1) a highly specific and saturable carrier-mediated

mechanism of transport that accounts for the passage of glucose,

ketone bodies, lactate, and amino acids (Oldendorf, 1973), and (2)

the Na^+-K^+-ATPase 'pump', an energy-mediated transport mechanism,

which maintains large ionic differences between intravascular and

extracellular spaces.

Another important component of the BBB is the glial cell.

These cells make up more than half the cellular volume of the brain

(Pope, 1978). Moreover, their astrocytic foot processes are tightly

applied to the capillary wall, covering about 85% of its surface

(Maynard et al., 1957). Astrocytes and endothelial cells interact to

control transport and exchange of water and solutes between vascular

and brain compartments (De Bault, 1980). The conclusion is that the

overall role of the BBB is to maintain a constant extracellular

milieu for the proper functioning of the neurons (Bradbury, 1984).

4.b Cerebral extracellular space

Quantification of fluid compartments within the brain has

proved technically difficult, and the various methods used to measure

the extracellular space have given different values. These methods

include freeze-drying (Van Harreveld et al., 1965), freeze-

substitution (Van Harreveld et al., 1966), the use of chemical

markers such as sodium, chloride, thiocyanate, iodide, sulfate,

sucrose and inulin, measurements of electrical impedance, and

electron microscopy with special fixation techniques. After a

comprehensive review of the results obtained with these techniques

Katzman and Pappius (1973) concluded that the extracellular space

corresponds to 12--25% of total brain volume.

The extracellular space of white matter is probably larger than

that of grey matter, due to the different properties of these

tissues. The former contains larger spaces, mainly because the nerve

fibers are cylindrical and run in all directions, whereas the cell

bodies in grey matter yield to accommodate one another smoothly

(Lee and Bakay, 1966). Moreover, under normal conditions the

extracellular space appears to offer no resistance to the passage of

substances of high molecular weight, such as horseradish peroxidase

(5-6 nm in diameter), and ferritin (10-11 nm) (Brightman, 1965) even

though the tortuosity of this space limits diffusion

(Fenstermacher, 1975).

It is now accepted that the fluid filling the cerebral

extracellular space communicates freely with the CSF and that the

chemical composition of both is the same (Bradbury, 1979; Davson,

1976; Milhorat, 1975). Furthermore, the capillaries of the brain

parenchyma produce 30% of the CSF and this flows via the interstitial

space (Pollay and Curl, 1967), the volume of which is regulated by

changes in regional cerebral blood flow (Fenstermacher, 1984).

4.c Starling's hypothesis of transcapillary fluid exchange

The functional significance of the blood--brain barrier (BBB),

and the effects of the BBB on regulation of the cerebral

extracellular fluid, can be further appreciated by taking into

consideration Starling's hypothesis of transcapillary fluid exchange

(Starling, 1896). This states that the driving force for water flow

across a membrane is given by the osmotic and hydrostatic pressures

on both sides of the membrane, and the permeability characteristics

of the latter:

$$Q = L \cdot S[(P_{mv} - P_{pmv}) - \sigma(\Pi_{mv} - \Pi_{pmv})] \qquad (1)$$

where Q = net rate of fluid movement across the vascular

endothelium (ml/min $\cdot$ mm Hg $\cdot$ cm^2), L = specific hydraulic conductance

(ml/min), S = surface area (cm^2), P = hydrostatic pressure (mm Hg),

σ = protein reflection coefficient, Π = protein osmotic pressure

(mm Hg), and mv and pmv correspond to microvascular and

perimicrovascular pressures respectively.

In the normal brain, the hydrostatic pressure difference

probably plays a negligible role in the production of interstitial

fluid. It is offset by the extremely high effective osmotic pressure

of plasma at the BBB, i.e., about 5700 mm Hg (Fenstermacher, 1984),

which in turn is due to the low permeability of brain capillaries to

proteins, electrolytes and water-soluble non-electrolytes (Rappoport, 1976; Bradbury, 1979). Thus, the low hydraulic conductivity of the BBB and the high osmotic activity of solutes in the intravascular and extracellular spaces are the main mechanisms regulating fluid volume within the normal brain. However, with the alterations in capillary permeability observed during brain edema, the hydrostatic pressure becomes one of the more important factors in fluid flow (see below).

Two mechanical properties of tissues contribute to the fluid homeostasis of the brain -- the tissue hydraulic resistance, which is defined as the impedance offered by the tissue to the flow of fluid, and the tissue compliance, which is the ability of the tissues to change form in response to changes in fluid volume (Marmarou et al., 1980). Under normal conditions the hydraulic resistance is very high, restricting the accumulation of fluid in the extracellular space, although it still allows the convective flow of solutes in the extracellular fluid. The interstitial fluid normally flows into the cerebral ventricles or the Virchow--Robin spaces and returns to the general circulation via the arachnoid villi.

The dynamic aspects of fluid regulation in the extracellular space can be explained as follows. The impermeability of the BBB to solutes counteracts any change in capillary hydrostatic pressure that tends to force fluid out of the intravascular space. Dilution by the solute-poor fluid that escapes into the extracellular space results in a decrease in its osmolality and an increase in the osmotic difference between blood and interstitial fluid. This, in turn, tends to force water back into the vessels. Moreover, the low

compliance of normal brain tissue limits the accumulation of fluid in the extracellular space due to marked increases in hydrostatic pressure that result from small increases in volume.

4.d Gibbs--Donnan equilibrium for regulation of cell volume

The Gibbs--Donnan postulate is the most widely accepted theory of cell-volume regulation (MacKnight and Leaf, 1977). It predicts that cells have a tendency to accumulate, from the extracellular fluid, ions such as K^+, Na^+, and Cl^- that can move from the intra- to the extracellular space or vice-versa. These ions, in turn, lead to an osmotic influx of water. Because of their non-permeant nature, proteins remain confined to either space. Their polyelectrolyte behavior attracts ions and, due to their higher concentration in the intra- than in the extracellular space, results in a tendency to draw Na^+ and Cl^- into cells. Cells avoid swelling by the active extrusion of Na^+, preventing its accumulation in the cells. This mechanism is known as the double--Donnan hypothesis for cell-volume regulation. A steady state is reached when the rate of extrusion equals the rate of ionic leak into cells. This active 'pumping' of Na^+ is mediated through the enzyme Na^+-K^+-ATPase, which in turn is activated by ATP.

Other active and passive mechanisms involving ion transport across membranes have been described (Bourke, 1980). Some of these involve the activity of two ionic antiporters that control intracellular pH and, indirectly, cell volume. Carbon dioxide produced by the normal metabolic activity of glial cells is converted to carbonic acid by the enzyme carbonic anhydrase, releasing hydrogen

ions and bicarbonate ions. To maintain optimal intracellular pH the glial cell extrudes excess H^+ in exchange for Na^+. The second antiporter involves the exchange of bicarbonate ions for Cl^- from the extracellular fluid. The increase in osmotic pressure due to the shift of Na^+ and Cl^- into the cell attracts water (Kimelberg and Bourke, 1982). It has been suggested that in pathologic conditions characterized by decreased oxygen availability, an increase of H^+ occurs, which produces swelling of the glial cells by this mechanism. (Siesjö, 1985).

5. Pathophysiology of Brain Edema

5a. Mechanisms operating in brain edema

The basic pathophysiologic alteration in cerebral edema involves a derangement of the mechanisms responsible for the homeostasis of water within the brain parenchyma. For descriptive purposes only, the process of brain edema can be divided into three distinct but inter-related phases. The formation phase involves disruptive agents that alter the normal fluid homeostasis of the brain. These noxious agents may act on several regulatory mechanisms (components of Starling's equation, see subsection 4c.) such as osmotic force, hydrostatic pressure, and permeability of the membranes. For example, alterations in osmotic pressure are observed in water intoxication, and of hydrostatic pressure in hypertensive edema. Alterations in the membrane-permeability characteristics of the BBB may be either structural as, for example, in tumors, or

functional, as in the early phases of ischemia. Membrane alterations

in brain cells that lead to cytotoxic edema are caused by similar

disruptive agents.

The second or spread phase is closely related to the formation

phase. It depends not only upon changes in osmotic and hydrostatic

pressures and membrane permeability, but also upon the inherent

biomechanical properties of the parenchyma such as tissue compliance

and hydraulic conductivity of tissue.

To be effective, the resolution phase requires loss of the

initial disruptive agent with a return to normal of Starling's

equilibrium components. However, it is important to note that

resolution mechanisms are operative immediately after the pathologic

process starts, and may achieve homeostasis -- although at a level

different from normal -- even when a noxious stimulus is present. An

example of this may be found in small and slowly growing neoplasms of

the central nervous system.

5b. Formation of Brain Edema

5b.1. Alterations in the blood--brain barrier

Brain edema is characterized by an increase in the fluid

content of the tissue. This fluid comes directly from the

intravascular space (Hossmann, 1976), except in hydrocephalus where

it comes from the cerebral ventricles (Milhorat et al., 1970). Thus,

alterations in the brain vessels are usually present in edema

(Lee, 1971). The disruption in the BBB may be structural, such as

that observed with abnormal capillary proliferation, or functional,
such as that mediated by chemical substances, or both.

Structural disruption of the BBB is commonly observed in the
late phase of a developing infarction (Olsson et al., 1971; Kamijyo,
1977, O'Brien, 1979). Change in permeability resulting in edema is
proportional to the severity and duration of the ischemic insult, and
is caused by necrotic changes in the capillary endothelium (O'Brien
and Waltz, 1974).

A structural breakdown of the BBB is also observed in brain
tumors from experimentally induced neoplasms (Hossmann et al., 1979;
Nishio et al., 1983) and in biopsy material from human tumors
(Long, 1970, Vick, 1980). It results from proliferation of abnormal
capillaries induced by angiogenesis factors released from the tumor
in its attempt to procure a vascular supply for itself
(Folkman, 1971). The abnormalities, which are associated with marked
extravasation of fluid, include increased number and diameter of
capillaries, increased mitotic activity, and hyperplastic changes of
endothelial cells. The abnormal endothelium also shows increased
pinocytotic activity, presence of fenestrations and loss of contact
between cells (Long, 1970; Vick, 1980). Similarly, in cerebral
infections, e.g., abscesses of the brain, a marked neovascularization
occurs around the lesion (Britt et al., 1981). Endothelial cells of
these newly formed capillaries lack tight junctions
(Cancilla et al., 1974), a condition which contributes to the severe
edema observed in these conditions.

Functional alterations in the BBB also lead to cerebral edema. For example, injection of hyperosmolar solutions into the carotid artery (Brightman et al., 1973; Houthoff et al., 1982) is associated with a reactive response of the endothelium which includes formation of vesicle and channel-like structures, and cytoplasmic pooling of protein tracers (Farrel and Shivers, 1984). These changes lead to extravasation of water, electrolytes, and tracers of high molecular weight, e.g., 40,000--160,000 daltons, into the extracellular space (Houthoff et al., 1982). Edema associated with arterial hypertension is also caused by functional breakdown of the BBB (Westergaard et al., 1977; Nag et al., 1979; Petito et al., 1977).

The permeability of the BBB during the initial stages of an infarction increases also (Hossmann, 1976; Petito, 1979; Lossinsky et al., 1979, Klatzo et al., 1984) and probably includes a functional rather than a structural alteration of the capillary endothelium of the brain. A substance or a series of them may be involved in this kind of alteration.

Many substances have been postulated as mediators of increased BBB permeability. The ones most studied include arachidonic acid, free radicals, lactate, monoamines, and cyclic AMP.

Free radicals are highly reactive chemicals that can combine with a wide variety of cell structures, and are especially damaging to cell membranes. (For a review see Demopoulos et al., 1980). Free radicals are probably generated in many forms of brain insult characterized by reduced regional blood flow, for example, ischemia and mass lesions. Reduced blood flow depletes the normally occurring

antioxidants and the enzymes responsible for control of free-radical
formation. The free radicals activate membrane phospholipases which
readily convert phospholipids into arachidonic acid and its
metabolites (Chan et al., 1981). Arachidonic acid injected into the
brain parenchyma of rats produces brain edema by altering the
permeability of the microvasculature (Chan et al., 1983a).

Lactate accumulation, and therefore lowering of pH, has been
associated with loss of regulation of blood flow and damage to the
BBB (Lassen, 1974). Lactate is produced in large amounts after an
ischemic insult (Lassen, 1966) and within brain tumors
(Jähde and Rajewsky, 1982).

Monoamines stimulate the formation of cyclic AMP, which has
been found in the endothelium of the rat brain
(Szumanska et al., 1984) and may mediate the endothelial transport of
macromolecules and water (Klatzo, 1983).

5b.2. Alterations in cell volume during brain edema

Many injurious processes cause alterations in brain cells that
are associated with cerebral edema; the energy depletion that
results from an ischemic lesion has been the most extensively
studied.

The double--Donnan hypothesis predicts that, with energy
depletion such as that occurring after an ischemic event, cells in
the nervous system will swell. It has been shown that the reduction
of ATP, responsible for driving the Na^+-K^+-ATPase pump, is associated
with swelling of neuronal cells (Siesjö and Wieloch, 1985). This

swelling involves a shift of water from the extra- to the
intracellular space as shown by a reduction in extracellular space
determined by cortical impedence methods (Van Harreveld and Ochs,
1956; Schuier and Hossmann, 1980). Moreover, even though the BBB
offers resistance to the passage of water (Raichle et al., 1976), and
Na^+ (Go and Pratt, 1975), there is a net increase of both in the
brain parenchyma, suggestive of movement of these substances from the
plasma (Hossmann, 1982). This increase in water from the plasma may
be due partly to an increase in brain osmolality during the ischemic
process (Hossmann, 1982). Because the endothelium in the early
stages of ischemia may retain some function, it is still able to
maintain an osmotic difference between brain tissue and blood
(Hossmann and Takagi, 1976). This difference, in turn, will tend to
equilibrate according to the mechanisms postulated by Starling's
hypothesis, accounting for some of the movement of plasma water but
not proteins into the brain parenchyma. Adrenergic stimulation of
brain vessels during ischemia may contribute to water accumulation by
increasing the blood flow and permeability of the microvasculature
(Raichle, 1976).

Chemical mediators that affect the permeability of the BBB also
result in a change in cell volume. Energy failure results in release
of K^+ and uptake of Ca^{++} (Siesjö and Wieloch, 1985), ions that cause
release of neurotransmitters, such as adenosine and noradrenaline,
that induce swelling of glial cells (Bourke, 1981). Release of
glutamate may lead to sustained depolarization of nerve cells and
swelling (Chan et al., 1979; Maier-Hauf et al., 1984). The increased

intracellular Ca^{++} mediates the formation of free fatty acids

(Harris et al., 1981), which produce cell swelling (Chan et al.,

1981), probably due to degradation of cell membranes. More

importantly, the presence of Ca^{++} at a concentration greater that 10μ

mol prevents the reactivation of Na^+-K^+-ATPase by interfering with

ATP synthesis (Nichols and Ackerman, 1982). Decrease in ATP leads to

formation of free radicals (Flamm et al., 1978) which inactivates

Na^+-K^+-ATPase with resultant cellular edema (Chan et al., 1983b;

Brody et al., 1974). Lassen (1968) observed suppression of enzymatic

activity in the brain associated with acidosis that was probably

produced by lactate accumulation. He suggested that because lactic

acidosis leads to cell swelling, some of the enzymes suppressed may

be those responsible for driving the ionic pumps. Siesjö (1985) has

suggested that swelling of glial cells results from increased

activity of Na^+/H^+ antiporters.

In summary, the changes in the fluid homeostasis of the brain ,

and, therefore, the formation of cerebral edema, are due to a

disturbance in the normal function of cell membranes. Vasogenic

edema results when the membrane changes occur in endothelial cells

whereas cytotoxic edema results when such membrane changes occur in

neuronal or glial cells. Most lesions resulting in brain edema

produce a combination of vasogenic and cytotoxic edema. Accumulation

of fluid occurs with disequilibrium of the factors responsible for

Starling's equation, and alterations in the double--Donnan steady

state.

Most studies of the spread of cerebral edema have been performed in animals subjected to lesions that produce vasogenic edema -- for example, cryogenic injury. Using this model, Klatzo et al. (1967) and Reulen et al. (1977) have shown that capillary hydrostatic pressure is the driving force for the extravasation of edema fluid. Transmission of hydrostatic pressure depends on the area of altered vascular permeability and the duration of opening of the BBB (Klatzo et al., 1967). In this model, the altered permeability of the BBB in the area of the lesion allows osmotic difference to equilibrate, while hydrostatic pressure gradients are generated. The pressure is highest in the area of the lesion and decreases with increasing distance from the site of the injury. The pressure gradient in the tissue is due at least in part to the opposing force generated by the resistance of the affected tissues. Studies by Marmarou et al. (1980, 1982) in which fluid was infused into the white matter of cats have shown that tissue hydraulic resistance and tissue compliance are responsible for changes in brain volume in vasogenic edema. However, it is important to note that white matter varies in its susceptibility to spread of edema. Clasen et al. (1962) observed that white matter under the postcentral gyri of monkey and of dog was more susceptible to spread of edema than that of the precentral gyri. This difference in resistance patterns is due to a greater number of criss-cross fiber patterns beneath the postcentral than the precentral gyrus. Similarly, in the corpus callosum and the internal capsule, a compact arrangement of parallel

the grey matter, the intermingled disposition of nerve cells and their processes makes this tissue very resistant to the spread of edematous fluid. Therefore, considerable hydrostatic pressures have to be reached before fluid accumulates in the grey matter or the corpus callosum.

The tissue pressure gradient created by the damaged cerebral microvasculature opens the intercellular channels between the parallel fibers of the white matter (Cserr et al., 1977). Initially a large increase in interstitial fluid pressure is required to cause these channels to dilate. Once this separation of fibers has occurred, a small increase in hydrostatic pressure produces a large increase in the movement of water and solutes (Fenstermacher and Patlak, 1976). Marmarou et al. (1980) have shown that tissue compliance increases exponentially with increases of up to 0.4 ml of infused fluid but reaches a plateau beyond this volume. They also observed that tissue resistance decreases exponentially with increases in infused volume. Thus, the spread of edema fluid in vasogenic edema is dependent on the distention of the extracellular space by a continuous leakage of fluid through a disrupted BBB that allows direct transmission of hydrostatic pressure. Once the BBB is repaired, the pressure gradients disappear and osmotic forces become the predominant factor responsible for the spread of edema fluid, and more importantly, resolution of the edematous process (Klatzo et al., 1980; Marmarou et al., 1982a).

the formation and spread of brain edema has been confirmed recently by several authors (Gazendam et al., 1979; Klatzo, 1980; Bodsch et al., 1982; Kuroiwa et al., 1985). These investigators demonstrated a close relationship between accumulation of serum proteins and increase in tissue water. They have suggested that the increment in serum proteins in the extracellular space reduces the transvascular oncotic pressure difference, which limits the reabsorption of fluid from the tissue into the blood vessel (Go et al., 1976; Klatzo et al., 1980). Therefore, as well as hydrostatic pressure gradients, tissue resistance and tissue compliance, serum proteins play a major role in the accumulation of water during vasogenic edema. In the cryogenic-injury model these forces acting together produce an approximately linear decrease in water content away from the site of the lesion (Reulen et al., 1977) an effect which, however, is only observed in white matter.

5d. Resolution of brain edema

Most organs of the body have a lymphatic system that specialises in the removal of the excess water and solutes that accumulate -- for example, during edematous processes. In the brain no such lymphatic system has been found. However, the extracellular space of the brain is in direct communication with the ventricular cerebrospinal fluid (CSF). The ependymal cells lining the ventricles offer little resistance to the passage of solutes, as shown by the appearance of substances of widely different molecular weights, such

parenchyma (Wald et al., 1978).

Bulk or convective flow is responsible for the clearance of edema fluid from the brain tissue via the CSF (Reulen et al., 1978). This clearance mechanism is dependent upon the existence of a hydrostatic pressure difference between the edematous tissue and the CSF. Therefore, this process is active only when there is a continuous escape of fluid into the brain from the microvasculature (Marmarou et al., 1982a). Once the BBB is repaired, i.e., within a few hours of cryogenic injury, outflow of plasma is reduced (Marmarou et al., 1976). Bulk flow is thus reduced, although some clearance of edema fluid may persist due to diffusion of solutes (Cserr, 1977).

If convective flow were the only mechanism responsible for clearance of edma fluid, then protein-poor and protein-rich fluids would be expected to disappear at the same rate. However, Marmarou et al. (1982a) showed that mock CSF infused into the brains of cats was cleared at a faster rate than infused cat serum. Studies by Klatzo et al. (1980) have shown that glial cells have a definite role in removing macromolecules such as albumin. The removal of albumin from the extracellular space and its subsequent digestion by glial cells lowers the oncotic pressure of the edema fluid and permits its re-entry into capillaries. Rubinstein et al. (1962) reported that this was associated with an increased metabolic activity of astrocytes. However, Bodsch and Hossmann (1983), working with rats with implanted brain tumors, showed that degradation of albumin was not significant. A possible explanation is that metabolic

disturbance of the brain associated with edema, as suggested by Pappius (1982) and Hossmann et al. (1986), results in impaired uptake and catabolism of serum proteins.

Other mechanisms of edema clearance may include a 'retrograde' pinocytosis across endothelial cells (Wagner et al., 1974; Vorbrodt et al., 1985); absorption of edema fluid in areas devoid of a BBB, such as the area postrema, the pineal gland, and the median eminence; and lymphatic channels draining some regions of the brain (Bradbury et al., 1981).

In summary, several mechanisms act simultaneously to restore the normal fluid homeostasis of the brain. Their contribution has been quantified by Marmarou et al. (1984) using a model in which the brain was continuously infused with fluid. Clearance via the CSF accounts for up to 38% of the infused fluid, uptake by the brain for about 56%, and uptake by the blood for about 6%.

6. Effects of brain edema on the cerebral function

It is not clear whether edema per se produces metabolic or functional alterations of the brain. For example, the proteins in the fluid present in vasogenic edema are taken up by astrocytes as previously discussed (Klatzo et al., 1980). This uptake is associated with cell proliferation and scar-tissue formation, which are clearly structural sequelae. However, the effect of the gliotic scar on changes in brain function has not been determined. Schaul et al. (1976) found that in rats with brain edema not associated with increased intracranial pressure, no changes in

electroencephalographic activity were observed. Measurements of short-latency somatosensory-evoked potentials in areas of edema in cats with cryogenic injury did not show alterations in wave amplitude and latencies (Sutton et al., 1980). Similarly, in patients with mass lesions and edema, no alteration in somatosensory-evoked potentials was observed in edematous areas of white matter (Penn, 1980). Therefore, normal neurologic and electrical function can be preserved in patients despite focal white-matter edema. However, widespread depression of local glucose utilization has been observed in rats with cold-injury (Pappius, 1982), and in the peritumor edema of animals with brain tumors (Yamada et al., 1983; Hossmann et al., 1986). The significance of these findings remains to be determined.

The most serious effect of brain edema on neurological function is caused by the increase in intracranial pressure resulting from an increase in brain volume within the rigid cranial cavity. There is a reciprocal relationship between the volumes of the brain tissue, the CSF and the cerebral blood such that a change in the volume of one results in changes in the other two. This relationship was recognized as early as 1783 by Alexander Monro and later modified by George Kellie, and so termed the Monro-Kellie Doctrine (quoted in Bell, 1983).

Compensating mechanisms, such as decreased production and increased absorption of CSF (Hochwald and Sahar, 1971; Weiss and Wertman, 1978), prevent the volume of the cranial contents from reaching excessively high levels. When the increase in volume of the

brain overwhelms these compensatory mechanisms, intracranial pressure increases. At this point, very small increases in volume lead to marked changes in intracranial pressure (Marmarou et al., 1975; Sullivan et al., 1979). The increase in volume leads to herniation of brain structures through the natural openings of the skull. The result is compression of vital centers causing the depression of circulation and respiration observed with uncal herniations (Tarlov, 1959). Herniations may also compress blood vessels with the resultant infarction of regions of the brain supplied by them (e.g., interruption of flow in the posterior cerebral artery with homonymous hemianopsia due to temporal lobe compression against the edge of the tentorium). In addition, the increase in intracranial pressure reduces cerebral blood flow (Wolff and Blumgart, 1929) and causes generalized brain ischemia. Increases in intracranial pressure per se have deleterious effects on the function of the vital centers (Cushing, 1901). In summary, the evidence suggests that accumulation of fluid in small, localized areas has little or no effect on the function of the brain. However, a large increase in volume leads to increased intracranial pressure, which is one of the commonest causes of death due to neurological disease.

PART II: METHODS EMPLOYED FOR THE STUDY OF BRAIN EDEMA

This section describes experimental methods used to obtain information on the pathophysiologic alterations that occur during brain edema, as well as clinical methods for examining patients with edema. It concludes with a review of the application of proton NMR to the study of the brain and other components of living systems.

Because cerebral edema is characterized by an increase in tissue fluid content, measuring the water content of the brain is the most direct method of determining its presence. Evaluating the biochemical composition of the edema fluid and the movement of labeled compounds in it provides information about the origin of the edema. The relationship between edema fluid and brain parenchyma is investigated by studies of morphology and the distribution of chemical compounds. Finally, pathophysiologic processes are interpreted by monitoring the dynamic relationship between changes in fluid content of tissue and its composition and distribution, and the reaction of the brain to fluid accumulation.

In clinical practice, accurate diagnosis of the pathologic conditions that produce edema is essential for proper management of patients. Monitoring the edematous process and its response to therapy is important to establish a prognosis. To reduce risk and discomfort to patients, its invasiveness should be minimal.

1. Determinations of Water Content

   To measure its water content a fresh tissue sample is weighed, dried at high temperatures, then weighed again. Using the values obtained, the amount of water in the sample is calculated by employing the Elliot--Jasper equation (1949):

$$\% \text{ tissue water} = \frac{\text{tissue fresh weight} - \text{tissue dry weight}}{\text{tissue fresh weight}} \times 100$$

A serious drawback with this technique is the assumption that the only volatile compound is water. Lipid molecules of the brain may be lost during this process, especially the degraded lipids that accumulate in areas of infarction. This problem can be corrected, at least partly, by freeze-drying under vacuum (Shigeno et al., 1982). Another advantage of the latter technique is that it leaves many of the organic constituents of the tissue unchanged and available for analysis in the dried sample. Methods not commonly used for quantification of water content in the brain include: recovery of tissue water by xylene distillation (McQueen et al., 1966), determination of fat-free dry weight (Aprison et al., 1960), and coulometric techniques (Le Bas et al., 1984).

   An indirect but popular method of determination of water in brain samples is the specific-gravity technique, originally described by Barbour and Hamilton (1923). Using body fluids they observed the time required for a drop of fluid to fall through a solution of xylene and bromobenzene, and compared it to the time taken by a solution of potassium sulfate of known density to fall through the same mixture. Nelson et al. (1971) modified this method for use with

edematous brain samples. They provided an equation to convert specific-gravity units into water-content units so that changes in water content can be calculated. This conversion is valid as long as the specific gravity of the tissue solids remains constant; however, in vasogenic edema the density of the tissue is increased with the increase in serum proteins. The protein content of the edema fluid can be compensated for by an equation developed by Marmarou et al. (1982b).

Many factors besides protein changes in the tissue affect the determination of specific gravity in tissue samples of edematous brains and thereby preclude comparisons of values obtained in different studies. Fujiwara et al. (1981) showed that the purity of kerosene and bromobenzene solutions, the size of the samples, and the temperature had marked effects on the observed values. By maintaining constant conditions under which measurement was made, it was possible to obtain reproducible values. They further concluded that these values cannot be extrapolated to absolute water content, although Bothe et al., (1984) suggested that this can be done due to the small effect such factors have on the values for specific gravity.

Fujiwara et al., (1981) have stated that the specific gravity method is 5--10 times more sensitive than heat drying and that samples as small as 1 mg can be used. The studies of Ferszt et al., (1980) and Shigeno et al., (1982) indicated the optimal weight of samples to be greater than 30 mg. By contrast, it has been recommended that the sample size for measurements of water content in

the drying method be larger than 100 mg (Shigeno et al., 1982; Bothe et al., 1984). Hence the advantage of the specific gravity method is its requiring smaller tissue samples than the drying method and may permit accurate determination of the distribution of brain edema as shown by Klatzo et al., (1980).

2. Biochemical composition of edema fluid

Distinguishing between normal tissue fluid and edema fluid poses technical problems in attempts to determine the chemical composition of the latter. Original investigators performed quantitative chemical analysis of edematous and normal tissue, and assumed that the difference between them represented the composition of the edema fluid (Stewart-Wallace, 1939; Aleu et al., 1964; Herzog et al., 1965; Reulen et al., 1969).

Sodium and potassium content were measured in studies on cats with cryogenic injury. When expressed as units of ions per dry weight, these measurements revealed an increase in sodium but no change in potassium content (Pappius and Gulati, 1963). As the levels of these ions were similar to those in plasma the authors concluded that the fluid originated from plasma. In extensive studies by Hossmann and collaborators on cats with vasogenic edema produced by different lesions, the amount of sodium in edema fluid was slightly lower than in plasma. They suggested that the production of idiogenic osmoles could account for a difference in osmolality, and thus in sodium content (Hossmann et al., 1979; Hossmann et al., 1983; Bothe et al., 1984). Alternatively, the lower

sodium content may have been due to a small increase of sodium in the

opposite hemisphere (Pappius and McCann, 1969). This increase may be

a source of error because reference values are usually obtained from

samples taken from the opposite hemisphere.

Direct measurements of the biochemical composition of edema

fluid in the cryogenic-injury model have been performed by either

centrifugation of tissue samples (Clasen et al., 1962 and 1982), or

by implantation of catheters (Gazendam et al., 1979). The values of

sodium were similar to those of plasma in both types of experiments;

however, potassium was very high in the fluid extracted by

centrifugation, while in the fluid obtained by catheter implantation

it was high initially, then decreased with time to plasma values. In

the centrifugation experiments Clasen et al. concluded that the high

potassium content was an artifact of preparation, whereas Gazendam et

al. concluded that the elevated potassium content in the initial

stages resulted from cell injury caused by the cryogenic lesion.

Measurement of proteins in edematous brain has provided further

evidence that edema fluid originates from plasma. It is well

established that the serum protein content of the normal

extracellular fluid of the brain is minimal (see above) and hence an

increase in these proteins would indicate the origin of edema fluid

as plasma. Klatzo et al. (1958), performing paper electrophoresis on

extracts of edematous brain subjected to cryogenic injury, showed a

marked increase in the albumin fraction of edematous white matter.

Similar findings were recorded by other groups (Kiyota, 1959;

Cumings, 1961; Karcher and Lowenthal, 1967). Increase in serum

albumin in brain tissue was monitored over time after cryo-injury in cats (Pappius, McCann, 1969). These investigators, employing radio-labeled serum albumin demonstrated an increase of albumin reaching a maximum at 48 hr, which corresponds to the time the BBB remained open to macromolecules (Klatzo et al., 1980). They also observed a relationship between an increase in albumin and in water in the formation phase of edema, which has been confirmed by Bothe et al. (1984), Hossmann et al. (1983), and Kuroiwa et al. (1985). Different groups of investigators, however, have found varying amounts of serum proteins in edema fluid. For example, Clasen et al. (1982) and Go et al. (1985) have reported serum-protein values similar to those in plasma, while Hossmann et al. (1983) found very low values (about one tenth those in plasma), and Kuroiwa et al. (1985) obtained values intermediate between these two. These discrepancies are mainly due to differences in method, although changes in protein concentrations have been observed in edema fluid from brains with different lesions (Bothe et al., 1984), and during the various phases of edema (Bodsch et al., 1982).

3. Measurement of Tissue Spaces

The volume of the extracellular space of the brain has been measured with substances that were assumed not to enter cells. These markers were adminstered intravenously or intracisternally and distributed evenly within the extracellular space. Substances used for this purpose include inulin (Bourke et al., 1965), sucrose, radioactive tracers such as ^{36}Cl, ^{35}S, ^{131}I (Reed and Woodbury, 1963),

and thiocyanate (Streicher et al., 1964). These techniques have several limitations; for example, markers may distribute in more than one space giving rise to error, or values may be altered by changes in the incubation temperature of the medium or its composition (Cohen, 1972). Consequently, these techniques are no longer used (for a comparative review see Katzman and Pappius, 1973).

Electrical impedance can be used to measure the size of the extracellular space indirectly, based on the assumption that the cell membranes' high electrical resistance allows electric current to flow only through the interstitial fluid. During vasogenic brain edema, the increase in extracellular fluid results in a direct increase in its conductance (reciprocal of the impedance). However, large scatter in the data and an uncertainty of 20% have been observed (Cohen, 1972). Another serious problem with the technique is that it assumes that cell membranes are impermeable to ions. Because membranes of certain cerebral cells may be highly permeable to ions (Bourke et al., 1980; Katzman, 1961), cortical impedance does not provide a true measure of the extracellular space.

4. Morphologic Methods

Pathologic characteristics of edematous brains have been well described, using macroscopic examination and light and electron microscopy (Greenfield, 1939; Long et al., 1966; Hirano, 1980). Many attempts to quantify the size of the tissue spaces were made after the introduction of the electron microscope. This technique, however, also has its limitations: Van Harreveld et al. (1965 and

artifacts in the tissue that alter the size of the extracellular space.

Despite some of its limitations, the electron microscope has helped prove that edema fluid accumulates in extracellular and in the intracellular spaces (Lee and Bakay, 1966). With the use of electron-dense material, electron microscopy has also helped define the anatomical basis of the BBB and some of its functions. Tight junctions between endothelial cells represent the BBB, as shown by the studies of Reese and Karnovsky (1967).

The electron microscope revealed that in brain edema induced by triethyltin intoxication, the edema fluid collected within the myelin sheath forming vacuoles by splitting the intraperiod lines (Aleu, 1963). The vacuoles are physically separate from the extracellular space (Hirano et al., 1968).

Physiologic studies of the BBB during cerebral edema began with intravenous injection of vital dyes. The more commonly used markers are Evan's Blue (Tschirgi, 1950) and fluorescein isothiocyanate (Klatzo et al., 1962). For electron microscopy the more frequently used markers are the electron-dense tracers horseradish peroxidase and microperoxidase (Westergaard, 1977). The functional changes affecting the BBB during the early phase of ischemia have been well documented by employing horseradish peroxidase (Kuroiwa et al., 1980). Also, studies with peroxidase-antiperoxidase techniques have provided information on resolution processes in brain edema (Klatzo et al., 1982). The limitations of these techniques are that no

the tracers can be accurately determined. Moreover, this distribution may not correspond with that of serum proteins due to differences in their transport, spread, and degradation throughout the compartments of the brain (Westergaard, 1977; Wolman et al., 1981).

5. Autoradiography

Quantitative autoradiography measures spatial distribution and concentration of radioisotopes in tissues. By labelling chemical compounds with radioactive tracers, it is possible to determine the rates of specific biochemical reactions. This method was developed in the 1940s, but was not generally applied to studies of the central nervous system until several years later (Landau et al., 1955; Reivich et al., 1969).

As this technique employs intravenous injection of a radioactive tracer, one must take into account the blood flow in the tissue of interest as well as the tracer's transport between blood and tissue, and its metabolic pathway (Sokoloff et al., 1977). This requires knowledge of chemical and enzyme kinetics and tracer theory. These depend upon a number of basic assumptions that are affectd by numerous factors, both static and dynamic. Moreoever, methodologic factors such as type of labeled compound, procedure for administering it, and time since administration, all markedly influence results. Hence the technique requires that the basic assumptions be validated at each stage of the procedure. If such complications are allowed

information can be obtained with this technique.

The application of autoradiographic methods to the study of brain edema has confirmed previous observations using other techniques. Blasberg et al. (1980), for example, employed ^{14}C-aminoisobutiric acid for assessing capillary permeability and ^{14}C-sucrose and ^{111}In-transferrin for the determination of fluid flow through brain parenchyma in rats with cryogenic injury. Their results showed that capillary permeability increased in the area of the lesion, and did not alter in the surrounding brain. They also demonstrated that the rate of movement of sucrose and transferrin was the same and limited chiefly to the white matter. This confirms previous studies showing that the spread of edema fluid after a cryogenic lesion is by convective flow.

Autoradiography has provided new information on the metabolism of the brain following various insults. In rats with cold injury, Pappius (1980) studied the relative rates of glucose utilization, which provides a measure of cerebral oxidative metabolism. Her results showed a marked decrease in glucose utilization in the affected hemisphere, and to a lesser extent in the opposite hemisphere. This effect was most marked in the cortical areas. From further experiments using the same methodology, Pappius and Wolfe (1984) concluded that depression of glucose utilization does not contribute to brain damage, and that edema per se did not cause a decrease in local cerebral glucose utilization. Hossmann et al. (1986) demonstrated a similar depression in the brains of rats with

determination of protein synthesis, Bodsch et al. (1984) reported

that depressed glucose utilization was associated with reduced

protein synthesis.

6. The Study of Brain Edema using Paraclinical Methods

Cerebral edema behaves as a mass lesion and, as such, it may

produce an increase in intracranial pressure. Intracranial pressure

is determined either by lumbar or ventricular puncture, with the

ventricular route reflecting intracranial pressure more accurately

than the lumbar route (Lehman and Parker, 1935). Because periods of

intracranial hypertension are followed by periods of relatively

normal pressure, ventricular puncture also more accurately monitors

these changes over time. These spontaneous variations in pressure

have been observed in a variety of disorders, and have been

attributed to "vasomotor instability" (Lundberg et al., 1965;

Langfitt and Kassell, 1966).

Intracranial manometry is not diagnostic of brain edema but of

any lesion that produces an increase in the contents of the skull.

Once edema is diagnosed, however, the continuous measurement of

intracranial pressure monitors quantitatively the development of

edema and its response to treatment (for a review see Gaab and

Heissler, 1984).

Imaging of the brain has provided a more direct approach for

the diagnosis of cerebral edema. Pioneered by Arthur Schuller (Bull,

1961), neuroradiology has evolved into a separate discipline, and

variety of techniques is a result of the complexity of the central

nervous system, its inaccessibility, and its vulnerability. The

limitations of plain x-ray films for the detection of cerebral edema

were evident from the beginnings of neuroradiology. Only certain

lesions causing edema, such as calcified tumors and the sequelae of

trauma, were amenable to diagnosis by x-rays (Bull, 1961). Working

at Johns Hopkins Hospital Dandy, in 1918--19, introduced air into the

cerebral ventricles of children with hydrocephalus, and into the

subarachnoid space, to delineate the ventricles and observe

distortions produced by a variety of conditions. Sicard, in 1921,

published his work on the use of positive contrast media. He

injected Lipiodol intrathecally in the lumbar region to detect

lesions that produce a mass effect in the spinal cord. Egaz Moniz is

credited with the discovery of angiography in 1927. He used sodium

iodide intra-arterially in an effort to delineate blood vessels. By

the end of the 1950s, the combination of plain x-rays, tomography,

air studies, and angiography provided neurologists and neurosurgeons

with a fairly accurate idea of the lesions they were encountering in

clinical practice, including their size, shape, and position.

The development of nuclear medicine began with George Moore

(1948) when he showed that fluorescein was taken up by certain tumors

and their outline could be well defined by using ultraviolet light at

the time of surgery. He then prepared di-iodofluorescein with ^{131}I

and injected it intravenously with subsequent location of tumors by

using a Geiger counter. The great advantage of this technique was

patients. The application of increasingly sophisticated techniques of nuclear medicine to brain scanning has revealed that this uptake of radioactive tracers by tumors and other lesions, is the result of an altered BBB (Bakay and Lee, 1965).

Godfrey Hounsfield (1973) revolutionized neuroradiology with his work on computed tomography. One of his breakthroughs was the digitization of the signal detected by sodium iodide crystals that scintillated when exposed to x-rays. Using the principle that crystals scintillate in proportion to the amount of x-rays they absorb, and that tissues absorb x-rays in proportion to their densities, Hounsfield obtained values for tissue densities from the scintillation produced by x-rays emerging from irradiated organs. These values, in digital form and derived from exposures taken at a large number of angles, were analyzed by computer to reconstruct an image. The image is formed by a large number of discrete areas (i.e. pixels) whose numerical values correspond to varying tissue densities. This development enabled neuroradiologists to detect brain edema directly and noninvasively for the first time.

In the early days of computed tomography (CT) combining a radionuclide scan and a CT scan of the brain was more accurate than either procedure on its own. With further technical developments, it was possible to replace the radionuclide scan with CT (Mettler et al., 1985).

It was hoped that the CT would provide an objective assessment of the extent and severity of edema. The studies by Clasen et al.

(1981) showed a good correlation between the size of the areas of decreased tissue density on scans, and the extent of cerebral edema as judged by histopathological methods. They also found a correlation between tissue density and severity of the edema. However, values representing tissue densities, i.e., CT numbers, are influenced by various factors, both intrinsic and extrinsic. Intrinsic factors, for example, include alterations in protein and salt content of the edema fluid (Clasen et al., 1981) and the thickness of the skull (Di Chiro et al., 1978). Extrinsic factors such as the energy of the x-ray tube affect CT numbers (Rutherford et al., 1976). Moreover, the sensitivity of x-ray CT to the small variations in tissue density is limited. These factors have precluded the widespread use of quantitative CT in clinical practice. Despite the limitations of quantitative CT, a few studies have shown that this technique is capable of objectively monitoring the evolution of cerebral edema after therapeutic intervention (Hatam et al., 1982; Ito et al., 1986).

The use of computers for manipulation of large amounts of data has permitted the evolution of isotope scanning into tomographic techniques such as single-photon-emission computed tomography (SPECT) and positron-emission tomography (PET). The former utilizes gamma-emitting radionuclides for the production of tomograms. The disadvantage of this technique is that the scan times are too long; faster methods are therefore required to make this technique practical.

PET provides information comparable to that obtained with autoradiography but with much less spatial resolution. The ability of this technique to provide, non-invasively, metabolic information from the brain that is spatially encoded, and the fact that such information can be quantified, makes it a very promising tool for research on brain edema (Raichle, 1980). At present, however, experience with PET scanning in cerebral edema is limited. Studies have indicated, for example, that areas of peritumor edema and some regions remote from it show a decrease in regional cerebral blood flow and regional cerebral metabolic rate for oxygen (Beaney et al., 1985); that a decrease in regional cerebral metabolic rate for glucose occurs in the peritumor grey matter and in the cerebellar cortex (De La Paz et al., 1983); and that the uptake of glucose in areas of peritumor edema is decreased (Ericson et al., 1985). These findings corroborate previous descriptions of metabolic changes within the brain of animals with experimental brain edema (Pappius, 1982). Much more work is needed, however, to define clearly the metabolic and functional alterations associated with this condition.

7. Proton Nuclear Magnetic Resonance (NMR)

Proton NMR, like PET, is another technique that has the potential to provide not only structural but also functional information, spatially defined and obtained noninvasively. Experiments carried out by the groups of Bloch in Stanford and Purcell in Harvard led to the discovery of NMR (Bloch et al., 1946; Purcell et al., 1946). It was not until the following decade,

however, that this technique was first used for systematic studies in biological systems (Odeblad and Lindstrom, 1955). These studies clearly demonstrated that water in tissues does not behave like pure water. Following work on silica gels, Zimmerman and Brittin (1957) proposed that water molecules in gel exist in at least two different physical environments. Based on this proposal, Bratton et al. (1965) conducted pulsed NMR experiments to measure proton relaxation rates of water (see section 7a.) in biological samples and reached a similar conclusion to that of Zimmerman and Brittin. Since then many studies have been carried out using proton NMR to define precisely the physical characteristics of water in biological systems (for reviews see Cooke and Kuntz, 1974; Hazlewood, 1979; Lynch, 1983; Bottomley et al., 1984a). This goal has proved elusive, however, because of the complex dynamic behavior of water molecules associated with biological macromolecules (Bryant and Halle, 1982). It is clear at present that macromolecules produce some ordering of water molecules in their vicinity. The proportion of these affected molecules to the total water content of the tissue, and the precise mechanism of this behavior, are still a matter for debate.

In the 1970s, groups in England (Hinshaw, 1974; Hutchinson et al., 1974; Mansfield and Maudsley, 1977) and in the United States (Lauterbur, 1973) were involved in the development of NMR imaging. Lauterbur is credited with publishing the first NMR image, which consisted of a pair of glass tubes filled with water. Considerable interest in NMR scanning for medical purposes was sparked by the suggestion by Damadian (1971) that proton NMR could differentiate

between normal and neoplastic tissues based on differences in relaxation rates. Damadian and his collaborators (1976) were later involved in the development of one of the first NMR scanners in the United States. At the same time, groups in England were publishing NMR images of human parts such as the hand (Mansfield and Maudsley, 1977; Andrew et al., 1977). The first description of cerebral abnormalities detected by NMR imaging and confirmed by pathological assessment came from a group at Nottingham (Hawkes et al., 1980). Since then, the brain has been the main organ of clinical interest for proton NMR scanning. This technique is still rapidly changing with the introduction of multiple-slice imaging (Crooks et al., 1982), progressive improvements in spatial and contrast resolution, faster scan times, use of spectroscopic imaging (Bottomley et al., 1984b), and the clinical use of paramagnetic contrast agents (Carr et al., 1984). NMR imaging now plays an important role in many neuroradiology departments (Andrew, 1984).

The introduction of NMR into clinical practice has turned attention towards the morphological characteristics of the body. Images obtained with proton NMR also permit the measurement of relaxation rates for diagnostic purposes as these have been shown to be highly sensitive to pathological alterations in tissue. It was soon recognized from in-vitro experiments using NMR that the altered rates of relaxation associated with neoplastic changes in tissue found by Damadian could also occur in a variety of other pathologic processes (Bakay et al., 1975; Go and Edzes, 1975; Beall et al., 1976). Similarly, researchers employing NMR imaging have noted the

high sensitivity of this technique for detecting changes in tissue.

Data from relaxation rates are relatively unspecific for diagnosing

brain disease; however, diagnosis is aided by other factors including

morphologic details revealed by the image and clinical manifestations

in the patient (Brady et al., 1983; Smith et al., 1985).

7a. Proton NMR relaxation

Many comprehensive reviews deal with the basic principles of

NMR and the experimental results obtained with pulsed NMR applied to

biological samples (Abragam, 1983; Farrar and Becker, 1971; Fullerton

et al., 1982; Mathur-De Vre, 1979; Foster, 1984; Hazlewood, 1979).

This section briefly describes principles of NMR as they relate to

mechanisms of proton relaxation in tissues. The principles of NMR

imaging are described in detail by Mansfield and Morris (1982).

A magnetic dipole in an individual nucleus results from its

finite spin angular momentum. When this magnetic moment interacts

with a static magnetic field, the torque it experiences causes it to

precess about the direction of this static field. The precession

frequency ω_o, known as the Larmor frequency, is proportional to the

strength H_o of the magnetic field, where the proportionality constant

is the magnetogyric ratio of the nucleus itself, as shown in the

following equation:

$$\omega_o = \gamma H_o \qquad \qquad (2)$$

The magnetogyric ratio is a constant specific for each elemental

nucleus. In the case of protons which have a nuclear spin quantum

number (I) of 1/2, two energy levels characterize the interaction

between the static magnetic field and a population of nuclei. One corresponds to protons aligned along the field's lines of force, the other to protons aligned in the opposite direction. The energy difference between these levels is ΔE, which is also proportional to the strength of the static field and the magnetogyric ratio. In thermal equilibrium, a larger proportion of nuclei occupy the lower energy level and result in a greater number of protons whose magnetic moments are pointing along the direction of the static magnetic field. The excess number of protons occupying the lower energy level is predicted by a Boltzmann population distribution, which states that the probability of occupying an energy level decreases exponentially with increasing energy.

The characteristics of NMR can be explained in detail only by a quantum mechanical model. For descriptive purposes, however, the classic mechanical model is a more appropriate one and gives results that are equivalent to the former model. Therefore, the basic characteristics of NMR described in this section use the classic mechanical model.

The sum of the magnetic moments of these nuclei gives rise to a net magnetization vector pointing parallel to the applied magnetic field H_o (M_z). This is due to the excess nuclei in the lower energy level in conditions of thermal equilibrium. By convention this direction defines the z axis of a laboratory frame of coordinates. To produce an NMR signal the magnetization vector is tilted into the x-y plane by applying an electromagnetic field H_1 at an angular frequency ω_o. This rotating magnetic field causes the proton

magnetization to precess away from the z axis. To describe the

motion of the magnetization vector, a rotating frame of reference is

employed. This frame rotates about H_o at the Larmor frequency and in

the same direction as that at which the magnetization vector

precesses. By analogy with the laboratory frame, which has co-

ordinates x, y, and z, the co-ordinates of the rotating frame are x',

y', and z'. The axes z and z' are the same for the two frames of

reference, whereas x' and y' rotate about the z axis. Therefore, the

magnetization vector tilted into the x'-y' plane will appear

stationary.

From the point of view of quantum mechanics, when

radiofrequency energy that matches the Larmor frequency ω_o is applied

the protons absorb this energy. This produces a transition of

protons from the parallel (low energy level) to the antiparallel

(high energy level) state, which is equivalent to the rotation of the

magnetization vector into the x'-y' plane. The term 'resonance' in

NMR originates from the transition of protons between energy levels.

Tilting of the magnetization vector progresses for as long as

the rotating magnetic field H_1, is applied to the proton population.

In the rotating frame, the field H_1, also called radiofrequency (RF)

pulse, is conventionally applied on the x' axis. This causes the

magnetization vector to rotate away from the z' axis into the y'

axis. The strength and duration of the RF pulse can be adjusted to

rotate the magnetization vector to any desired angle, the commonest

used for studies of proton NMR in tissues being those that induce

rotation of the vector by 90° or 180°.

When the RF pulse is interrupted, components of the magnetization will be left precessing in the x-y plane due to the torque that protons experience from the static field H_o. The precession in the x-y plane generates an electromotive force (EMF) in a specially tuned receiver coil. The amplitude of the signal is proportional to the magnitude of the magnetization vector in this plane (M_{xy}) and the amount of protons in the sample. Because the protons tend to return to thermal equilibrium by a process called relaxation (see below), the detected signal decays with time. This time-dependent signal receives the name of free induction decay (FID). This return to equilibrium involves a combination of two processes: loss of energy by dissipation into the surrounding environment (longitudinal relaxation), which describes the realignment of the magnetization vector along the z axis. Secondly, interactions between protons without exchange of energy leads to loss of the magnetization on the x-y plane (transverse relaxation).

The rates describing the relaxation processes are designated R_1 for the longitudinal relaxation, R_2 for the transverse relaxation, and $R_{1\rho}$ for the longitudinal relaxation in the rotating frame. The commonly used values, however, are the reciprocal of the rates T_1, T_2 and $T_{1\rho}$. In this study the rates are going to be used because of their direct relationship with the efficiency of relaxation.

7a.1. Longitudinal relaxation

The mechanisms responsible for relaxation occur at the molecular level. For longitudinal relaxation to occur, the excited

protons must release the absorbed energy to their surroundings, which is accomplished by electromagnetic fields. These fields are provided by the surrounding nuclear environment or lattice. In the case of protons of water, the lattice fields are produced by neighboring protons, especially that of the same water molecule. The lattice must fluctuate to promote transfer of energy from the excited protons to the surrounding environment and the fluctuations are provided by the thermal (Brownian) motion of the molecules. When the rate of fluctuations matches the Larmor frecuency, the most efficient relaxation is achieved. The return of magnetization to thermal equilibrium is usually described by an exponential recovery process. In other words, the magnetic interaction involving nuclei is modulated by the thermal motion of the environment. This magnetic interaction, which causes each nucleus to experience a local magnetic field, when modulated gives rise to a time-varying magnetic field at each nucleus. The amplitude of these magnetic interactions can be transformed to its equivalent frequency domain representation by employing a mathematical expression known as Fourier transform, which enables a quantity that varies with time to be analyzed in terms of its frequency components. Plotting the resultant spectral densities $J(\omega)$ against the frequency components of samples containing protons that experience variable tumbling rates (Fig. 1) gives an idea of the efficiency of relaxation to be expected from a sample at particular resonant frequencies. Longitudinal relaxation is more efficient when the molecular fluctuations occur at $J(\omega_o)$.

7a.2. Transverse relaxation

The RF pulse induces coherence in the precession of nuclei and is responsible for the component of transverse magnetization detected by the receiver coil. The transverse magnetization decay is the characteristic of an exponential decay process that occurs due to loss of phase coherence within the transverse magnetization of a population of protons. The nuclear magnetic moments get out of phase because they posess slightly different precessional frequencies, which are the result of (1) intrinsic fields within the system caused by the magnetic fields of neighboring nuclei, and (2) imperfections of the static magnetic field that intensifies the dephasing of protons. R_2 describes the loss of transverse magnetization and is caused by the intrinsic fields, whereas R_2^* describes the decay of transverse magnetization caused by intrinsic fields plus that induced by lack of homogeneity in the magnetic field. Therefore, $R_2^* > R_2$.

The inherent fields are the result of nuclei experiencing the resonant frequency of its neighbor. For example, the protons of a water molecule in ice have a very slow thermal motion and experience different resonant frequencies because of their difference in orientation relative to each other. Similarly, their water molecules experience different resonant frequencies because their different orientation in space. The result is that protons in ice have a very broad range of resonant frequencies that lead to a fast dephasing of the transverse magnetization (i.e., an efficient transverse relaxation or a high value of R_2). On the other hand, water molecules at room temperature have a fast rate of tumbling, which

cause the relative orientations of the various nuclei to fluctuate randomly. This fast motion tends to average the interactions between nuclei resulting in a much smaller range of resonant frequencies and a slow dephasing of protons.

Lack of homogeneity in H_o contributes to the range of resonant frequencies experienced by the nuclei. The greater the non-uniformity of the magnetic field, the greater spread of frequencies and thus a more efficient transverse relaxation.

R_2 is affected not only by intrinsic fields caused by protons tumbling at very low rates (static component of the spectral density function, J_o), but is also affected by the same mechanisms that cause longitudinal relaxation. The latter contribute to R_2 in a much less important manner, however, and thus the efficiency of transverse relaxation decay is greater with larger molecules because the intrinsic fields generated at zero reorientational frequency are larger than those observed in small molecules (Fig. 1).

Figure 1. Plot of the spectral densities (i.e. amplitude of the magnetic interactions) against thermal motion of molecules (τ_c) and their effect on the efficiency of relaxation. In the case of the longitudinal relaxation, the most efficient relaxation is achieved at motional frequencies near the Larmor frequency ω_0 and is given by medium-sized molecules. Very small molecules have a broad distribution of motional frequencies and thus a low amplitude of the magnetic interaction that results in inefficient relaxation. A similar situation is observed with very large molecules that have a limited distribution of motional frequencies. For the transverse relaxation, components of motion at the Larmor frequiency contribute to the dephasing of the magnetization; however, the static components of the spectral density function J(o), have a strong contribution to this type of relaxation, making it very sensitive to slow molecular motion characteristic of very large molecules (or of diffusion processes). The mechanisms facilitating longitudinal relaxation in the rotating frame are similar to those inducing longitudinal relaxation with the added component of slow molecular motion that tunes in to the Larmor frequency of the applied radiofrequency field J(ω_1). The RF field can be varied within a limited range of strengths (ω_1), which can tune in to a distribution of τ_c values providing information on a limited range of molecular motions. The K in the equations is an interaction constant that takes into account the internuclear distance.

Spectral Density $J(\omega)$

Molecular Motion (τ_c)

$J(0)$ $J(\omega_1)$ $J(\omega_0)$ $2J(\omega_0)$

large molecules

medium-sized molecules

small molecules
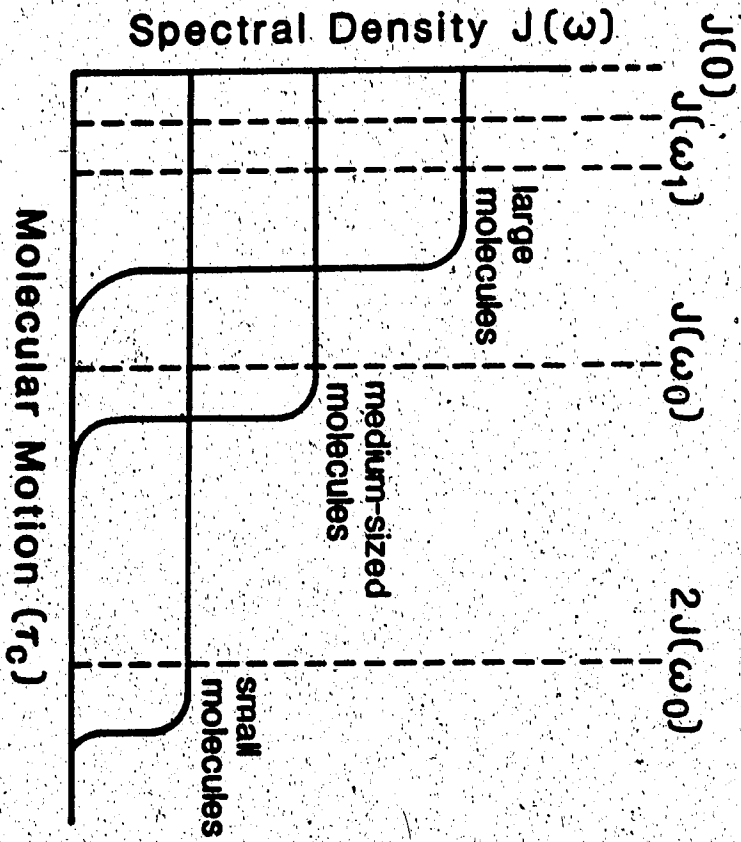
$$R_1 = K_1 [J(\omega_0) + 2J(\omega_0)]$$

$$R_2 = K_2 [J(0) + J(\omega_0) + 2J(\omega_0)]$$

$$R_{1\rho} = K_3 [J(\omega_1) + J(\omega_0) + 2J(\omega_0)]$$

7a.3. <u>Longitudinal relaxation in the rotating frame</u>

The longitudinal relaxation in the rotating frame is also an exponential process corresponding to the decay of the magnetization when it is aligned along an RF field H_1, rotating in the x-y plane. This decay corresponds to the return of proton magnetization to the z direction and is facilitated by fluctuating magnetic fields that occur at the resonant frequency ω_1. Because the Larmor frequency of protons in this weak field is very low, the efficiency of relaxation of $R_{1\rho}$ is facilitated by slow molecular motion characteristic of large molecules in addition to those occurring at $J(\omega_o)$.

Another factor that contributes to proton relaxation is that occurring when two nuclei undergo simultaneous transitions between energy states. The transition is in the same direction if there is a component of molecular motion at a frequency equal to the sum of the Larmor frequencies of the two nuclei and is represented by $2J(\omega_o)$ (Fig. 1). This factor contributes equally to longitudinal, transverse, and longitudinal in the rotating frame relaxations.

7a.4. <u>Measurement of R_2</u>

The measurement of transverse relaxation is central to the present work and thus is going to be described in some detail. To determine the decay of transverse magnetization it is necessary to eliminate the contribution to the decay caused by lack of homogeneity in the static magnetic field. This is achieved by generating an echo or a series of them after a 90° RF pulse is applied to the sample under study. The echo is generated by applying a 180° RF pulse after

a period of time $T_E/2$ in which T_E is the time between 180° pulses.
The observed effect is that after the 90° pulse the magnetization
dephases with a decay rate R_2^* due to imperfections in the
homogeneity of the static magnetic field. The loss of phase
coherence results from some nuclei precessing faster than others in
the x-y plane. The 180° pulse inverts the various components of the
magnetization; because each component precesses at the same frequency
after the 180° pulse, all the components of magnetization will tend
to reach coherence at the -y' axis of the rotating frame of
reference. This can be visualized in the laboratory frame as protons
that precess faster are placed 'behind' those precessing more slowly
by the 180° pulse. Therefore, the former protons 'catch up' with the
slower-precessing protons and give rise to an echo at a time $T_E/2$
after the 180° pulse. The signal induced by the generation of an
echo is of opposite phase as that of the signal observed after the 90°
pulse and its amplitude is given by the intrinsic transverse
relaxation, provided that the effects of proton diffusion are
negligible during this time (see Chapter II, Study B, Discussion for
an explanation of the diffusion effects in solid tissues such as
muscle and brain). Therefore, the amplitude of the echo is
diminished over that induced by the 90° pulse by a factor
$[\exp(-T_E \cdot R_2)]$.

To monitor the decay of the transverse magnetization, a series
of 180° RF pulses are applied at fixed intervals following a 90°
pulse. The resultant amplitude of each echo gives the decay of
magnetization as a function of time. This method, however, has the

inconvenience that any inaccuracies of the 180° pulse are summed
every time a 180° pulse is applied in the sequence. To correct for
this, Meiboom and Gill (1958) proposed the application of 180° pulses
at 90° out of phase relative to the 90° pulse. The effect is that
errors in the 180° pulse cancel every other echo and thus the decay
of the magnetization can be accurately measured employing the even
echoes only. This pulse sequence is called Carr--Purcell--Meiboom--
Gill (CPMG) sequence and its analog for imaging is the multiple-spin-
echo (MSE) sequence.

7a.5. Relaxation rates in heterogeneous systems

Theoretical explanations of proton relaxation processes take
into account the structure and molecular dynamics of the spin
population. They are adequate for simple systems, but their
application to heterogeneous systems such as biological tissues is
limited by the large number of factors that have to be considered
simultaneously. Molecular dynamics or Brownian motion are assumed to
be random processes that can be described in terms of a correlation
time (τ_c), which is an average of the time a molecule spends between
collisions.

Molecular motion is most effective in inducing longitudinal
relaxation when the reciprocal of τ_c (i.e., the average frequency of
collisions) is close to the Larmor frequency. Pure water, for
example, has a very fast Brownian motion relative to the Larmor
frequency, which is reflected by the relatively inefficient
longitudinal relaxation. The water in tissues, however, has a slower

molecular motion which results in more efficient longitudinal relaxation. Most authors have used models in which the cell water comprises at least two populations of water molecules existing in environments that have different dynamic and physical characteristics. In the first place, water associated with macromolecules in the tissues is so ordered that its molecular tumbling is much slower than that of water molecules in the second environment that resemble pure water. This longer τ_c for the associated water is responsible for a more efficient relaxation process. The rest of the water, which is thought to be similar to pure water in its behavior does not promote such efficient relaxation. A further assumption that is usually made is that a fast exchange of water molecules occurs between these two environments, averaging the relaxation rates of both populations, and thus giving a single observed R_1 value. This two-environment fast-exchange (TEFE) model is represented in the following form:

$$R_{1\ obs} = (R_{1a} \cdot p_a) + (R_{1b} \cdot p_b) ; \qquad p_a + p_b = 1 \qquad (3\ a,b)$$

where p is the relative population of water molecules in each environment, and a and b are the associated and free populations of water respectively.

Equation (3a) can be rearranged into:

$$R_{1\ obs} = p_a (R_{1a} - R_{1b}) + R_{1b} \qquad\qquad (4)$$

Because R_{1b}, the relaxation rate of the free water moleucles, is constant under conditions of constant temperature (Hallenga and Koenig, 1976), the variables in the model are the proportion of water molecules in the associated environment and their relaxation rate,

R_{1a}. This means that either an alteration in the relative amounts of water in each environment and/or in the nature of the associated water affecting R_{1a} will change the observed R_1.

NMR determinations in diseased tissue have generally revealed a smaller value of R_1 than in normal tissues (Damadian, 1971; Hollis et al., 1973; Kirikuta and Simplaceanu, 1975; Bakay et al., 1975; Go and Edzes, 1975). Damadian (1971) initially suggested that an alteration in the ordering of water in cancerous tissues was responsible for the smaller R_1, while later investigators suggested that in this case, the effect was produced both by the altered properties of the associated water, and an increase in the relative proportion of the free water molecules (Fung, 1974; Peemoeller et al., 1979). Changes in R_1 are therefore not specifically indicative of cancer, but of any process characterized by alterations in either water content of, or macromolecular conformation within, tissues.

The TEFE model may also describe the transverse relaxation of tissues. The macromolecules of tissues restrict the degree of mobility of neighboring water molecules, which results in a greater time-average magnetic field, which in turn causes a fast dephasing of water protons at these sites. In the free environment, however, the fast tumbling of water molecules averages out the local magnetic fields giving rise to a slower dephasing of the magnetization and thus a smaller value of R_2. The exchange between these two environments should be fast relative to the rates of dephasing in order to observe a single averaged relaxation decay.

A slower molecular motion with the characteristic of a diffusion process between compartments in tissues is another factor that contributes to the nature of transverse relaxation decay. If the diffusion or exchange between compartments is slow enough relative to the rates of dephasing, then the transverse magnetization decay rate will show more than one exponential component. Such slow diffusion or exchange processes have been well documented by researchers studying erythrocyte suspensions (Conlon and Outhred, 1972; Andrasko, 1976). Their findings -- an exchange time of 8 ms at 37°C -- suggest that there is a relatively slow exchange of water molecules between the intracellular and the extracellular spaces of the erythrocytes. Measurements of R_2 in muscle have also shown that transverse relaxation in this tissue shows more than one rate of decay (Hazelwood et al., 1974; Foster et al 1976; Pemoeller et al., 1980). This multicomponent relaxation behavior is also thought to arise from anatomical compartments within tissues such as the intracellular and extracellular spaces (Hazelwood et al., 1974; Diegel and Pintar, 1975; Foster et al., 1976). It is assumed, however, that fast exchange between two populations of water molecules still occurs within each compartment (Diegel and Pintar, 1975).

$R_{1\rho}$ is another parameter that may provide useful information about the dynamic properties of water in tissues. The mechanisms that facilitate longitudinal relaxation in the rotating frame are similar to those responsible for longitudinal relaxation, but are strongly affected by slow molecular motion that tunes into the

frequency $\omega_1 = H_1$ (Diegel and Pintar, 1975). Therefore, by varying the strength of the radiofrequency magnetic field H_1, it is possible to obtain information on various ranges of slow molecular motion.

In summary, it can be said that longitudinal relaxation is mainly affected by the nature of the interactions between water and macromolecules. If the structure of the macromolecules in tissues stays approximately constant, then R_1 will be a sensitive index of water content in such tissues. On the other hand, transverse relaxation and longitudinal relaxation in the rotating frame are affected not only by the dynamic relationship between water and macromolecules, but also by any slower diffusive processes. The latter two, therefore, are complex parameters that provide information on the water content of the tissues, are very sensitive to the macromolecular conformation within such tissues, and are affected by anatomical barriers, such as membranes, which restrict diffusion of water.

7b. Proton NMR in brain edema

From the preceding discussion it is clear that the measurement of relaxation rates in tissues should provide information on the distribution and physiologic properties of water in tissues in normal and pathologic states. Indeed, NMR imaging (Asato et al., 1983; Brant-Zawadzki, 1984; Shirakuni et al., 1985) and in-vitro NMR studies (Bakay et al., 1975; Go and Edzes, 1975; Naruse et al., 1982) in animals with experimental brain edema have revealed the high sensitivity of these techniques to alterations in water content of

the brain following different types of insult. The extent of the edema as shown by the NMR images corresponds with that indicated by macroscopic inspection. Changes in R_1 and R_2 were found to relate closely to changes in water content of the brain. Changes occurring in cryogenic-induced lesions over a period of time were followed and found to resemble closely the development of edema in a similar model evaluated by Klatzo et al. (1980) using water-content determinations and histopathologic assessment. The previous studies reported single exponential decay rates for normal brain tissues; however, for edematous white matter the transverse relaxation was usually biexponential. The change from monoexponential to biexponential decay of the transverse magnetization was found to occur at 4 hr after inducing a cold lesion, or 3 days after starting oral administration of triethyltin (Naruse et al., 1982). The presence of two exponential decays suggests that the pathologic process is associated with decreased diffusion of water in tissue compartments.

A question that remains to be answered is whether NMR can differentiate between cytotoxic and vasogenic edema. Because the latter is associated with a net increase in serum proteins within the cerebral parenchyma, it is expected that relaxation rates would differ according to whether brain edema is vasogenic or cytotoxic. In addition, because these two forms of edema differ with respect to which compartment the edema fluid collects in, different rates of relaxation are to be expected. Moreover, due to variable distribution of the edema fluid, i.e. white or grey matter or both depending on the type of edema, relaxation rates are expected to

differ according to the anatomical location of the process.

Bartkowski et al. (1985) have observed different rates of relaxation

in brain samples from animals with various types of edema, even

though the water content was similar in such samples. Therefore the

possibiltiy exists that NMR may be capable of differentiating between

cytotoxic and vasogenic edema. This has important clinical

implications because the response to treatment of each condition is

usually different (Hossmann, 1982; Long, 1985). Thus the clinical

application of NMR for the objective assessment of various types of

cerebral edema and their secondary effects upon the brain should lead

to the development of better forms of treatment.

The Present Studies

Experimental work consisted of studies A and B

Study A: Evaluation of the proton NMR relaxation characteristics in
a model of brain edema fluid.

Study B: Experimental cerebral edema in cats: comparison of proton
relaxation rates in vivo and in vitro, and content of
water, total and soluble protein, and albumin in vitro.

I. Study A

1. Objectives:

i.   Examine the relative sensitivity of the different relaxation
rates to chemical composition of edema fluid.

ii.   Ascertain whether the use of the two-environment fast exchange
model of solvent relaxation is a good approximation for
vasogenic edema fluid.

iii. Produce a quantitative database of relaxation rates from which
criteria for distinguishing between cytotoxic and vasogenic
edema might be established.

61

parameters can be selected to optimize contrast in the resultant images.

2. Materials and Methods

2a. Rationale

The extracellular fluid of the brain is an ultrafiltrate of plasma. Its protein concentration is 0.2--0.4 g/liter, and it plays a substantial role in the production of CSF (Pollay and Curl, 1967). The anatomical continuity between extracellular spaces and cerebral ventricles suggests that the chemical composition of the interstitial fluid is similar to that of CSF (Milhorat, 1975).

Vasogenic brain edema is characterized by an accumulation of water, ions, and serum proteins in the interstitial space (Klatzo, 1967). In attempting to distinguish between vasogenic and cytotoxic edema by proton NMR, it is necessary to study relaxation rates in a model of edema fluid. Human CSF provides a simplified model of extracellular edema fluid; we varied its chemical composition to simulate changes observed in vasogenic edema fluid. To vary concentrations of serum proteins, characteristic components of vasogenic edema fluid, we used solutions of human serum to establish the magnitude of the changes to be expected in vivo. We also used individual proteins and their mixtures, to determine the effect of mixing various proteins found in human serum.

strength were also investigated. Previous studies have clearly established that vasogenic edema is associated with marked increases in sodium content of the brain (Hossmann et al., 1983), and there is evidence that changes in the ionic composition of edema fluid alter relaxation rates (Halle et al., 1981). Electrolytes could, for example, decrease relaxation rates by displacing protons from the population of associated water molecules. According to the two-state fast-exchange model, small changes in this fraction of water produce marked changes in the observed relaxation rate. In this study sodium content of albumin solutions was varied from 50% to 200% of normal CSF sodium concentrations.

Changes in pH in areas of peritumor edema have been reported. A decrease of about 1 unit has been observed in rats with transplanted brain tumors, probably due to accumulation of lactate (Jähde et al., 1982). Reduced hydration of proteins when the pH is lowered has been observed in studies of ^{17}O NMR relaxation of albumin solutions (Halle et al., 1981). Thus, we also studied the effect of varying pH on relaxation rates using albumin solutions.

Alterations in strength of magnetic field produce marked changes in relaxation rates (Koenig, 1985). It was not possible to vary the field strength of the magnet used in this experiment. The measurement of $R_{1\rho}$ at various spin-lock field strengths (H_1), however, provided information on the relaxation rates within a limited range of field strengths. The mechanisms of relaxation of $R_{1\rho}$ are similar to those of R_1, but they are also affected by slow molecular motions

that tune into the applied radiofrequency field, H_1. This molecular

motion is intermediate between the slow motion contributing to R_2

relaxation and the fast motion contributing to R_1. Such information

may provide further insight into the molecular motions that produce

proton relaxation in vasogenic edema fluid.

Changes in temperature affect molecular tumbling rates and thus

the rates of fluctuation in magnetic fields responsible for the

relaxation mechanisms. As the temperature of biological systems in

vivo normally lies within a limited range, the effect of temperature

was not assessed in this study.

2b. <u>Preparation of samples and biochemical measurements</u>

The model of extracellular edema fluid consisted of 24 samples

(2--3 ml) of human CSF taken from patients undergoing lumbar

myelography. The clinical picture of these patients was consistent

with disorders that infrequently cause elevations in the protein

content of the CSF (i.e., usually low-back pain syndrome). Each

sample was immediately centrifuged to remove cellular elements and

divided into aliquots for biochemical and NMR determinations. The

samples were either tested at once or stored for up to 7 weeks at

$-20°$ C. Frozen samples were thawed at room temperature before

testing.

Concentrations of CSF total protein and glucose were determined

by spectrophotometry (ACA III; Du Pont Instruments, Willington, DE),

and albumin and IgG were measured with a laser nephelometer (Behring

model; Hoechst Pharmaceuticals, Frankfurt, W. Germany). Sodium and

potassium were measured with ion-specific electrodes, and chloride

was determined with a coulometric generator (Astra 8; Beckman

Instruments, Brea, CA); pH was obtained with a Fisher Accumet meter,

model 610A. The nuclear relaxation rates were determined for each

sample.

The remainder of each CSF sample was pooled and the resulting

sample divided into three lots: one was diluted two-fold with

distilled de-ionized water, one had NaCl added to yield approximately

twice the sodium concentration of normal CSF, and the third was not

altered. All three lots were subjected to the same biochemical and

NMR measurements. Additional CSF samples from a different series of

patients were pooled for use as the solvent for some of the proteins.

The third unaltered lot (normal CSF) was used as a solvent for

various concentrations of proteins. The proteins used (Sigma, St

Louis, MO) were lyophilized, human proteins selected to span a wide

range of molecular weights and were employed in the concentration

range 0--50 g/liter, which corresponds to that expected for vasogenic

edema fluid. They were albumin (MW 69,000 daltons), IgG

(MW 150,000 daltons), fibrinogen (MW 340,000 daltons), and

alpha-macroglobulin (MW 725,000 daltons), together with lyophilized

human serum. In the pooled CSF lots with altered ionic concentration

(i.e., diluted and with NaCl added), albumin alone was used as the

solute. NMR relaxation rates were measured in solutions of albumin

using either double-distilled water or saline solution as the

solvents.

2c. NMR measurements

The NMR determination of relaxation rates of protons was carried out initially with a 30 cm bore imaging magnet, and subsequently with a 40 cm bore magnet (Bruker Instruments, Kalsrhue, W. Germany), both operating at 2.35 Tesla and a field homogeneity of at least 1 ppm over a 2 cm diameter sphere. A modified CXP Bruker spectrometer (Bruker Instruments) excited protons using hard pulses and detected nuclear signals. The inversion recovery sequence was used to determine R_1, with a repetition time (T_R) of 10 times $1/R_1$ to ensure re-establishment of thermal equilibrium. At least 10 different inversion times (T_I) were used to fit an exponential recovery curve where the amplitude of the NMR signal $[M(T_I n)]$ is related to R_1 by:

$$M(T_I n) = M_o [1 - 2 \exp (-R_1 \cdot T_I)] \qquad (5)$$

in which M_o corresponds to the magnetization at thermal equilibrium.

A Carr-Purcell-Meiboom-Gill (CPMG) sequence (Meiboom and Gill, 1958) was employed to obtain R_2. This pulse sequence monitored the amplitude of the spin-echo, $M(T_E n)$, as a function of the time interval between pulses, T_E. R_2 and $M(T_E n)$ are related by the function:

$$M(T_E n) = M_o \cdot \exp (-R_2 \cdot T_E n). \qquad (6)$$

The measurement of $R_{1\rho}$ requires a sequence that incorporates a 90° pulse followed immediately by a second pulse of amplitude H_1, with a duration T_S, and phase-shifted by 90°. $R_{1\rho}$ was obtained by

monitoring the amplitude $M(T_S n)$ of the free induction decay (FID) following the second pulse:

$$M(T_S n) = M_0 \exp (-R_{1\rho} \cdot T_S n) \qquad (7)$$

The temperature inside the radiofrequency coil enclosure, monitored with probes (Tele-thermometer, Yellow Springs Instrument Co., Yellow Springs, OH), was kept constant at $37 \pm 0.2°C$ by a flow of warm air. Samples were placed inside the coil enclosure and tested when they reached $37°C$. The probes had no apparent effect on the homogeneity of either the static or radiofrequency magnetic field across the sample. Initially, NMR measurements were performed on 1 ml samples of CSF in cylindrical vials with an external diameter of 0.9 cm; later samples in glass spheres of external diameter 0.4 cm and a capacity of about 20 μl were used.

2d. Statistical analysis

The signal intensity values from the NMR experiments were transformed to their natural logarithms and linear regression was used to calculate the slope of the lines, which correspond to the rate of relaxation. Subsequently, curvilinear regression analysis of the magnetization values obtained with the CPMG and spin-lock sequences was carried out to calculate R_2 and $R_{1\rho}$ respectively. In the latter analysis, either one or two exponential terms were used for curve fitting. The relationship between protein content of CSF and the relaxation rates was also analyzed by regression methods, with statistical comparison of regression lines. Values are expressed as means $\pm$ standard deviation.

3. Results

3a. Relaxation rates and biochemical composition of normal CSF

In the individual samples of CSF taken directly from patients, concentrations of electrolytes were within normal range and concentrations of albumin and total protein were normal or slightly elevated (Table 1). The pH was elevated in all samples, probably as a result of loss of CO_2 after extraction coupled with the poor buffering capacity of CSF. No relationship was found between the concentrations in these ranges and the relaxation rates.

3b. Sensitivity of relaxation rates to protein concentration

In the pooled CSF batch in which protein concentration was varied, (Table 1), an increase in protein concentration increased the rates of relaxation. This relationship for the relaxation rates R_1, R_2, and $R_{1\rho}$ respectively is illustrated in Figures 1 to 3. The gradients of concentration dependence (G_1, G_2, and $G_{1\rho}$) were more than 10 times greater for R_2 than for R_1, and about 1.6 times greater for R_2 than for $R_{1\rho}$, measured at 15 kHz (Table 2). A very close relationship was found between the molecular size and the sensitivity of the relaxation rates to protein concentration for macromolecules of 340,000 daltons or less. This relationship, however, did not hold for a-macroglobulin, whose molecular weight is 725,000 daltons.

3c. <u>Sensitivity of relaxation rates to ionic content</u>

Linear regression analysis used to compare albumin-concentration dependence of longitudinal and transverse relaxation of solutions containing distilled water, saline, or CSF revealed slightly more efficient transverse relaxation in the solutions without CSF (Table 3). There was no statistical difference in the dependence of the longitudinal relaxation rates G_1 on albumin concentration between the three solutions. The dependence of the transverse relaxation rates G_2 on albumin concentration, however, varied significantly ($p < 0.05$) between saline and CSF solutions. Scatter in the data for the albumin solutions containing distilled water prevented comparison with the other data.

Values of G_1 and G_2 for CSF-albumin solutions with three concentrations of electrolytes (diluted CSF, CSF with double the normal concentration of NaCl, and normal CSF) are compared in Table 4. Multiple linear regression analysis showed a statistically significant difference for G_2 between the diluted CSF and the normal CSF ($p < 0.05$), whereas differences for the other data were not significant.

3d. <u>Effect of pH on albumin--CSF solutions</u>

The dependence of R_1 and R_2 on pH in albumin-CSF (30 g/liter) is shown in Figure 4. The relaxation efficiency for R_2, but not for R_1, is maximal at around the physiologic pH, and decreases with variations from this range.

3e. <u>Sensitivity of the longitudinal relaxation in the rotating frame</u>
<u>to changes in strength of the spin-lock field (H_1)</u>

Table 5 shows the effect of varying strengths of magnetic field H_1 on the dependence of the longitudinal relaxation rate in the rotating frame ($G_{1\rho}$) on various albumin concentrations in CSF solution. At very low fields more efficient relaxation of the protons was observed. The field dependence of $R_{1\rho}$ for solutions of various proteins in CSF at a concentration of 50/g liter is shown in Figure 5. The sensitivity of $R_{1\rho}$ to field strength was proportional to the molecular size of the proteins throughout the range of resonant frequencies tested (i.e., from 5 to 40 kHz). This relationship, however, did not hold for α-macroglobulin, which induced relaxation comparable to that of fibrinogen, a molecule that is less than half its size.

Table 1. Chemical composition and proton-relaxation rates of human cerebrospinal fluid (CSF).

	n	Mean ± SD	Na 50%	Na Normal	Na 200%
		Individual CSF Samples		Pooled CSF	
Albumin (g/liter)	24	0.27±0.12	—	0.27	0.27
Total protein (g/liter)	24	0.49±0.18	—	0.43	0.44
Sodium (mmol/liter)	23	145.0±2.5	80.0	146.0	286.0
Potassium (mmol/liter)	23	2.9±0.2	1.6	2.8	3.0
Chloride (mmol/liter)	23	128.0±3.2	62.0	125.0	268.0
pH	24	9.00±0.25	9.03	9.28	8.79
R_1 (s^{-1})	23	0.26±0.01	0.26	0.26	0.26
R_2 (s^{-1})	24	0.38±0.03	0.38	0.40	0.38
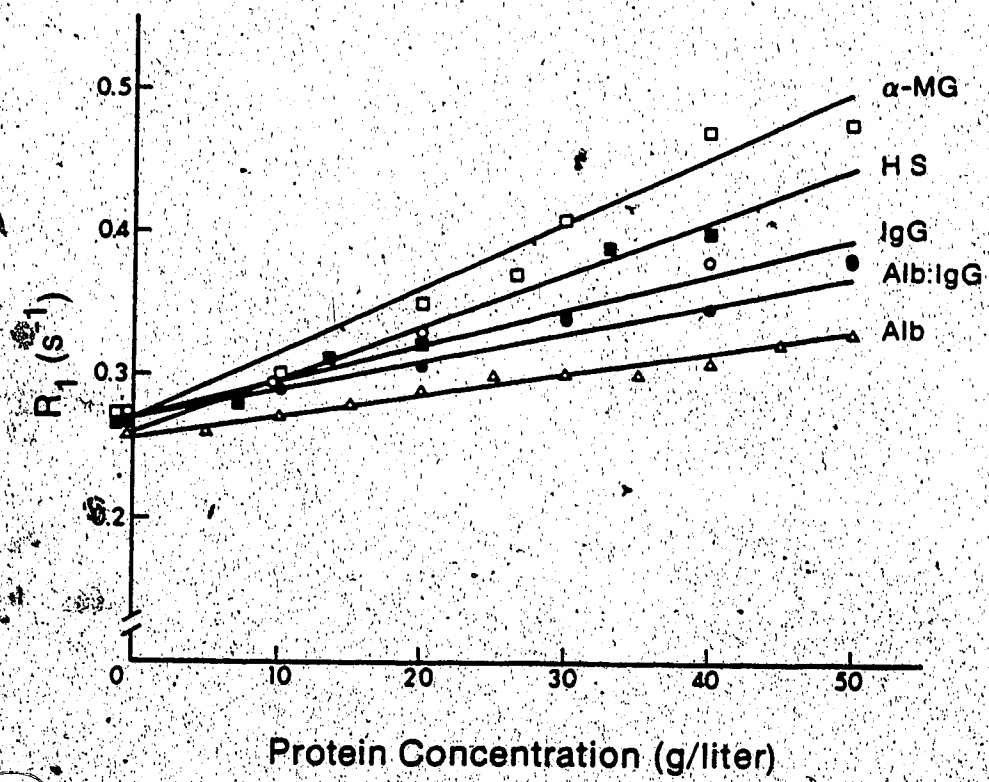
Figure 2. Effect of increasing protein concentration on the proton longitudinal relaxation rates of pooled CSF. Albumin (△), IgG (○), albumin : IgG mixture (●), human serum (■), and α – macroglobulin (□).
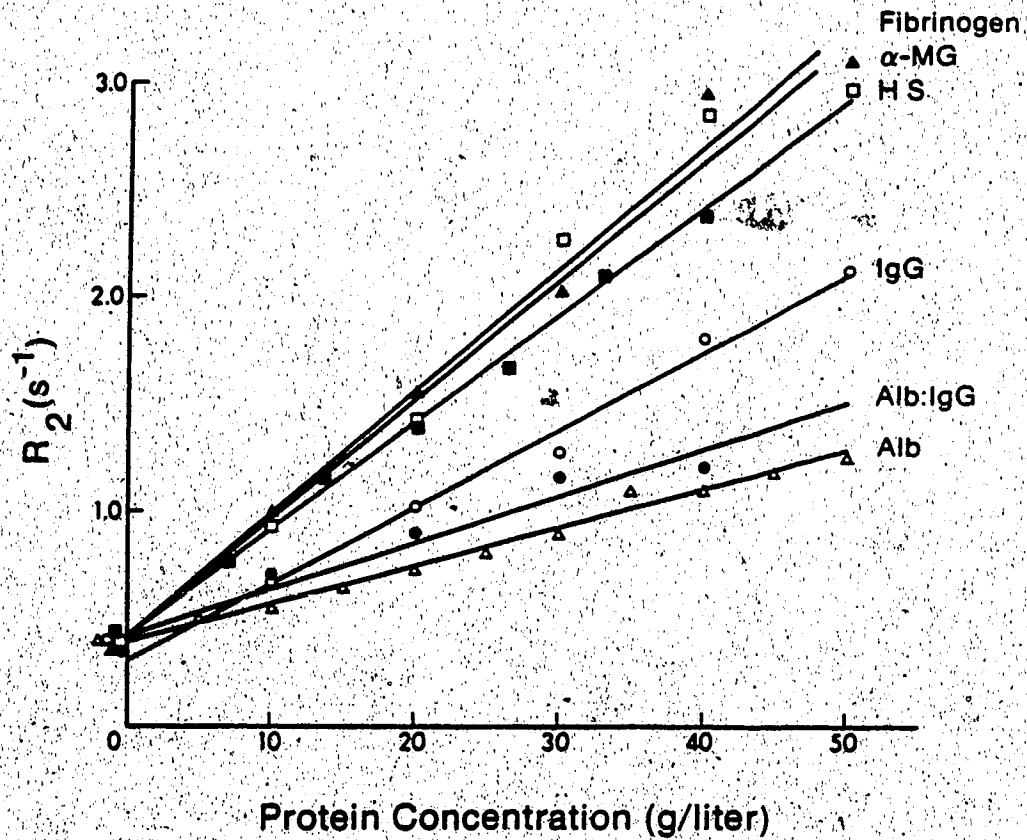
Figure 3. Effect of increasing protein concentration on the proton transverse relaxation rates of pooled CSF. Albumin (△), IgG (○), albumin : IgG mixture (●), human serum (■), fibrinogen (▲), and α-macroglobulin (□).
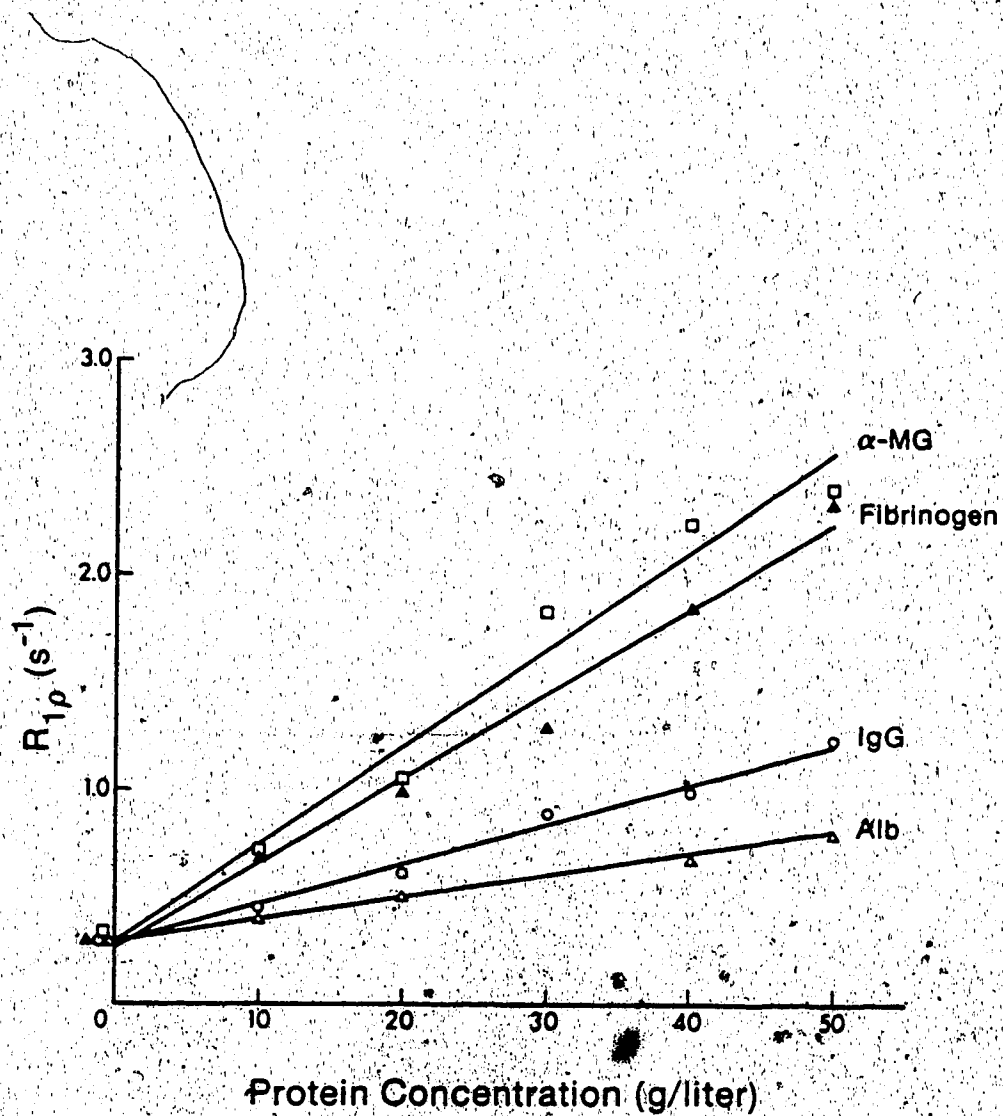
Figure 4. Effect of increasing protein concentration on the proton
$R_{1\rho}$ rates of pooled CSF. Albumin (△), IgG (◯), fibrinogen (▲),
and α-macroglobulin (□).

Table 2. Sensitivity to protein concentration in CSF of R_1, R_2, and $R_{1\rho}$ ($\omega_1 = 15$ kHz).

Protein	G_1 ($\times 10^{-3}$ s^{-1}/g/liter)	G_2 ($\times 10^{-3}$ s^{-1}/g/liter)	$G_{1\rho}$ ($\times 10^{-3}$ s^{-1}/g/liter)
Albumin	1.4 ± 0.1	17.6 ± 0.7	9.8 ± 0.3
IgG	2.4 ± 0.2	36.0 ± 1.0	18.8 ± 0.9
Alb : IgG*	2.0 ± 0.2	22.0 ± 3.0	--
Fibrinogen	--	56.8 ± 3.9	39.7 ± 2.5
α-Macroglobulin	4.5 ± 0.5	55.7 ± 4.6	45.6 ± 3.6
Human serum (a)	--	33.2 ± 3.2	20.4 ± 2.3
Human serum (b)	3.7 ± 0.3	49.0 ± 2.0	--

* The mixture of albumin and gamma globulin was a 2.8:1 ratio.

Table 3. Effect of solvent type using albumin as solute on the concentration dependence of R_1 and R_2.

Solvent Type	G_{1alb} (x10^{-3} s^{-1}/g/liter)	G_{2alb} (x10^{-3} s^{-1}/g/liter)
Distilled water	1.70±0.22	23.5±2.8
Normal saline	1.05±0.28	20.5±0.5*
CSF	1.38±0.08	17.5±0.7

* Significantly different from CSF, p<0.05

Table 4. Effect of electrolyte content of CSF using albumin as solute on the concentration dependence of R_1 and R_2.

Sodium Concentration	G_{1alb} (x10^{-3} s^{-1}/g/liter)	$G2_{alb}$ (x10^{-3} s^{-1}/g/liter)
50%	1.26±0.07	20.2±1.2*
100%	1.38±0.08	17.5±0.7
200%	1.54±0.15	18.0±1.0

*Signifcantly different from CSF with normal electrolyte content, p<0.05
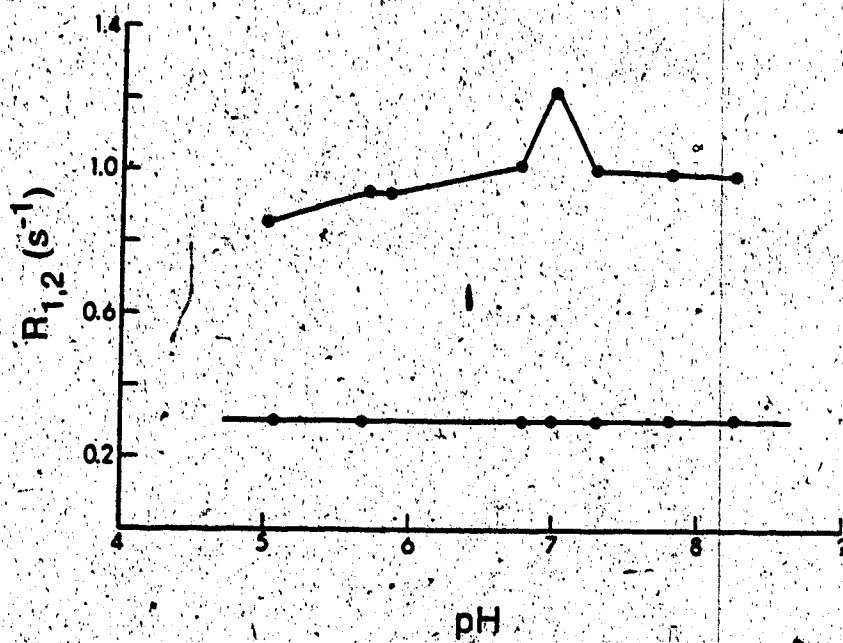
Figure 5. Effect of varying the pH of a solution of CSF containing
   albumin (30 g/l) on the longitudinal and transverse relaxation
   rates.

Table 5. Effect of the magnetic field strength (H_1) on the concentration dependence of CSF albumin solutions.

H_1 (G)	ω_1 (kHz)	$G_{1\rho\ alb}$ (x10^{-3} s^{-1}/g/liter)
1.2	5	12.0±0.7
3.5	15	9.8±0.3
5.9	25	9.7±0.4
7.1	30	8.6±0.7
8.3	35	7.1±1.1
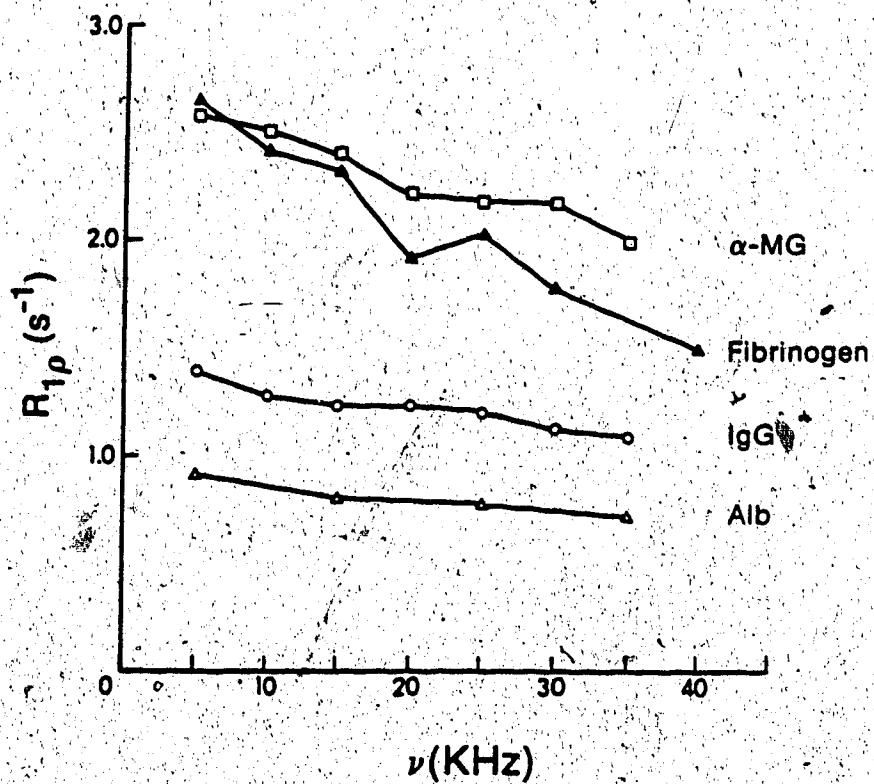
Figure 6. Effect of increasing the magnetic field strength on the
proton $R_{1\rho}$ rates of various proteins (50 mg/ml) dissolved in
pooled CSF. Albumin (△), IgG (○), fibrinogen (▲), and
α-macroglobulin (□).

4. Discussion

The observed relaxation rates were strongly affected by the concentration and type of protein dissolved in CSF. This finding is discussed in terms of a model of proton relaxtion that provides some insight into the effect of proteins on water around them. Such a model also provides information on the amount of water affected by the proteins. This parameter is used to explain the effects of protein type, ionic concentration, pH, and radiofrequency field strength on the observed relaxation rates.

4a. Two-environment fast-exchange model of proton relaxation

The development of a simplified model of proton relaxation applicable to brain edema fluid should assist in determining the physiologic role of water and proteins in this condition. According to the model of proton relaxation derived by Zimmerman and Brittin (1957) and further developed by others (Daskiewicz, et al., 1963; Clifford et al., 1968; Oakes, 1976; Fullerton et al., 1984), most water molecules behave like those in pure water. The rest are associated with the macromolecules as decribed previously (see Sections 3 and 4). These two environments have different rates of relaxation, which however become averaged due to fast exchange of water molecules between them. This two-environment fast-exchange (TEFE) model predicts that water molecules associated with the macromolecules are restricted in their motion due to the slower correlation time, τ_c of the macromolecule. The nature of this interaction is not fully understood but it is possible that hydrogen

bonding forces and other associations between water and macromolecules can result in restricted orientation and mobility of water molecules. In addition, the different chemical environments on the surface of a macromolecule, such as uncharged polar and apolar groups, and anionic and cationic residues (Halle et al., 1981), contribute to a wide range of molecular motions of the associated water protons. This is one of the main difficulties in producing an adequate model of proton relaxation in protein solutions (Bryant and Halle, 1982).

Because of this difficulty, other models have been developed. Several investigators measuring relaxation rates in protein solutions have proposed a three-environment model. Two of these environments correspond to those described by the TEFE model, and the third represents water molecules very closely associated with macromolecules (Cooke and Kuntz, 1974; Belton and Packer, 1974; Grosch and Noack, 1976; Fullerton et al., 1982). Such studies, however, were performed using very high protein concentrations. It has been shown that at the dilutions employed in our experiments, the contribution of the third environment becomes negligible (Grosch and Noack, 1976; Halle et al., 1981).

An extension of the previous models of proton relaxation of water molecules in dilute protein solutions has been developed by Koenig and coworkers by studying the magnetic field-dependence of proteins in solution. Hallenga and Koenig (1976) have shown that the motion of water molecules is affected in two general ways. First, when water exists in close proximity to macromolecules, its

correlation time decreases, while at a certain distance it is unaffected. This accords with the TEFE model and was observed with proteins ranging from 14 kdaltons to 450 kdaltons. Second, the molecular motion of all the water molecules is changed slightly by the relatively slow tumbling of macromolecules. The τ_c of macromolecules ($\approx 10^{-7}$ s) is sumperimposed on that of the water molecules and at low magnetic field strengths its contribution to R_1 increases by several orders of magnitude as slow molecular motions produce more efficient relaxation. The result is a marked field dependency of the longitudinal relaxation rate (called by Koenig relaxation dispersion). At magnetic fields greater than 0.2—0.4 T, however, the dominant relaxation is that corresponding to the TEFE model, because the Larmor frequency at these fields is too high relative to the frequency of tumbling macromolecules to induce relaxation. This model describes adequately the behavior of longitudinal relaxation. The criticisms arise mainly from the fact that four unknowns were employed in the fitting of a curve to the data points. Further work is required to prove the existence of these variables.

Assuming that this model applies to the present experiments, at the magnetic field strength used in our studies (2.35 T), the TEFE model, which assumes no contribution from the low frequency dispersion mechanism to relaxation of water in the free environment, is appropriate to describe the longitudinal relaxation. On the other hand, the high sensitivity of the transverse relaxation to slow

molecular motion (Abragam, 1983) means that R_2 is affected by macromolecular motion even at 2.35 T.

4a.1. Proof for the existence of fast exchange between environments

A single exponential recovery or decay was observed in all the measurements performed. This suggests that fast exchange occurred between the water environments as a slow exchange relative to the rates in each environment would result in a decay described by a biexponential curve. The monoexponential behavior of relaxation rates in the mixture of albumin and IgG, and in serum further suggests that a fast exchange took place in all environments. Similar conclusions have been presented by Blicharska et al. (1970), Cooke and Wien (1971), and James and Gillen (1972).

The TEFE model postulates that there are two environments of water that have different relaxation characteristics due to the different molecular motion that occurs within each environment, a and b. Thus the magnetization recovery or decay is described by:

$$M(T_I n) = p_a''[1 - 2 \exp (-T_I \cdot R_{1a}'')] + p_b'' [1 - 2 \exp (-T_I \cdot R_{1b}'')] \quad (8a)$$

$$M(T_E n) = p_a'' \exp (-T_E \cdot R_{2a}'') + p_b'' \exp (-T_E \cdot R_{2b}'') \quad (8b)$$

$$M(T_S n) = p_a'' \exp (-T_S \cdot R_{1\rho a}'') + p_b'' \exp (-T_S \cdot R_{1\rho b}'') \quad (8c)$$

where M is the amplitude of the magnetization at the various index numbers of the time periods T_I, T_E, and T_S. p is the population size of each environment and the biprime (") notation represents the observed populations and rates of relaxation, which are affected by the rate of proton exchange between environments.

An assumption that is made is that the resonant frequency for each of the environments of water is the same. Therefore, no compensation for this effect is attempted in this discussion.

A single exponential recovery or decay of the magnetization is observed when the exchange rate is fast relative to the relaxation rates of each environment. On the other hand, when the exchange rate of protons is slow relative to the rates of relaxation, a biexponential decay is observed. The exchange rates are given by $1/\tau_a$ and $1/\tau_b$ in which τ is the life time of a water molecule in a particular environment, a or b. In this case the exchange rate between environments (τ_{ex}) is given by:

$$\tau_{ex} = \frac{\tau_a \cdot \tau_b}{\tau_a + \tau_b} \tag{9}$$

To provide numerical values to τ_{ex} it is known that τ_a (the life time of a water molecule in the environment of water molecules associated with macromolecules) is about 10^{-5} s (Diegel and Pintar, 1975). Blicharska et al. (1970) have observed that in dilute protein solutions $p_b \gg p_a$, therefore the term τ_b can be considered negligible and τ_{ex} becomes approximately equal to τ_a. Under these conditions $R_{1b}'' \approx R_{1b}$ and $R_{1a}'' \approx R_{1a}$, thus to satisfy the fast exchange condition $\tau_{ex} \cdot R_{1a} \ll 1$. Allen et al. (in press) have provided values of R_{1a} in dilute protein solutions studied at 100 MHz. The highest relaxation rate was observed for the transverse magnetization of water molecules in the associated environment (i.e., about 70 s^{-1}). From this is clear that the fast exchange condition

is met for the three types of relaxation rates measured in this study.

4b. Determination of amount of water associated with proteins

Daskiewicz et al. (1963) showed that, for protein concentrations of less than 100 g/liter, the proton relaxation rates are linear functions of the concentration, c:

$$R_i = R_{ib} + cG_i \qquad i = 1,2 \qquad (10)$$

G_1 and G_2 are constants specific for the kind of protein (see section 3b) and R_{1b} and R_{2b} are the longitudinal and transverse relaxation rates respectively of pure water. A similar relationship occurs with measurements of $R_{1\rho}$. The linear plots on Figures 1 to 3 conform to equation (8) and extrapolation to zero protein concentration gives the ordinate intercept $R_i b$, which is known to be constant at different field strengths and at constant temperature. (In our studies these values were 0.26 s^{-1} for R_1 and 0.38 s^{-1} for R_2.) G_i, which represents the dependence of relaxation rates on protein concentration in CSF, can also be used as an index of the amount of water associated with macromolecules; a greater G_i corresponds to a larger amount of water in the associated environment:

$$G_i = (R_{ia} - R_{ib})h \qquad (11)$$

where h is the degree of hydration in grams of water per gram of protein.

To provide numerical values for hydration it is necessary to know the relaxation rate of water in the associated state. Fullerton et al. (1984) observed that the population of water molecules

associated with macromolecules had a relaxation time (i.e., the reciprocal of the relaxation rate R_{1a}) that was directly proportional to the strength of the magnetic field. They analyzed the relaxation times of associated water reported by a number of investigators and concluded that the longitudinal relaxation time is affected largely by the local environment of the macromolecules but not by their surface characteristics. Computing the relaxation rate of associated water at 100 MHz, we obtain a value for R_{1a} of 4.8 s^{-1}. Using the G_1 values from Table 2 the hydration of proteins was calculated for each protein (Table 6).

The significance of the hydration parameter is relative in the present studies because no attempt was made to define precisely the dynamic state of the associated water. The values are used in a semiquantitative manner to explain alterations in hydration of proteins under different circumstances and to establish a model of hydration for studies of brain edema.

Table 6. Amount of water associated to proteins (h) predicted from equations (8 and 9).

Protein	h ml/g protein
Albumin	0.3
IgG	0.5
Alb : IgG	0.4
α-Macroglobulin	1.0
Human serum (b)	0.8

Using the calculated values of hydration we observe that there
is a linear dependence between molecular size of the protein and
degree of hydration except for a–macroglobulin in which we obtained a
hydration value of 1 ml/g protein; whereas according to the TEFE
model as modified by Fullerton et al. we would expect a hydration of
1.8 ml/g protein..   It is known that at the protein concentrations
used in the present study a linear increase in hydration is observed
and at high protein concentrations this linearity is lost (Daskiewicz
et al., 1963).   At least two mechanisms account for this loss:
first, a high protein content, results in overlapping of hydration
regions of protein molecules resulting in exclusion of water
molecules from the associated environment; second, the correlation
time of water increases due to electrostatic repulsion between the
protein molecules resulting in increased ordering of water (Halle et
al., 1981).   For example, Oakes (1976) found that at high
concentrations of bovine albumin, the latter effect was dominant and
accounted for the disproportionately fast relaxation of such
solutions.   Similarly, Passen et al. (1985) suggested that
aggregation of β–lactoglobulin resulted in greater ordering of water
molecules and faster relaxation rates.   On the other hand, Cooke and
Wien (1971) suggested that protein aggregation and an associated
reduction in hydration was responsible for the decreased efficiency
of proton relaxation in solutions of muscle proteins.   Therefore,
these two mechanisms oppose each other and one may dominate,
depending on the concentration and type of protein.

With the α-macroglobulin, which shows an extreme tendency to
aggregate in aqueous solutions (Jones et al., 1972), the aggregation
process probably resulted in a decreased number of protein sites
available for hydration. If this is the case, then we ought to take
such factors into account in proton NMR studies of tissues. Proteins
in tissues are highly ordered, forming very large aggregates that
probably affect the ordering and amount of water molecules in the
associated environment. For example, changes in macromolecule
ordering in tissue culture have been reported to affect R_1 (Beall et
al., 1976). On the other hand, we would expect neither of these
mechanisms to affect appreciably the relaxation characteristics of
brain edema fluid in which proteins exist in comparatively low
concentrations.

4d. Effects of ionic content on proton relaxation

Our results showed an increased sensitivity of the transverse
relaxation to protein content when studied using solutions of low
ionic content (i.e., albumin in CSF diluted two-fold or albumin
solutions employing distilled water as a solvent). This suggests an
increased hydration of albumin molecules at ionic concentrations that
are well below normal physiologic levels. This finding contradicts
that of Cooke and Wien (1971) in which they showed that a decreased
ionic content of muscle protein solutions was associated with
decreased hydration of macromolecules. The presence of a reduced
concentration of ions may facilitate protein aggregation, which, as
shown above, may have opposing effects on the relaxation rates, the

dominant effect being dependent on the type and concentration of the protein.

4e. Effect of pH on proton relaxation

Decrease in R_2 with deviations of pH from neutral in CSF solutions of albumin suggests that there is a decreased hydration of albumin in both acidic and alkaline environments. A similar reduction in protein hydration has been reported by Tanford (1962) and Halle et al. (1981). The effect is probably due to a reduction in number of charged protein groups, or to conformational changes. An example of a conformational change is the unfolding of the albumin molecule reported at extremes of pH (Harrington et al., 1956; Decker and Foster 1967) which may result in a reduction of associated water.

The alterations in ionic content and of CSF induced in the present studies represent extremes that are not observed physiologically. Moreover, the small effect ions had on the relaxation rates may justify regarding their role as negligible. This conclusion is supported by the fact that ionic content varies little, as shown by the relatively small changes in osmolality measured in vasogenic edema fluid (Gazendam et al., 1977). The effect of pH on relaxation rates deserves further study.

4f. Sensitivity of $R_{1\rho}$ to field strength

The hydrodynamic effect of macromolecules on the relaxation of protons as shown by Hallenga and Koenig (1976) probably accounts for the relaxation dispersion determined by $R_{1\rho}$ measurements at various

field strengths (4kHz to 30 MHz). This model explains why proteins of low molecular weight show a small magnetic field dependence, whereas those of high molecular weight produce a more marked relaxation dispersion. The tumbling of small proteins is expected to produce a smaller hydrodynamic effect than that produced by larger ones because the much larger volume of the latter affects motion of a greater number of surrounding water molecules. It also explains why the relaxation is not affected to a large degree by the surface characteristics of the macromolecule and its charge as was indicated by the relaxation measurements at various ionic concentrations and pH (Hallenga and Koenig, 1976).

We can expect, therefore, that edema fluid has a small field dependence, whereas tissue has a marked field dependence due to its high content of macromolecules and their complex ordering. The slow molecular motion to which $R_{1\rho}$ is very sensitive can be expected to produce an even greater effect on R_2. This, in turn, may introduce additional factors to be taken into account in the interpretation of transverse relaxation in brain edema.

4g. <u>Implications for the study of brain edema</u>

The present experiments show that the TEFE model describes the relaxation behavior of edema fluid. Such fluid may or may not contain plasma proteins depending on the type of edema — vasogenic or cytotoxic. In vasogenic edema fluid we can expect a more efficient relaxation due to the presence of proteins, whereas in

cytotoxic edema fluid the lack of macromolecules should cause a relaxation similar to that of pure water. -.

Brain tissue comprises various types of macromolecular surfaces each with a particular degree of hydration. This is, in fact, the basis of the difference in relaxation rates among various tissues and hence of contrast in NMR images. Edema is expected to alter the hydration of brain tissues, which in turn changes the relaxation rates of affected regions. This is supported by the findings of several groups that have shown a high sensitivity of proton NMR to brain edema (Bakay et al., 1975; Go and Edzes, 1975; Naruse et al., 1982; Asato et al., 1983; Shirakuni et al., 1985; Brant-Zawadzki et al., 1984). This sensitivity is especially evident in proton NMR images that are dominated by R_2 processes such as the spin-echo sequence with long interpulse times (T_R). This is due, as shown in this study, to the much higher sensitivity (greater than 10 times) of R_2 to changes in the macromolecule--water interactions than R_1.

Some problems arise in trying to assess edema in the brain using NMR. If the edema fluid were only water, the change in tissue hydration could be readily determined, provided the hydration of normal brain was known. The protein content of vasogenic edema fluid, however, alters the macromolecular content of edematous tissue which in turn increases the relaxation rates. This counters to a certain degree the decrease in relaxation rates that results from the increase in water. Therefore, the relaxation rates are not only functions of water content in tissues but other factors such as macromolecular content. Such complex behavior cannot be readily

assessed by the measurement of a single relaxation rate. However, more than one exponential component of the transverse relaxation has been observed in areas of white matter edema (Bakay et al., 1975; Go and Edzes, 1975; Naruse et al., 1982) and a study of the separate components may be used to provide further information.

In summary, the data from the present experiment provide information that elucidates some of the differences in relaxation rates from areas of brain edema. They show: 1) that the amount and type of protein strongly affects relaxation rates, especially R_2 and $R_{1\rho}$ when it is measured at low spin-locking fields; 2) that protein aggregation such as that expected in tissues, may affect relaxation rates; 3) that changes in ionic content of edema fluid may have a negligible effect on relaxation rates; 4) the magnitude of changes in relaxation rates produced by the edema fluid under various concentrations of proteins that lie within the range expected in brain edema; 5) that the TEFE model predicts not only the behavior of single-protein solutions but also the mixtures of them that are to be expected in cerebral edema; and 6) that slow molecular motion, probably produced by macromolecular tumbling, influences the values of R_2 and $R_{1\rho}$ at the field strength used in this study. Such an effect may be more marked in tissues due to a greater restriction of the mobility of macromolecules.

Study B: Experimental cerebral edema in cats: comparison of proton

relaxation rates in vivo and in vitro, and content of

water, total and soluble protein, and albumin in vitro.

1. Objectives:

i. Provide quantitative data that might permit discrimination

between cytotoxic and vasogenic edema in vivo.

ii. Determine whether the transverse relaxation rate measured in

vivo is the same as that measured in vitro.

iii. Ascertain the ability of proton NMR imaging to provide an index

of water content in brain tissues.

iv. Determine the applicability of the two-environment fast-

exchange model of proton relaxation to normal and edematous

brain tissues.

v. Examine the relationship between changes in tissue protein and

water content of edematous tissue.

vi. Document the efficacy of NMR in showing severity and extent of

brain edema and its causative lesions.

vii. Provide quantitative data that will help optimize NMR machine

parameters for improved diagnosis and monitoring of edema.

2. Materials and Methods

2a. Rationale

The main objective of Study B was to develop a series of NMR criteria to discriminate between cytotoxic and vasogenic edema in vivo. Animal models were required whose edema closely resembled the clinical situation, and represented a 'pure' form of either type.

Various models of edema have been reported, including those that develop after trauma, cerebral compression, hypertension, cryo-injury, water intoxication, gamma and ultraviolet irradiation, brain abscess, brain tumor, intoxication with TET and lead, hydrocephalus, anoxia, and ischemia. The most-studied cause of vasogenic edema is cryo-injury (Klatzo et al., 1958). It was not chosen for this study because its pathophysiology differs from that of the clinical situation. The development of an experimental tumor model in an sanimal with a relatively large brain, in which reproducible peritumor edema develops, has been reported by Hossmann et al. (1979). Edema associated with experimental brain tumors in cats is predominantly vasogenic and closely resembles that observed in patients. Hypertensive opening of the BBB does represent a pure form of vasogenic edema (Kuroiwa et al., 1985), but as it is not a common clinical problem, we decided to use the experimental tumor model.

In the selection of an experimental model of cytotoxic edema two models were considered. One was the induction of focal cerebral ischemia in monkeys, which closely reflects the clinical situation; however, the edema that occurs in this type is very complex, with an

initial cytotoxic phase followed several hours later by a vasogenic

phase (Hossmann, 1976). Also, the cytotoxic phase is usually

confined to grey matter and therefore would prevent direct comparison

with peritumor edema, which occurs most frequently in white matter.

We considered also a model of a pure form of cytotoxic edema that

follows TET intoxication, which is not commonly observed but occurs

in white matter. The advantages of this model include simplicity of

the procedure, very high reproducibility of brain changes, rapid

course, very rare necrosis, and absence of reactive inflammation.

Hence we concluded that the model of TET intoxication more

appropriately satisfied the objectives of our study.

Water content was measured to determine the presence of edema.

Freeze-drying rather than drying at high temperatures was employed to

preserve the protein conformation in the samples. Heat drying would

have denatured the proteins and might have led to errors in water

determination due to loss of volatile lipids. The gravimetric

technique was discounted because, although more sensitive than the

freeze- or heat-drying techniques, it is subject to some degree of

error due to protein changes in vasogenic edema. In addition, the

error introduced when tissue-density units are converted to water

content units may offset its advantages. In preliminary studies we

found that freeze drying gave reproducible values of water content

using samples of 30--50 mg, providing that the container used was not

larger than 300 mg.

Protein content was determined: an increase in serum albumin

would indicate the presence of vasogenic edema. In addition, the

effect of increases in protein on the observed relaxation rates could

be evaluated. For this purpose it was necessary to wash out

intravascular proteins to minimize the background contribution of

serum proteins to the albumin measurements.

Correlation of histopathology with NMR images were expected to

indicate the value of NMR imaging as a technique for revealing the

extent and severity of edema non-invasively. The injection of vital

dyes such as Evans blue to determine the extent of the edema or the

BBB breakdown was not used because the former could be assessed by

histopathology alone, while information on the area of BBB breakdown

was considered unnecessary as long as changes in protein content were

demonstrated. Moreover, the presence of dye would have interfered

with protein determinations.

The observation that R_2 is multiexponential in some tissues,

and that its components may represent relaxation occurring

independently in the intracellular and extracellular spaces, would

have made the measurement of tissue spaces attractive. However,

because of severe errors associated with their measurement, it was

considered inappropriate for this study.

Another objective of study B was to compare the transverse

relaxation rate measured _in vivo_ and _in vitro_ using proton NMR

imaging for the former and conventional relaxation rate measurements

of tissue samples for the latter. This comparison was expected to

provide an assessment of the accuracy of the measurement of R_2 _in_

vivo. The transverse relaxation was chosen mainly for two reasons.

First, due to the higher sensitivity of R_2 to changes in

macromolecular content in edema fluid than R_1 and $R_{1\rho}$ as shown in

study A, R_2 was expected to detect the difference in relaxation rates

produced by the protein-rich fluid that accumulates in vasogenic

edema as compared to the protein-poor fluid accumulating in cytotoxic

edema. Second, the measurement of R_2 from images is probably

subjected to less errors than either that of R_1 and $R_{1\rho}$ because in a

single imaging sequence, several echoes can be generated, which

produce an equal number of images. These, in turn, are used to

calculate R_2 by obtaining the signal amplitude from specified regions

throughout the series of images. Measurement of R_1 and $R_{1\rho}$ is

limited by the number of images that can be generated because only

one image is produced per imaging sequence. Therefore, the length of

time required to obtain an adequate number of scans for calculation

of relaxation rates may result in errors of position due to movement

of the subject.

2b. Preparation of Animals

Mongrel cats of either sex weighing between 2.0 and 4.8 kg were

allocated to three groups. Group I consisted of five cats that

served as a control; Group II consisted to eight cats subjected to

xenotransplantation of 9L glioma cells in the white matter for the

production of tumors and peritumor edema; and Group III of eight cats

injected intraperitoneally with a single dose of triethyltin bromide

(TET) for the production of cytotoxic edema.

The anesthetic procedure in all cases was as follows: after

fasting overnight the cats were anesthetized with intramuscular

injection of atropine sulphate, 0.04 mg/kg of body weight (BW), (Glaxo Laboratories, Mississauga, Canada), xylazine, 1.5 mg/kg BW (Rompun, Cutter Laboratories, Mississauga, Canada), and ketamine, 20 mg/kg BW (Rogarsetic, Rogar/S.T.B., London, Canada). The anesthesia was prolonged as necessary by repeated injection of ketamine every 45 min at one half the original dose for up to about 2.5 hrs.

2b.1. Xenotransplantation of 9L glioma cells

The 9L glioma cells obtained from the Brain Tumor Research Center (San Francisco, CA), were kept frozen at -70°C in a suspension of 10% DMSO. They were prepared for injection as follows. Two days before injection they were thawed at room temperature and placed in minimum essential medium (MEM) containing 5% fetal bovine serum (FBS), 500 μg streptomycin/ml, 500 i.u. crystalline penicillin/ml, and 20 mmol L-glutamine. The cells were incubated at 37°C for about 48 hr until they were in logarithmic phase of growth and the resultant monolayer was incubated in 2.5 ml of 0.25% trypsin containing 200 μg/ml EDTA, for 10 min at 37° C, followed by a second incubation in fresh solution. The suspension was placed in 15 ml of MEM with 5% FBS and the cells were counted using a hemocytometer chamber. To obtain the desired cell concentration, the cells were centrifuged at 1000 RPM and 4°C for 5 min and the resultant pellet was suspended in an appropriate volume of medium. The cells were utilized within 6 hr after preparation during which time they were kept at 4°C.

The surgical procedure in Group II cats was as follows. The dorsal aspect of the head was shaved and prepared for surgery by scrubbing with betadine. The animal was placed in the prone position and its head secured using a specially designed holder. A midline skin incision was made, running from a point at 1.0 cm caudal to the supraorbital ridges and extending caudally for 4.0 cm. The right temporalis muscle was partly reflected from its parietal insertion and the coronal and sagittal sutures were identified. An electric drill was employed to make a burr hole of 2 mm in diameter at 5 mm lateral to the sagittal suture and at 5 mm caudal to the coronal suture. The dura was opened and the surface of the brain was inspected to select a point of injection free from large cortical blood vessels. A graduated micromanipulator attached to the frame holding the cat's head was employed to permit precise determination of the depth of the injection site. A Hamilton microsyringe (of 50 μl capacity) was secured to the micromanipulator and the 9L glioma cells (10^6 suspended in 50 μl of the medium) were injected gradually over $\approx$1 min at 6 mm below the surface of the suprasylvian gyrus. To minimize reflux of the cell suspension and allow spreading of the cells from the site of injection, the needle was left in place for $\approx$3 min. Subsequently the syringe was withdrawn, the burr hole covered with bone wax, and the skin incision closed.

2b.2. Injection of TET (triethyltin)

The cats in group III were injected intraperitoneally with a saline solution containing 30 mg/ml of TET bromide (Tiokol, Danver,

MA) and buffered to a pH of 7.5 with sodium bicarbonate. The dose was 2.5 mg/kg BW and the animals were observed closely for a period of 30 min after the injection, and at intervals for the next 12 hr.

2c. NMR imaging

Proton NMR imaging was performed in all cats after they had been anesthetized but before any other procedure was done to them. Such control images were used for comparisons between groups of animals, and for comparison of calculated R_2 values in the unaffected hemisphere of group II cats before and after a tumor had grown. Group II animals were scanned at approximately 2 weeks post-implantation. Group III cats were scanned at 48--72 hr post-injection of TET.

The same anesthetic regimen described previously was employed to keep the animals immobile during imaging. Heart and respiration rates were monitored by a plastic stethoscope placed on the left side of the chest. Rectal temperature was monitored with probes and the animal was kept warm within the magnet by a flow of air passing through an electrical resistance.

A specially designed plastic cradle was used for installing the cat in the supine position and was secured by velcro straps. The orbitomeatal line was used as external reference for aligning the head in the proper position to obtain transverse images of the brain. The reference angle relative to the long axis of the body was 100° -- 105° for all animals, except the younger ones for which angle

was 95° -- 100° (Fig. 6). At least two series of images were taken at different levels.

A 40-cm bore magnet (Bruker Spectrospin, Karlsrhue, W. Germany) operating at 2.35 T was employed for all NMR studies, including measurements of relaxation rates from images (in vivo) and from excised tissues (in vitro). The same spectrometer used for the CSF experiments (see study A, section 4b) was used to carry out both sets of measurements. It was connected to a VAX 11/750 computer for transferring the images and their subsequent storage on magnetic tapes.
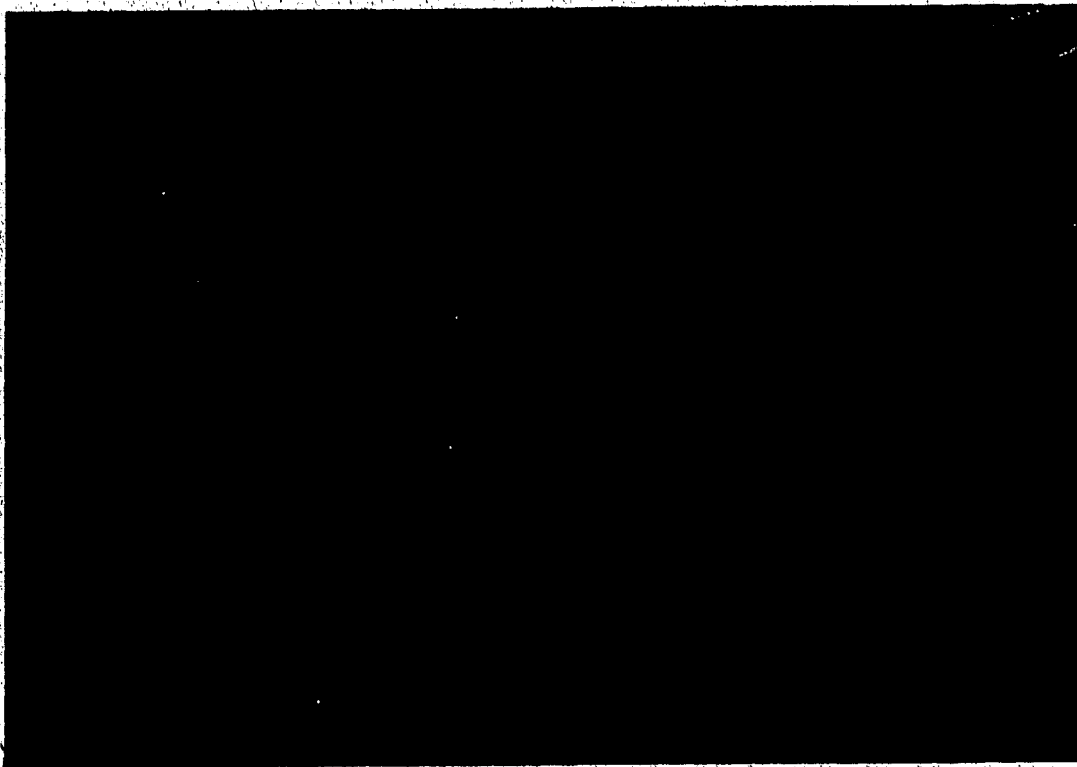
Figure 7. Lateral x-ray film of a cat head showing the orbitomeatal line (broken line) and the two levels at which NMR imaging was usually performed (solid lines).

A multiple-spin-echo (MSE) imaging sequence was used with a series of eight echoes employing a repetition time (T_R) of 4.3 s and an echo interpulse time (T_E) of 32.5 ms. We tried a 16-echo MSE sequence using the same timings to compute the biexponential decay of the transverse relaxation but obtained good results for only two cats in group III. For all images, 128 frequency-encoding steps were employed, with each pulse sequence performed twice for signal averaging. The FID data were processed by two-dimensional Fourier transform algorithms for image reconstruction of a 256 x 256 pixel matrix.

Calculations of R_2 from images were performed using the Grinnell imaging system, kindly provided by the Department of Applied Sciences in Medicine of the University of Alberta, using a program developed by K.S. Knudsen. This program allows the user to define regions of interest (ROI) within the first image, and transfers the spatial coordinates to the remaining images. The average signal intensity is computed for each ROI, and is employed to fit a least squares monoexponential regression curve to the values in a specific region.

2d. **Measurements of proton NMR relaxation in tissue samples in vitro**

The control cats were sacrificed within 24 hr of the imaging, whereas the cats in groups II and III were sacrificed immediately after the last imaging session. They were killed by intracardiac injection of 1 ml of sodium pentobarbital (Euthanyl). A procedure to wash out the blood vessels of the brain was then followed. A

longitudinal incision was made from the suprasternal notch to about the level of the umbilicus. The left costal cartilages were cut and the contents of both thorax and abdomen were exposed. A 15-gauge catheter was inserted in the left ventricle, blood flow to the caudal part of the body was interrupted by clamping the thoracic aorta, and the right ventricle was cut open. One liter of Ringer's lactate solution was infused through the catheter in the left ventricle at a pressure of 140 mm Hg. The brain was then extracted and placed in a metal container on ice. (Lowering of brain temperature reduces the rate at which the tissues undergo necrotic changes, increases the consistency of the brain for more adequate cutting in the desired plane, and reduces water loss due to evaporation.) The container was sealed with parafilm to avoid excessive condensation of water on its walls. After 5--10 min on ice, the brain was sliced in the transverse plane at two levels. One cut passed from the cruciate sulci to the coronal surface of the cerebellum; the second cut was at 5 mm below this plane. The coronal and the caudal segments were placed in 10% formalin and the middle was left in the container for subsequent sampling. The coronal and middle slices corresponded to the NMR imaging planes.

Samples of grey and white matter, and of tumor in group III cats, were carefully dissected from the middle slice of the brain. They were taken from the frontal, parietal, and occipital white matter, from the parietal cortex in the area of the sylvian and ectosylvian gyri, and from the caudate nuclei. Instead of obtaining samples from the occipital white matter in group II cats, the

parietal white matter was sampled at two locations. The samples were placed at the bottom of microcentrifuge vials (of 500 μl capacity and weight 300 mg). To obtain tissue fresh weight the vials were weighed on a Mettler AE 163 scale (Mettler Instruments Corp., Hightstown, NJ) before and after the sample was inserted. The vials were sealed with parafilm and placed on ice until NMR relaxation measurements were determined (from 2--12 hr after death).

These measurements were performed with the same magnet used for imaging, employing a double-turn coil of 2 cm diameter. The temperature was kept at 38°C (normal temperature of the cat) by a flow of warm air and monitored with probes. The inversion recovery (IR) pulse sequence was used for the determination of R_1 allowing 10 times $1/R_1$ between scans for recovery of magnetization equilibrium in the sample. At least 10 points were used to fit an asymptotic curve representing recovery of magnetization. R_2 was measured by using the CPMG pulse sequence with a T_R of at least 10 times $1/R_1$ and a T_E of 32.4 ms to provide similar data to those obtained by the imaging sequence with a T_E of 32.5 ms. Two or more averages were obtained for each measurement of R_2. Furthermore, R_2 rates were measured several times using a T_R of 4.3 s to determine wether the repetition time had an effect on transverse relaxation rate. Measurements of R_2 in brain samples were repeated after 10 hr to see if the transverse relaxation rate was affected by postmortem changes. From 12 to 30 points were used to fit a curve to the decay of magnetization. $R_{1\rho}$ was measured using a spin-lock pulse sequence with a field strength 10% weaker than that of the 90° pulse (ω_1 = 5 kHz). The low field

strength used was with the purpose of obtaining a high sensitivity of $R_{1\rho}$ to changes in tissue water content. Eight or 16 points were employed to fit a curvilinear decay with one or two exponential terms. $R_{1\rho}$ was measured only in the animals of groups I and III.

2e. Determination of water content

Immediately after the NMR measurements were done, the samples were frozen at $-70°C$ until they could be freeze-dried, usually within 3 days. The samples were placed on a Wheaton dry sealing dessicator (Fischer) at a temperature below $0°C$. Air was extracted from the dessicator which was then connected to the freeze drying apparatus (Freezemobile 24, Virtis Co., Gardiner, NY) for 48 hr at $-70°C$ and <100 mtorr. The samples were then weighed on the same scale used for determining the fresh weight. The difference between the original weight of the vial and the weight of the vial plus the dried tissue was taken as the dry weight. The water content per unit of dry weight was obtained as follows:

$$\text{water content (g/gDW)} = FW - DW/\ DW \qquad (12)$$

where FW is the fresh weight and DW is the dry weight of the sample. The reciprocal of the water content per unit dry weight (dry weight per unit tissue water and refered here as dry-tissue content) was employed for plotting against the relaxation rates. The reasons for this are explained in Chapter III (see also Hazlewood, 1979). To check for changes in water content during the NMR procedure, one half of the brain samples of control animals was frozen after weighing and the other half was kept on ice for about 10 hr, the time required to

¶ complete the NMR measurements. Each sample of the latter group was kept at 38°C for the 45 min period during which relaxation measurements were performed.

Two weighted empty vials for each set of samples were also subjected to freeze drying to determine the effect of the procedure on the weight of the vials. After weighing, the dried samples were kept at -70°C until further measurements could be performed.

2f. Measurements of total and soluble protein

To determine content of total protein, the dried samples were first homogenized using manual glass homogenizers (Radonti Glass, Monrovia, CA). One hundred and fifty vols. of buffer solution containing tris-HCl 0.01 M at pH 7.5 were employed for white matter samples and 300 vols. were used for grey matter samples. Homogenization was done for about 3 min for white matter and about 2 min for grey matter until all particulate matter was dispersed. One and one-half ml of homogenate were put in microcentrifuge vials, of which 1.0 ml was diluted with 2 ml of the buffer solution and centrifuged at 45,000 RPM for 45 min in a Beckman ultracentrifuge (Beckman Instruments, Model L5-65, Palo Alto, CA). One and one-half ml of the supernatant were kept for determinations of soluble protein.

Protein content was measured by the Bradford method (1976) using a commercial preparation of the reagents (Bio-Rad Laboratories, Ltd., Mississauga, Ontario). For determination of total protein , 50 μl of homogenate were diluted with 50 μl of buffer solution and

5 ml of dye reagent were added. The samples were agitated for 3 min
and the ultraviolet light absorbance was measured at a wavelength of
595 nm in a spectrophotometer (Unicam SP 1700 Brinkman Instruments).
For the soluble protein determination, the samples were not further
diluted (i.e., 100 μl of the supernatant were utilized).

2g. Measurement of albumin content

Polyacrylamide gel electrophoresis (PAGE) was performed
according to the method described by Laemmli (1970) with some
modifications. The acrylamide concentrations used were either 10% or
13% in a separating gel buffer of pH 8.8. The pH of the stacking gel
was 6.8 using an acrylamide concentration of 6%. The mixtures of
acrylamide and buffer were placed under vacuum for at least 10 min
before addition of ammonium persulfate (Bio-Rad) and
tetramethylenediamine (TEMED). Best elasticity of the gels was
obtained when 100 μl of ammonium persulfate solution and 10--15 μl of
concentrated TEMED were used.

Sample preparation was with a solution of the stacking gel
buffer containing 12.5% of glycerol, a 12.0% solution of sodium
dodecyl sulfate (SDS), and 10 mg/ml of bromophenol blue (Sigma).
Fifty μl of the buffer were mixed with 50 μl of the sample homogenate
and 10 μl of beta-mercaptoethanol. This sample was heated at 100°C
for 2 min and 50 μl of it were poured in each of the wells of the gel
slabs. The preparation was subjected to continuous current in a Bio-
Rad Protean II vertical electrophoresis system using a Bio-Rad power
supply (Model 500/200).

The gels were fixed for 1 hr in a solution containing 80% water, 10% acetic acid and 10% methanol. Subsequently, they were stained in a solution of 60% water, 30% methanol, 10% acetic acid to which 2 g/liter of Coomasie brilliant blue R-250 (Eastman Kodak Co., Rochester, NY) was added. Destaining was performed in a solution of the same composition as the fixative solution.

The destained gels were placed in plastic bags, a photographic record was obtained, and densitometry was performed using a Joyce-- Loebl laser densitometer (Vickers Instruments Inc., Malden, MA) with a filter giving a wavelength of 626 nm. The relative proportion of each protein band was determined and that of the albumin peak was transformed into absolute values by multiplying its relative proportion by the total protein content measured with the Bradford method.

2h. Histopathology

The brain slices were fixed in formaldehyde for 2 weeks, then dehydrated in 80% ethyl alcohol (ETOH) for 2 days, 95% ETHO for 2 days, and absolute ETOH for 2 days, and cleared in xylene for 3 hr. The samples were subsequently transferred to a xylene and wax bath at 60°C for 1 hr, then embedded in wax for 3 hr and left overnight in this bath. The wax blocks were sectioned at 8 μm and the sections stained with hematoxylin and counterstained with eosin. The slides were examined and photographed in a Zeiss microscope. A photographic record of the tissue slides was also obtained.

2i. <u>Statistical analysis</u>

A least squares minimization routine employing one exponential term was used to calculate R_2 from images. For the transverse relaxation decay data obtained <u>in vitro</u>, a similar fitting routine was used incorporating either one or two exponential terms. Data were input manually on an Apple Macintosh personal computer. For the decay data of the transverse magnetization, both even and odd echoes were used for the calculation of R_2, it was found that this did not have a significant effect when compared with the R_2 calculated from even echoes only. The greater number of echoes would allow a greater accuracy for the calculation of R_2 from images.

Linear regression was applied to the relationships between tissue water content and relaxation rates. Multiple linear regression analysis of the regression lines was then performed. Student's t-test or Wilcoxon's signed rank tests were used with normally distributed or skewed data respectively. Values are reported as means ± standard deviation.

3. Results

3a. Clinical findings

Cats with tumors were usually sacrificed before clinical signs developed. In some animals, however, decreased activity was observed around the 13th to 15th day post implantation. Additional findings were mild motor ataxia and in one animal focal seizures of the left hind limb.

In cats intoxicated with TET, an immediate reaction was observed after injection. The animals appeared distressed and seemed to be in pain. Increased salivation and vomiting was observed in most animals. After 30 minutes paresis of the hind limbs and stupor were observed. Tachypnea and tachycardia with peripheral vasodilation was observed in one animal. Urinary and fecal incontinence were common after 24 hr. In all the animals slight improvement of the paresis occurred after about 6 hr but worsened at 12 to 24 hr with progressive decline afterwards. Two animals died within 24 hr of injection and were excluded from the study.

3b. Pathologic findings

3b.1. Macroscopic

The brains of cats with tumors of the right parietal lobe showed adherence of the dura to the site of the injection, as well as effacement of the lateral and ansate sulci. The parasylvian and marginal gyri showed a grayish discoloration and diminution of the

consistency of the cortex at this point. An increased volume of the

right hemisphere was observed in several cats. On brain section the

tumor usually appeared as a grey, spherical mass, well delineated

from the surrounding brain, and under pressure as shown by its

protrusion through the surface of the cut. The tumor size was quite

variable ranging from 2 to 11 mm in diameter. Tumor cysts were found

in two animals and hemorrhage around the tumor--white matter

interphase was observed in one. Edema in white matter of the

affected hemisphere was observed in most brains and was more severe

in the animals with larger tumors. These also produced a marked mass

effect with compression of the contralateral hemisphere (Fig. 8).

The brains of cats with TET intoxication showed effacement of

sulci and the sections demonstrated marked increase in the volume of

white matter (Fig. 9).

3b.2. Microscopic

On H+E-stained sections of the brains with tumors, the neoplasm

showed a clear demarcation from the surrounding brain (Fig. 10). The

tumor consisted of spindle-shaped cells with large nuclei and

abundant mitotic figures throughout. Areas of necrosis were frequent

in the larger neoplasms (Fig. 11). Hemorrhage was observed in the

center of one and in the white matter--tumor interface of another.

The smallest tumor showed a marked round-cell infiltration with loss

of demarcation between the neoplasm and the surrounding brain. In

the peritumor region a rim of compressed tissue was observed around

the larger neoplasms and marked perivascular lymphocytic infiltration

was observed in the small vessels of the region (Fig. 12). Marked
edema of the white matter, but not grey matter, was observed around
most tumors except one that grew almost entirely within the grey
matter. The edema was characterized by the formation of clear spaces
that were largest a few millimeters from the tumor, and diminished
progressively with distance from it. They were also small in the
immediate proximity of the neoplasms, probably due to compression
effects of the latter (Fig. 13).

The brain sections of TET-intoxicated animals showed a
characteristic distribution of edema. Although all the white matter
was affected, the subcortical U-fibers showed the most severe edema
(Fig. 14). The grey matter, however, was not affected severely and
did not differ from controls (Fig. 15).

Figure 8. Brain section of a cat with an implanted glioma tumor in
the right parietal region (arrow). The center of the tumor
shows a large cyst and the white matter is markedly increased in
volume. Mass effect of the tumor is shown by displacement of
the interhemispheric fissure to the left.
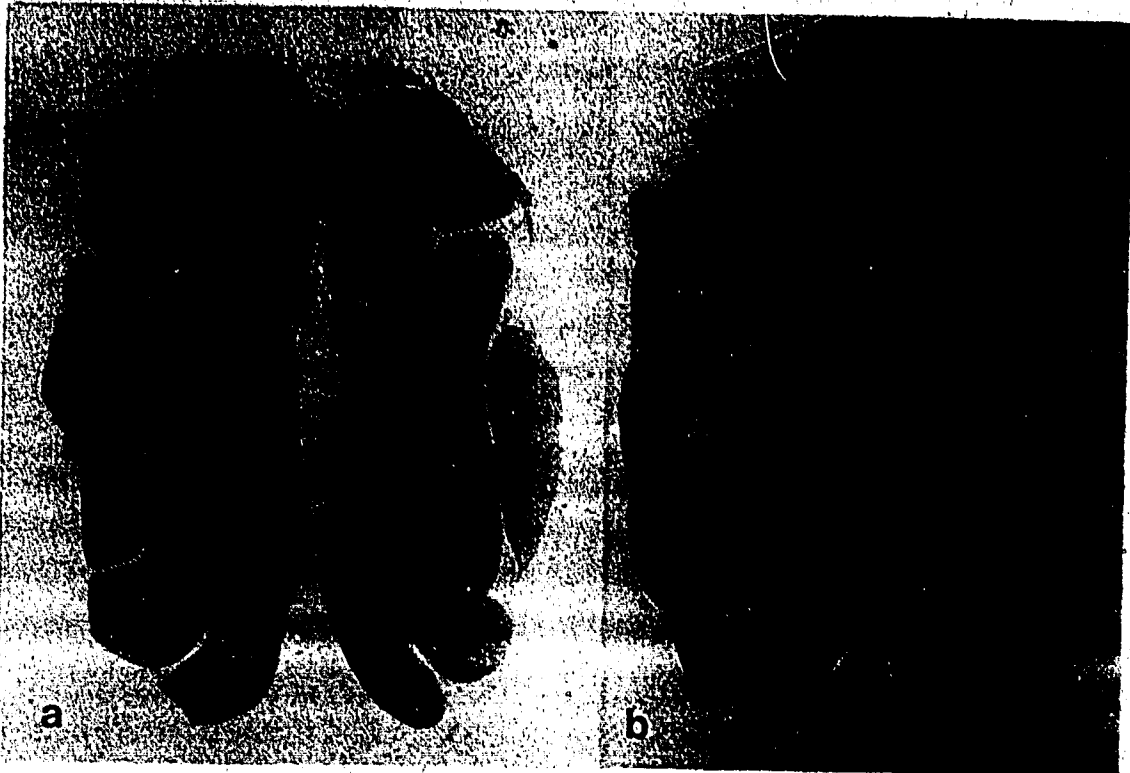
Figure 9. Brain section of a normal cat (a) used for comparison with
a brain section of a cat intoxicated with TET (b), which shows
marked enlargement of the white matter and compression of the
grey matter.

Figure 10. Brain sections of cats with implanted glioma tumors in
the right parietal region (a,b). Good demarcation between the
tumor and the surrounding tissue is observed. Photomicrographs
of the same tumors showing the tumor—peritumor interface (c,d).
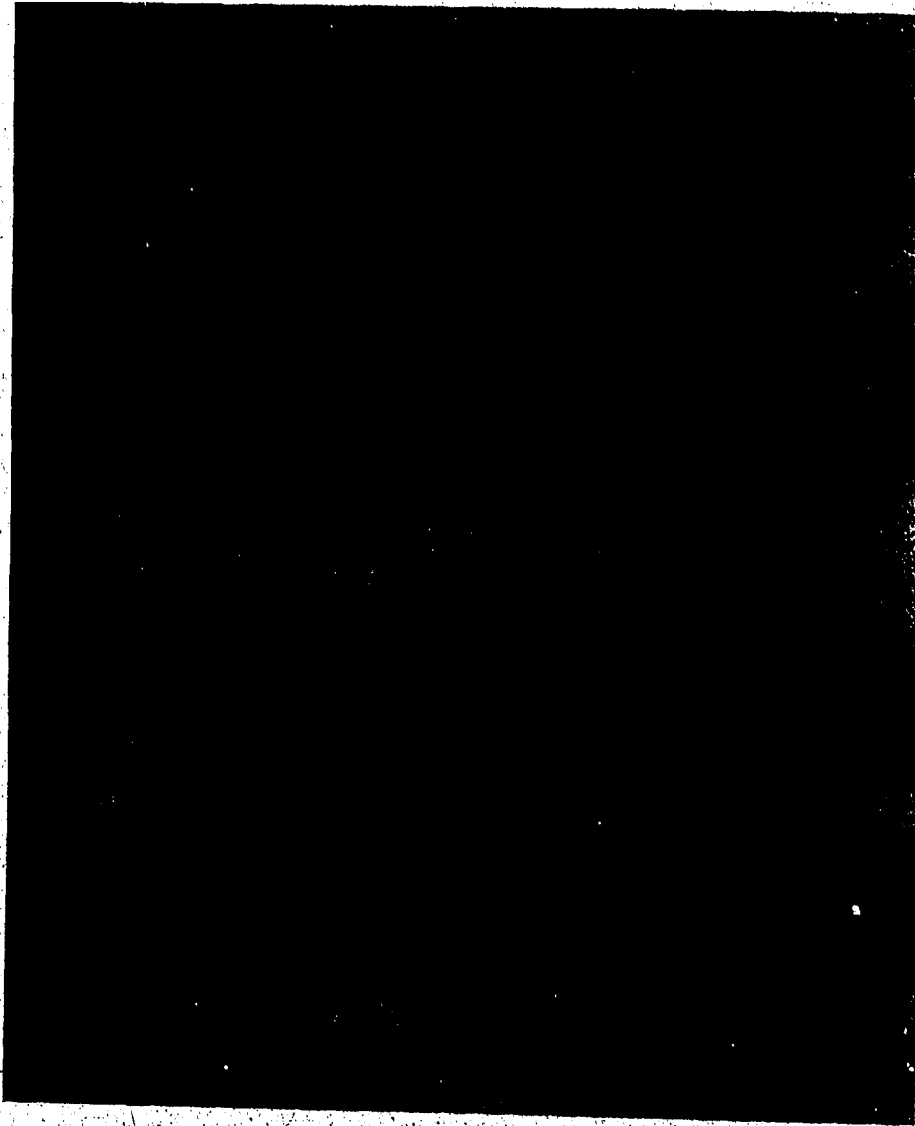
Figure 11. Photomicrograph of a xenotransplanted brain tumor showing areas of necrosis (arrows).
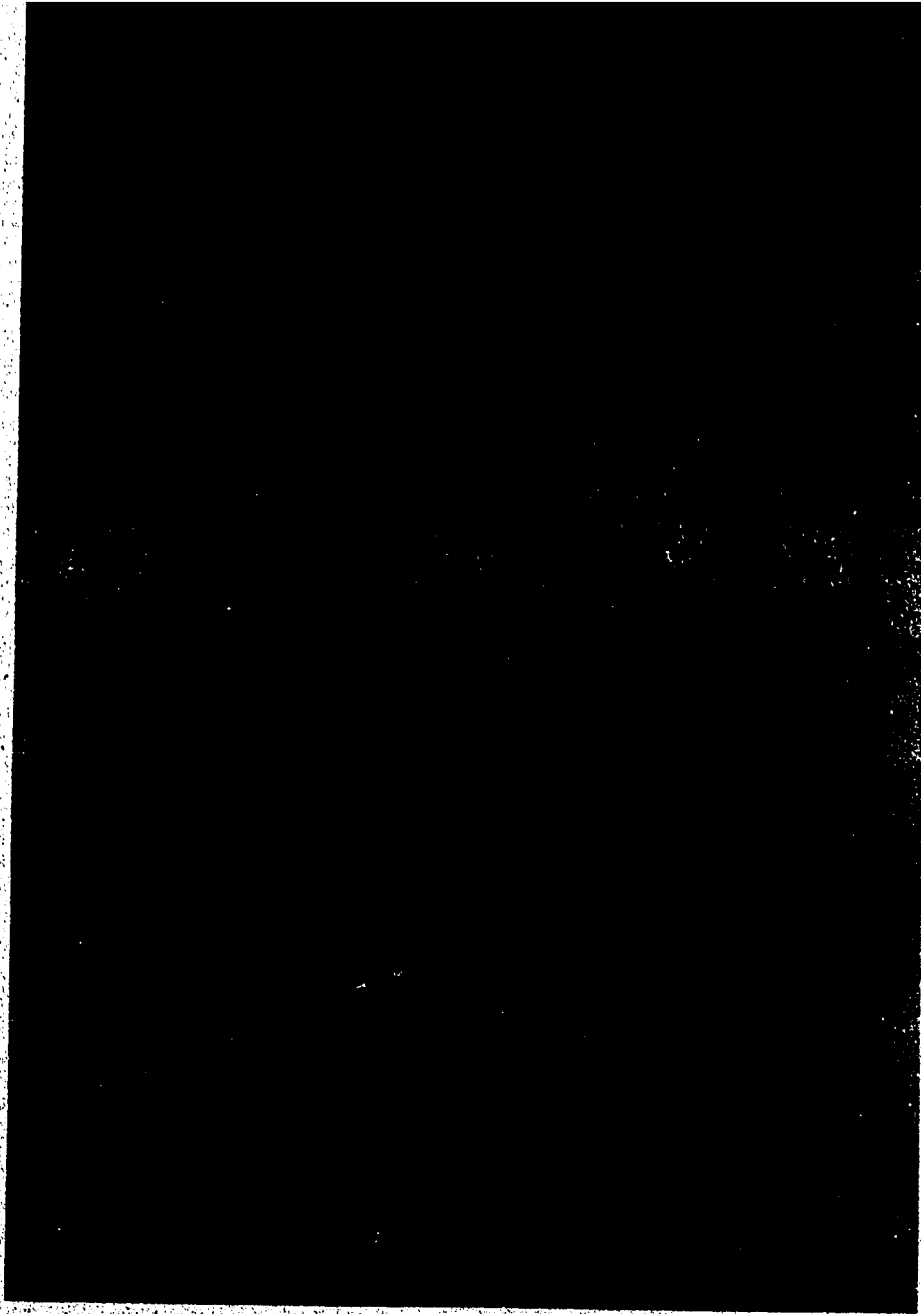
Figure 12. Marked accumulation of lymphocytes in the Virchow—Robin
   space was observed in all cats with brain tumors (a). Migration
   of lymphocytes into the surrounding neuropil (arrow) was
   observed in some of these animals (b).
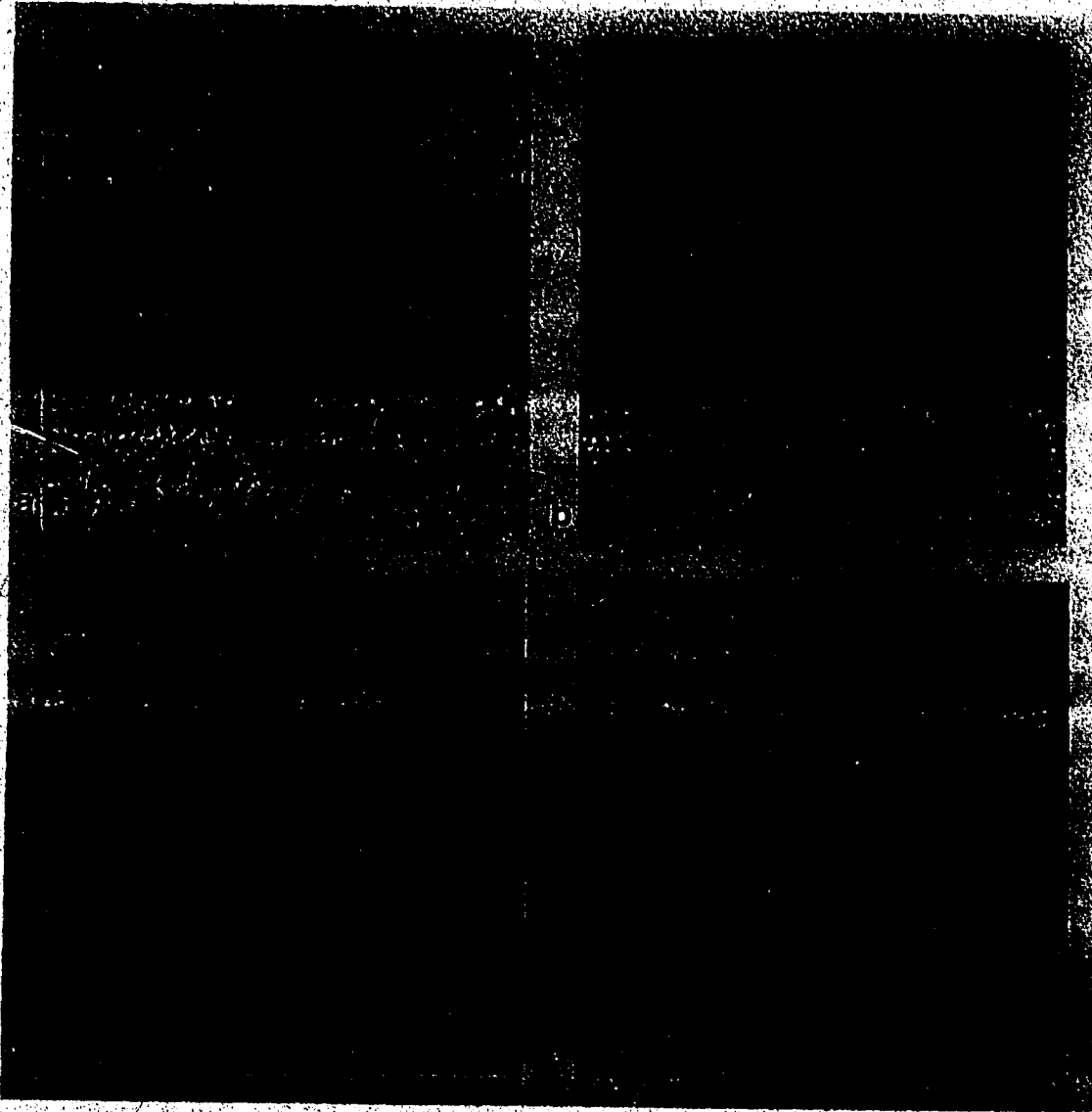
Figure 13. Photomicrographs of peritumor edema of the white matter.
Tumor—peritumor interface showing compressed peritumor tissue
(a), peritumor wihte matter at 0.8 radii from the tumor showing
a more severe degree of edema (b), peritumor white matter at 1.2
radii from the tumor where the edema is less prominent (c),
white matter at 2.4 radii from the tumor showing a minimal
degree of edema (d).
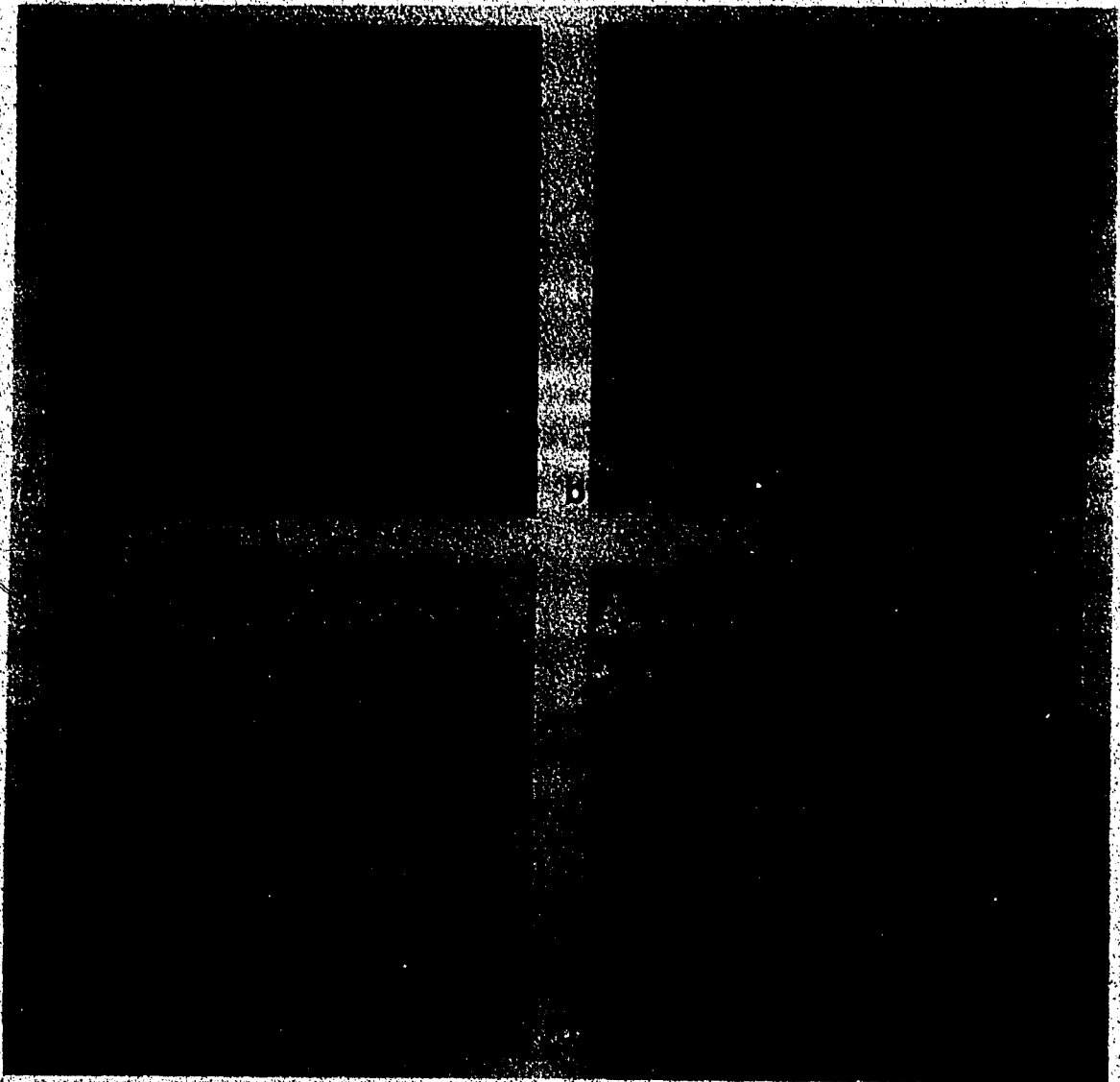
Figure 14. Low-power photomicrographs of white matter of cats with TET intoxication. A more severe degree of edema is observed in the subcortical U-fibers (arrows) than in the central white matter (a,b). High-power photomicrographs showing diffuse spongiosis of white matter (c,d).
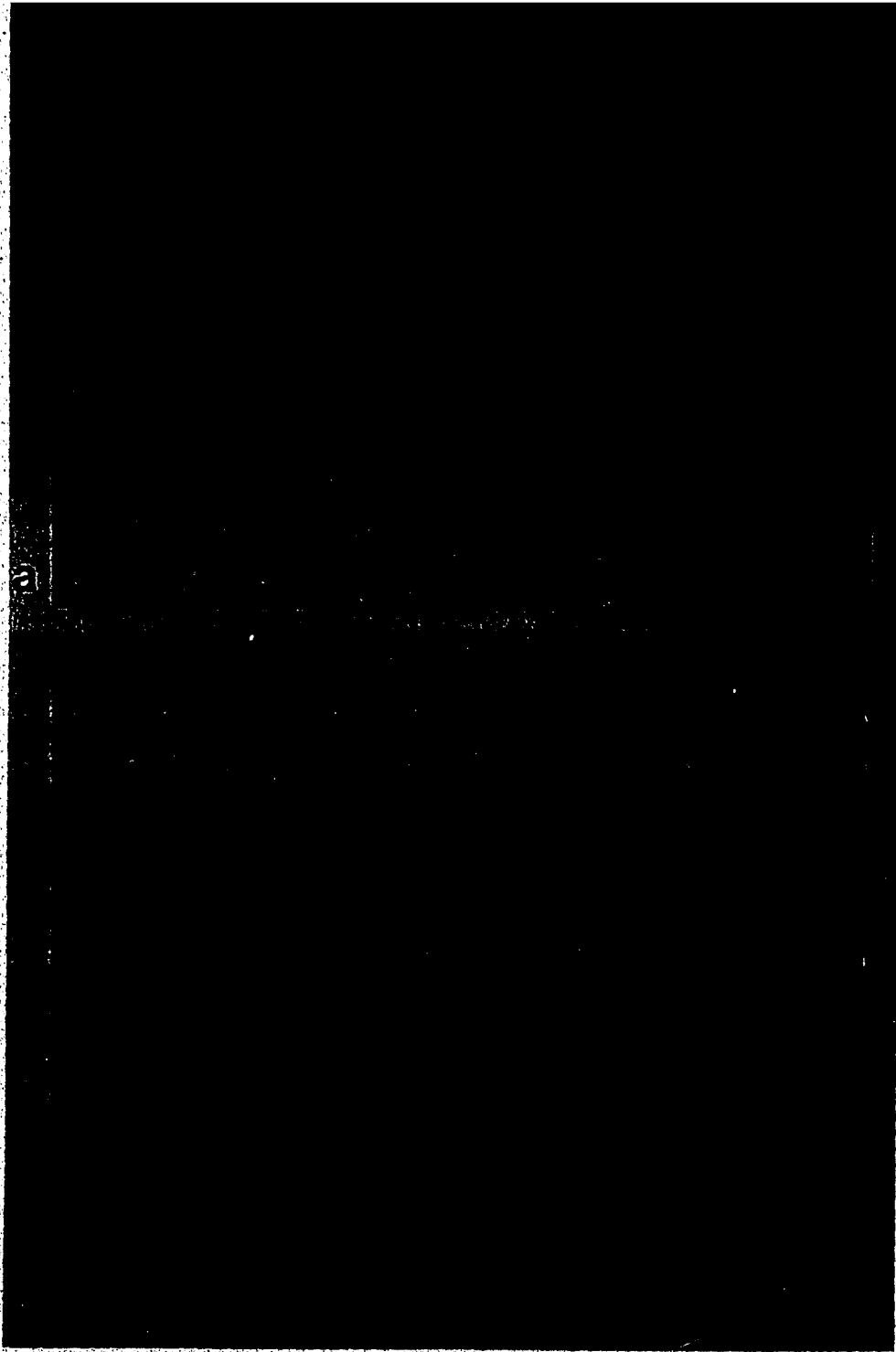
Figure 15. Photomicrographs of parietal grey matter. Control animal(a), TET-intoxicated animal (b). No difference in this structure could be detected between the two groups of animals.

3c. NMR imaging

3c.1 Image quality: comparison with pathologic state

The NMR images employing the MSE sequence provided very good spatial and contrast resolution. Spatial resolution is given by an image-slice thickness of about 3 mm and of Gaussian profile. The pixel size of the 256 x 256 display matrix represented an area of 0.5 x 0.5 mm. The volume of tissue corresponding to one pixel is therefore 0.75 mm^3; however, the true resolution of the image was not determined. The surface characteristics of the brain showed up clearly due to the marked contrast between CSF and brain tissue. On the other hand, the very small size of the ventricles of the cat brain precluded their visualization except in a few cases. In control animals the outline of the cerebral cortex and of the deep grey-matter structures, such as the caudate nuclei and the hippocampi, were distinguished. The diffuse lateral borders of the thalami, intermingled with white matter, however, prevented adequate visualization of their borders (Fig. 16). Contrast between grey and white matter was best in the first image (i.e., echo at 32.5 ms) and decreased progressively with increasing T_E. Comparison with brain slices showed very good correlation (Fig. 17).

NMR images of cats with brain tumors demonstrated a very close agreement with the histopathology slides. For example, in a cat with a 4 mm tumor the spherical mass was clearly separated by a rim of lower intensity signal. The edema of the white matter was well delineated with a maximum signal intensity just outside the rim and

decreased progressively to values for normal white matter (Fig. 18).
The mass effect produced by the larger tumors on both hemispheres was
clearly shown (Fig. 19). In the cats with hemorrhage or cysts, NMR
showed such areas as of low and high intensity respectively. In
tumors that showed signs of rejection histopathologically, and thus a
loss of clear demarcation between neoplasm and peritumor tissue, a
loss of demarcation was also observed in the NMR images.

The correlation between the appearance of the distribution of
brain edema induced by TET as shown by histopathology and by NMR
images was very good. On the echoes occurring towards the end of the
MSE sequence (i.e., T_E = 97.5 ms or greater) the more severe edema in
the subcortical white matter, as shown by the high signal intensity
in this region, became clearer. The grey matter, on the other hand,
appeared unaffected (Figs. 20, 21).
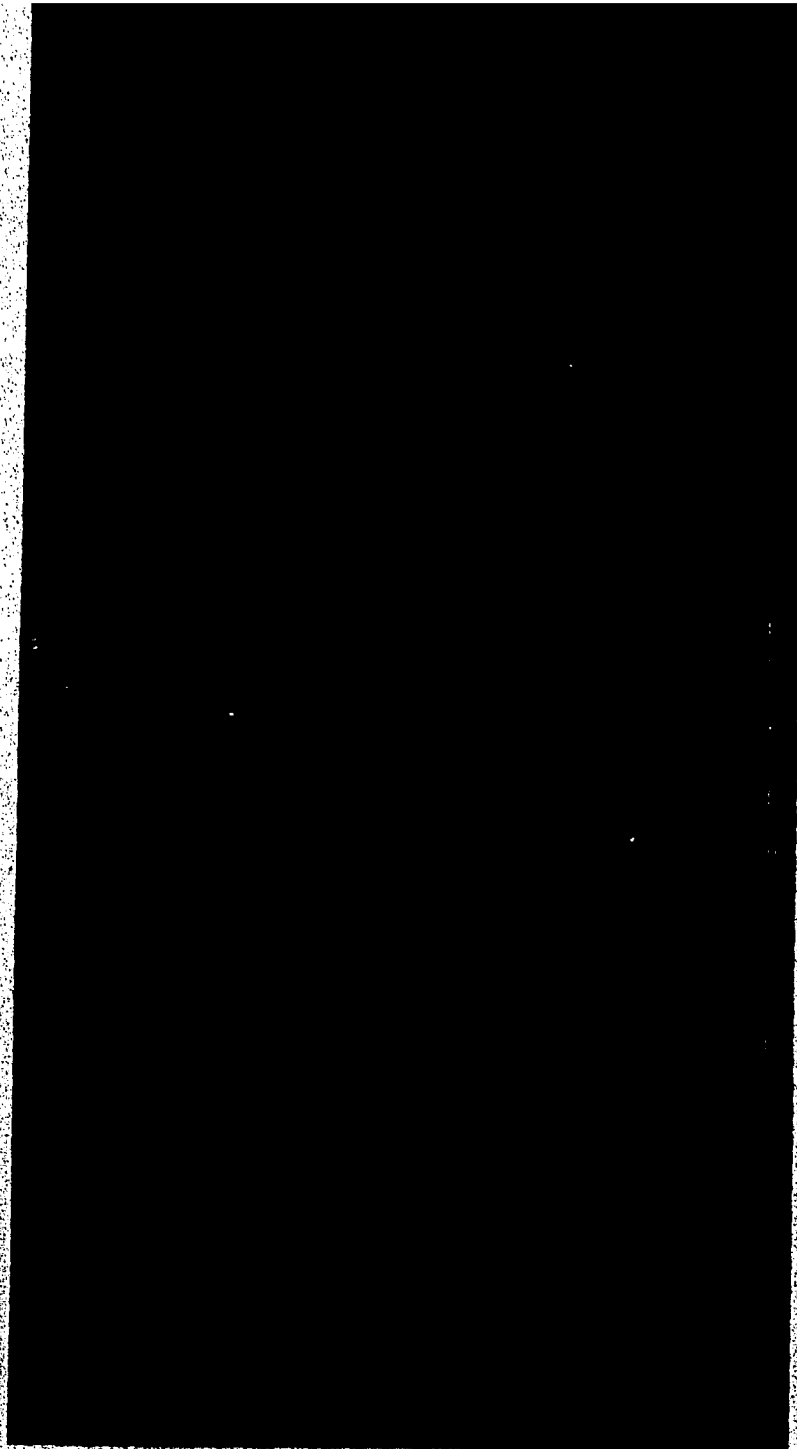
Figure 16. MSE images of head of a control cat, $T_E = 32.5$ ms (a), $T_E = 65.0$ ms (b), showing good delineation of anatomical strucutres of the brain. Good contrast between grey and white matter allows discrimination between deep grey matter structures: 1 - caudate nucleus, 2 - thalamus, 3 - hippocampus.
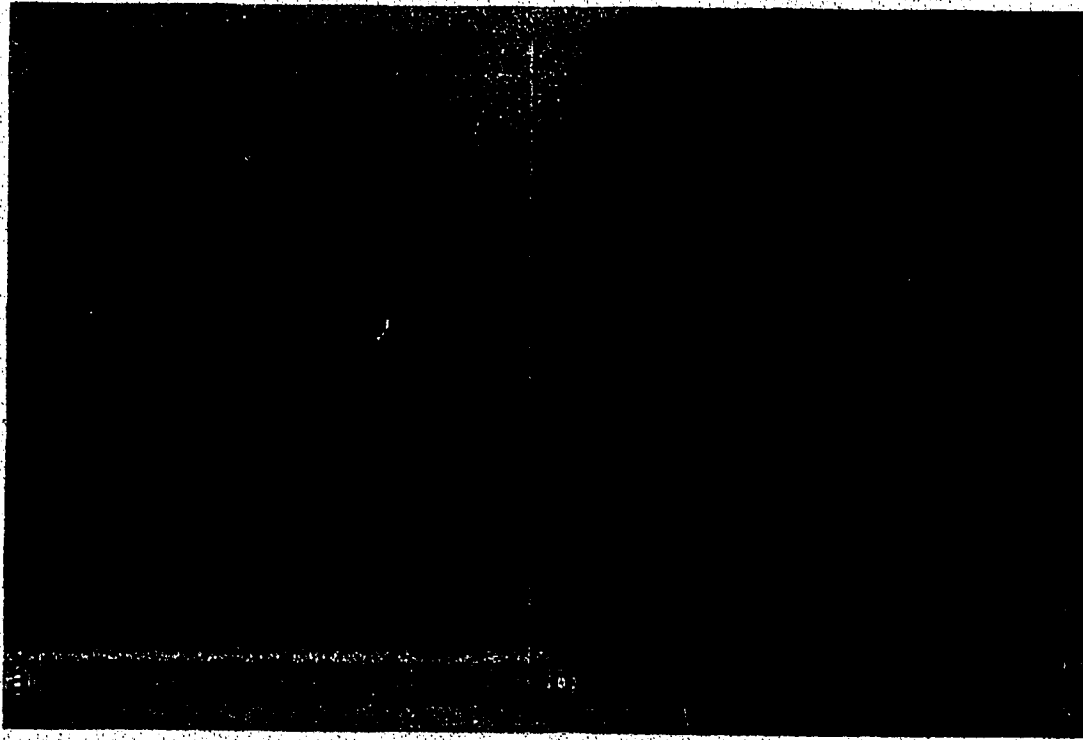
Figure 17. Comparison of an H+E-stained section of brain of a control cat (a), with corresponding MSE image (b), $T_E = 32.5$ ms.
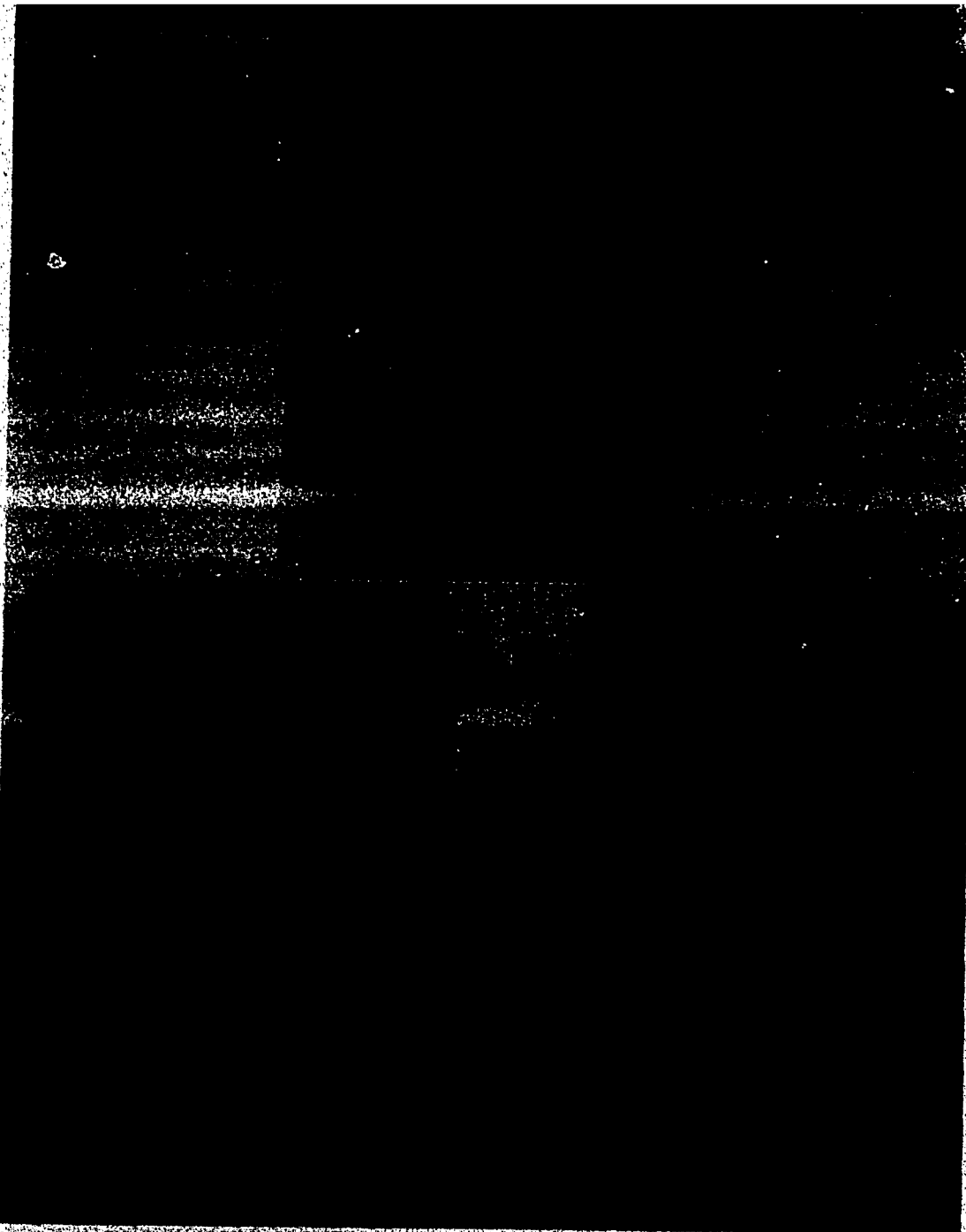
Figure 18. Comparison of (a), H+E-stained section of brain of a cat
with an implanted glioma tumor (arrow), with (b) and (c), MSE
images of the same animal before sacrifice. The tumor (arrow)
is surrounded by a rim of decreased signal intensity with
neighboring peritumor edema showing as regions of high signal
intensity.
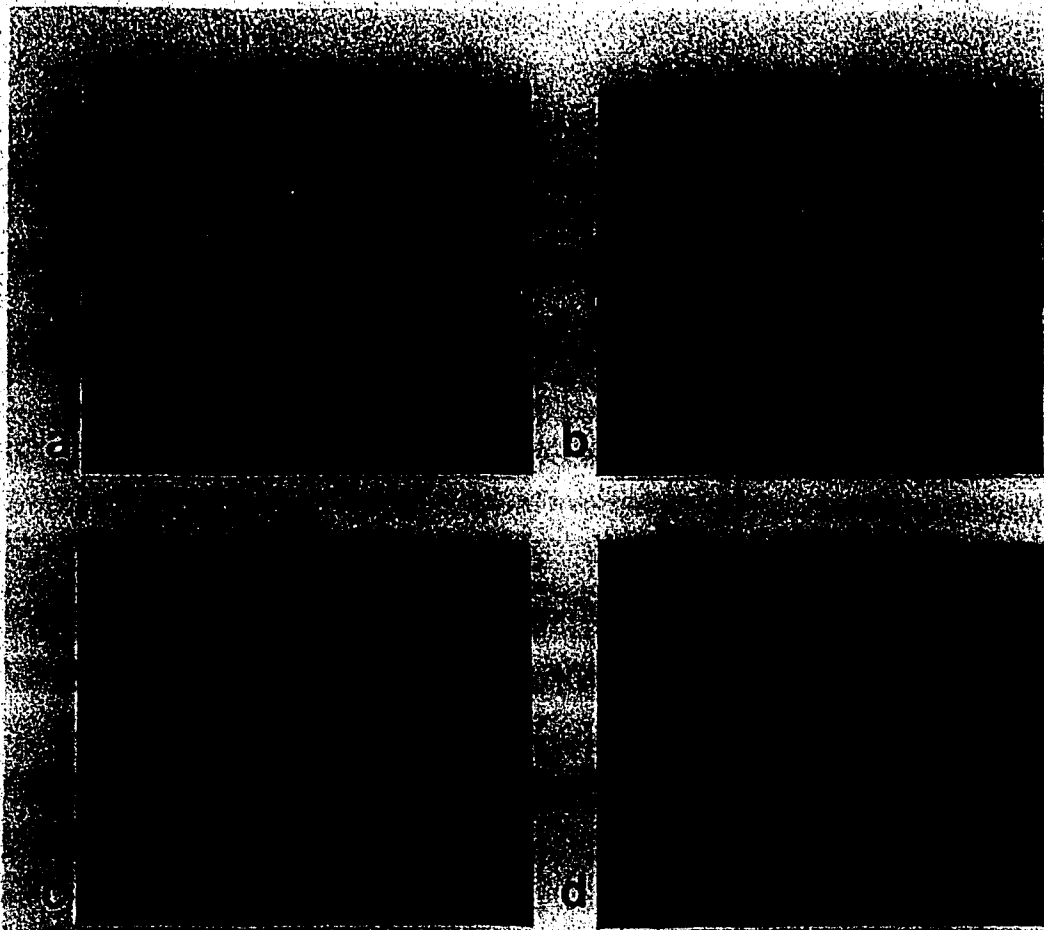
Figure 19. MSE sequence of images of head of a cat with an implanted glioma tumor. The tumor is spherical (arrow) and surrounded by a rim of low signal intensity. The edema (areas of high signal intensity) is restricted to the white matter and together with the tumor produces marked mass effect as shown by the shift of the midline to the left. T_E = (a) 32.5 ms, (b) 97.5 ms, (c) 162.5 ms, (d) 227.5 ms.
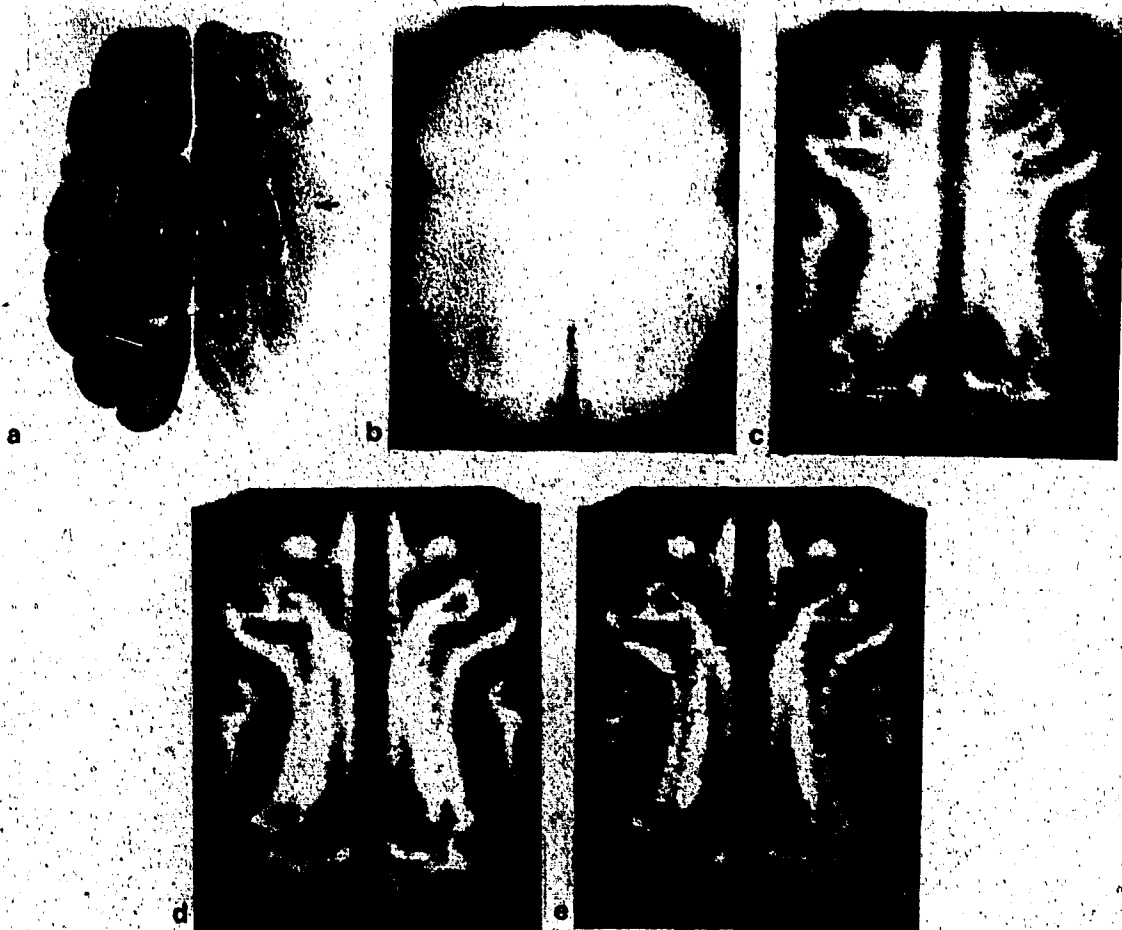
Figure 20. (a) H+E-stained brain section of a cat intoxicated with
TET. Lucency of the subcortical U-fibres is clearly shown
(arrows). (b) to (e) Corresponding MSE images. (b) The first
echo image, $T_E = 32.5$ ms, shows loss of contrast between grey
and white matter. The later echo images, $T_E = 97.5$ ms,
162.5 ms, and 227.5 ms, show increasing contrast between them,
however. The greater severity of the edema in the U-fibers is
clearly shown in the images.
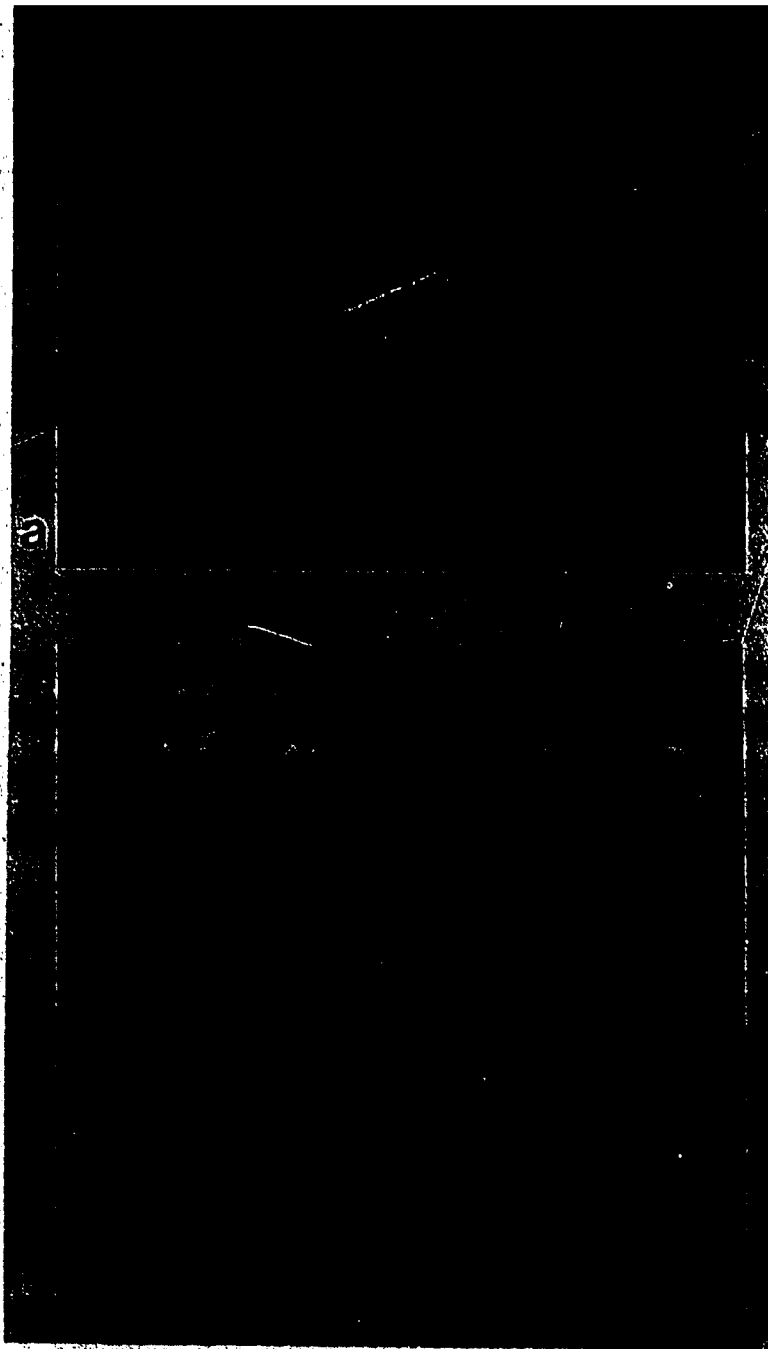
Figure 21. MSE images of head of a TET-intoxicated cat. At this more caudal level some degree of edema in the subcortical U-fibers is also apparent. T_E = (a) 97.5 ms, and (b) 162.5 ms.

The calculations of R_2 from ROI in the MRI images gave rise to

standard deviations of the fitted exponential curve of an average of

2.6% in white and grey matter of control animals. The size of the

ROI most commonly employed was 10 pixels; however, ROI from

4 to 14 pixels gave similar values to those obtained with 10 pixels.

A single exponential decay could be used to describe the transverse

relaxation of all brain structures within the time-frame of this

experiment which covered over one order of magnitude of signal decay

for the in-vivo R_2 measurements.

In cats with cerebral neoplasms, the transverse magnetization

could be described by a single exponential decay in regions of white

and grey matter of the left hemisphere and of grey matter and tumor

of the affected hemisphere. In regions of peritumor white matter,

this decay was marginally non-linear when plotted on semilogarithmic

paper. Due to the limited number of points and the limited time

frame of the observations, however, a biexponential fit could not be

applied. Thus, a monoexponential R_2' was obtained from the eight-

echo decay (Fig. 22). Fig. 23 demonstrates the biexponential decay

of the transverse magnetization obtained in vitro for a sample of

white matter with severe peritumor edema. The magnetization decay in

vivo in white matter of cats with TET intoxication showed definite

multiexponential behavior; however, eight data points and the short

time-frame employed were not sufficient to discriminate reliably

between two exponentials. Thus, a single R_2' was computed from this

set of data points. In addition, it was found that calculation of R_2'

cats. This was interpreted as the effect of partial volume averaging

in the ROI due to the contribution of severe edema in the subcortical

U-fibers of white matter. (Partial volume averaging is the averaging

of the magnetization signals coming from different tissues. In this

case, the convoluted nature of the cortex--white matter interphase

results in both types of tissue being included in the parallelepiped

described by the pixel.)
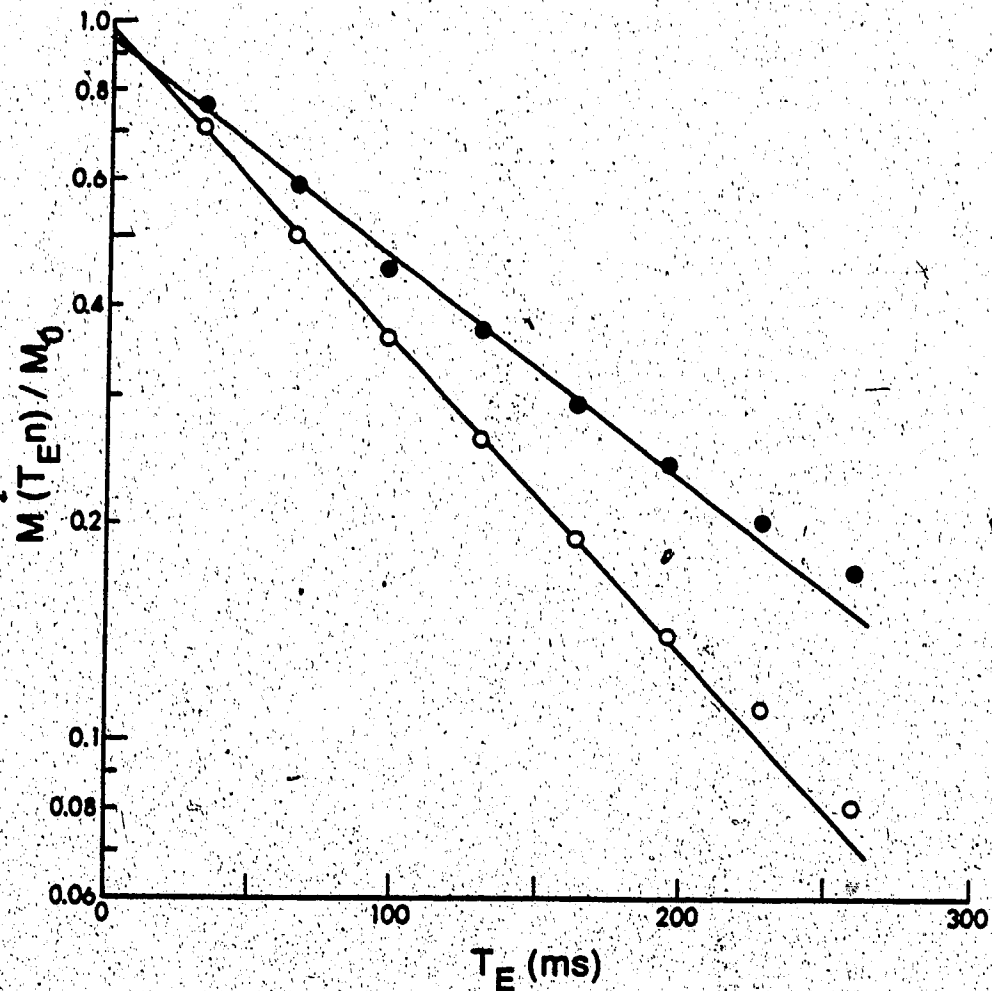
Figure 22. Normalized transverse relaxation decay obtained
in vivo in cats with severe peritumor edema (●) and mild
peritumor edema (○). A slight curvature is observed in both
sets of data suggesting more than one exponential component;
however, the limited time-frame of the observations precludes
separation of the components. The solid lines represent the
curvilinear fit to the data points using a single exponential
term, the slope of which is given by R_2'.
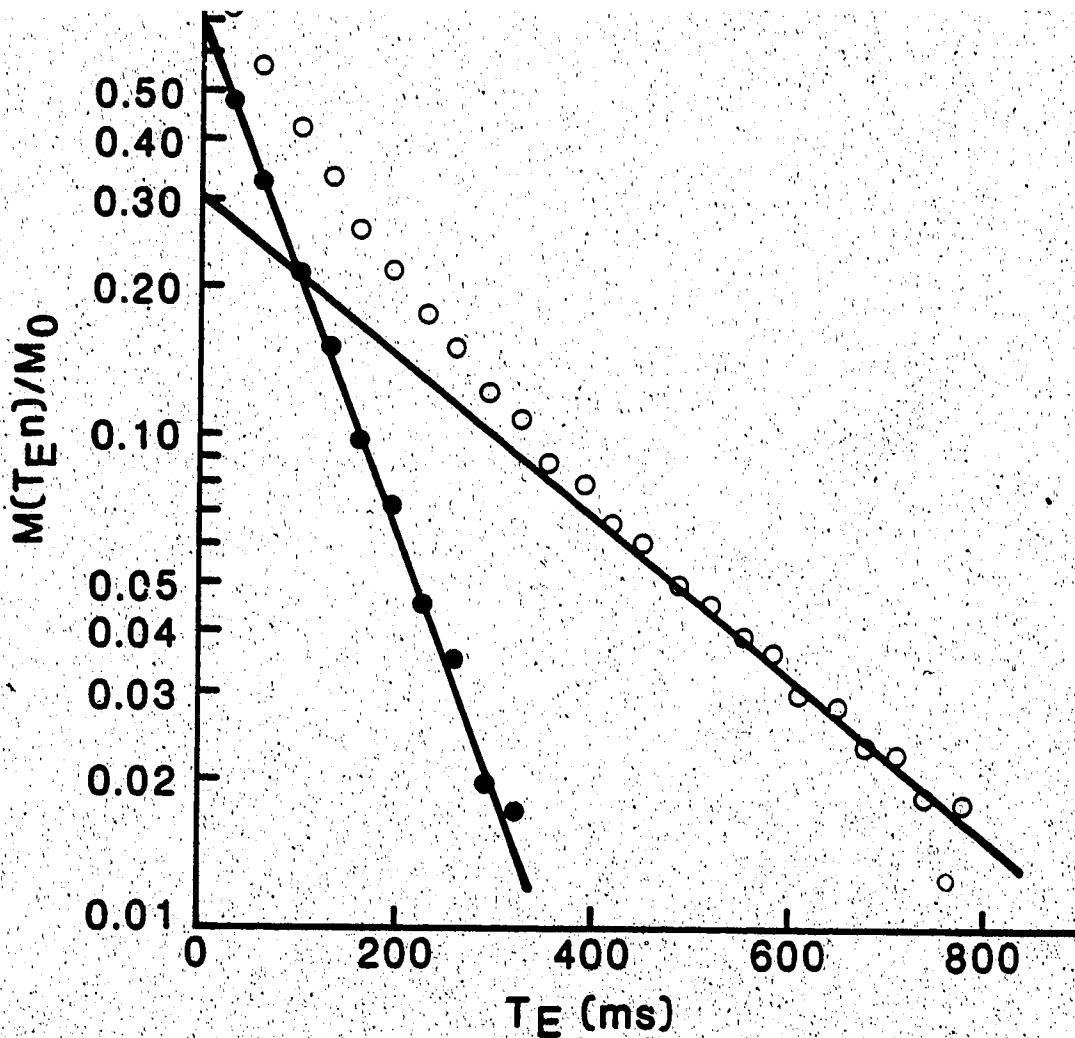
Figure 23. Normalized transverse relaxation decay obtained
in vitro from a sample of white matter of a cat with severe
peritumor edema (○). A marked curvature is observed in the
data. Separation of the components of the decay is shown. The
slow component is given by the slope of a line fitting the
points at longer T_E, and substraction of the predicted from the
observed values gives the points describing the fast component
(●). In fact, the solid lines represent the curvilinear fit to
the data points using two exponential terms for the least
squares minimization routine. The slopes correspond to R_{2f} and
R_{2s}, which are the fast and slow components respectively, and
the intercepts correspond to the proportion of the proton signal
accounting for each component.

Each relaxation rate measured, namely R_1, R_2, and R_1 , provided

different information. Although R_1 showed least change in actual

units, the relative difference between grey and white matter was more

marked than that observed in R_2 and $R_{1\rho}$ (Tables 7--9). The latter

two were similar when the relative difference between the values of

white and grey matter was compared. No indication of

multiexponentiality could be determined from the data on control

animals. Moreover, the longitudinal relaxation recovery could always

be described by a monoexponential curve in all tissue samples from

all groups of cats. The magnetization values from R_2 and $R_{1\rho}$

measurements from edematous white matter, however, could be described

by biexponential decay in most cases (Fig. 23). In these data the

sum of squares for the residuals for a mono- and bi-exponential fit

to the data demonstrated a much improved fit if two exponentials were

employed. Areas of mild peritumor edema in samples from group II

animals, however, could not be described by multiexponential

transverse relaxation decay. On the other hand, all samples of white

matter from cats with TET edema showed this type of decay (Table 10).

The slow component of the relaxation decay (R_{2s}) for peritumor edema

was significantly different from that of TET edema. Grey matter

samples including those from caudate nuclei from groups II and III

could be described by a single-exponential transverse relaxation

decay. $R_{1\rho}$ could not be measured in the group of cats with brain

tumors; in cats with TET intoxication it showed similar

characteristics to R_2 (Table 9).

Table 7. Longitudinal relaxation rate of brain samples from the three groups of cats.

Sample	Control(s^{-1})	n		Tumor(s^{-1})	n	TET(s^{-1})	n
WM	1.06±0.04	(16)	L	1.14±0.06	(17)	0.91±0.09	(32)*
			R	0.70–1.20	(18)+		
GM	0.67±0.03	(8)	L	0.72±0.07	(6)	0.70±0.02	(10)‡
			R	0.69±0.03	(6)		
Caudate	0.71±0.02	(4)	L	0.70±0.01	(4)	0.70±0.02	(10)
			R	0.69±0.01	(4)		

WM = white matter, GM = grey matter

L = left hemisphere, R = right hemisphere

* Significantly different from control, p<0.001

+ The range is given instead of the mean because the data is skewed by variation in size of tumor.

‡ Significantly different from control, p<0.025

Table 8. Transverse relaxation rates of brain samples from the three groups of cats.

	Groups		
	Control(s^{-1}) n	Tumor(s^{-1}) n	TET(s^{-1}) n
WM	12.79±0.38 (16)	L 13.15±0.66 (17) R 7.91–14.10 (17)[+‡]	10.96±1.50 (36)[*‡]
GM	11.13±0.32 (7)	L 11.84±0.83 (6)[★] R 11.82±0.65 (6)[☆]	11.50±0.64 (10)
Caudate	12.18±0.45 (5)	L 12.09±0.36 (4) R 11.80±0.27 (4)	11.94±0.74 (10)

WM = white matter, GM = grey matter

L = left hemisphere, R = right hemisphere

* Significantly different from control, $p < 0.001$

+ The range is given instead of the mean because the data is skewed by variation in size of tumor.

‡These values represent a weighted average of a two-component relaxation decay.

★Significantly different from control, $p < 0.05$

☆Significantly different from control, $p < 0.025$

Table 9. Longitudinal relaxtion rates in the rotating frame measured at
5 kHz for brain samples from control and TET-intoxicated cats.

	Group			
	Control	n	TET	n
WM	9.10 ± 0.48	(16)	7.98 ± 1.09	(29)[*+]
GM	7.95 ± 0.33	(7)	8.21 ± 0.31	(8)
Caudate	8.74 ± 0.61	(5)	8.61 ± 0.71	(7)

WM = white matter, GM = grey matter

* These values represent a weighted average of a two-component
relaxation decay.

+ Statistically different from control, $p < 0.001$

Table 10. Comparison of components of two-exponential transverse relaxation decay obtained _in vitro_ in samples of edematous white matter.

	Peritumor edema (n=12)	TET edema (n=36)	p
R_{2s} (slow component), s^{-1}	5.26±1.89	3.83±0.81	<0.012
R_{2f} (fast component), s^{-1}	12.82±2.50	13.70±1.49	n.s.
%f (amount of signal contributing to R_{2f})	78±8	72±5	<0.012

Control values of R_2 determined in vitro are compared with R_2 values determined in vivo at day 0 for each group of cats in Fig. 24. There was no difference in the R_2 of white matter measured in vitro and in vivo; however, for areas of grey matter the in-vitro values were significantly lower than those obtained in vivo.

In each group of animals the ROI within the NMR image were selected to match the regions later sampled for in-vitro relaxation measurements, namely grey and white matter from specific areas in each hemisphere. Employing a set of eight data points (one from each echo) in-vivo, and in-vitro R_2' rates were computed and compared. Although a tendency was observed towards higher in-vitro values relative to their in-vivo counterparts, no statistically significant difference was established between the two R_2' determinations from areas of white matter in the normal cats or from the unaffected hemisphere of the cats with brain tumors. The in-vitro R_2' values, however, were significantly greater than those determined in vivo for both peritumor and TET-induced edema (Figs. 25 and 26).

In two cats of group III, when a 16-echo MSE imaging sequence was used, it was possible to establish two component exponentials in the decay of the transverse magnetization. The various components of this two-exponential decay for both in-vivo and in-vitro measurements are given in Table 11. It is of interest to note the marked difference in the rates of decay and in their relative contributions (p < 0.001). Of importance was the finding that the weighted average of R_2 was about the same for both in-vitro and in-vivo measurements.
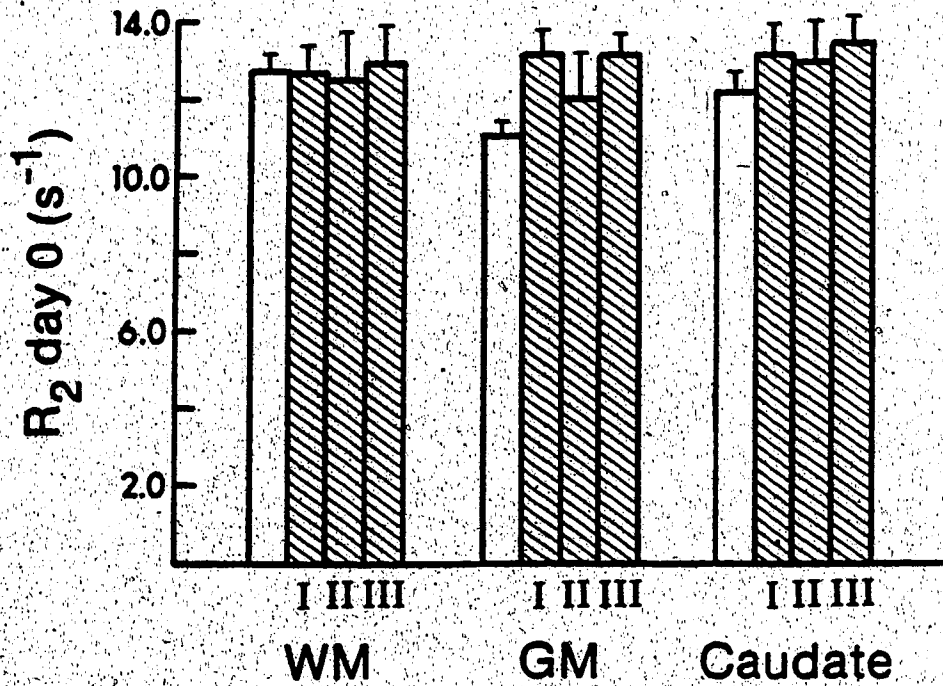
Figure 24. Comparison of control values of the transverse relaxation rate obtained _in vitro_ (empty bars) with similar values obtained _in vivo_ at day 0 for the three groups of cats (hatched bars). I: control cats, II: cats to be subjected to brain tumor implantation, and III: cats to be injected with TET. WM - white matter, GM - grey matter, caudate - head of caudate nuclei.
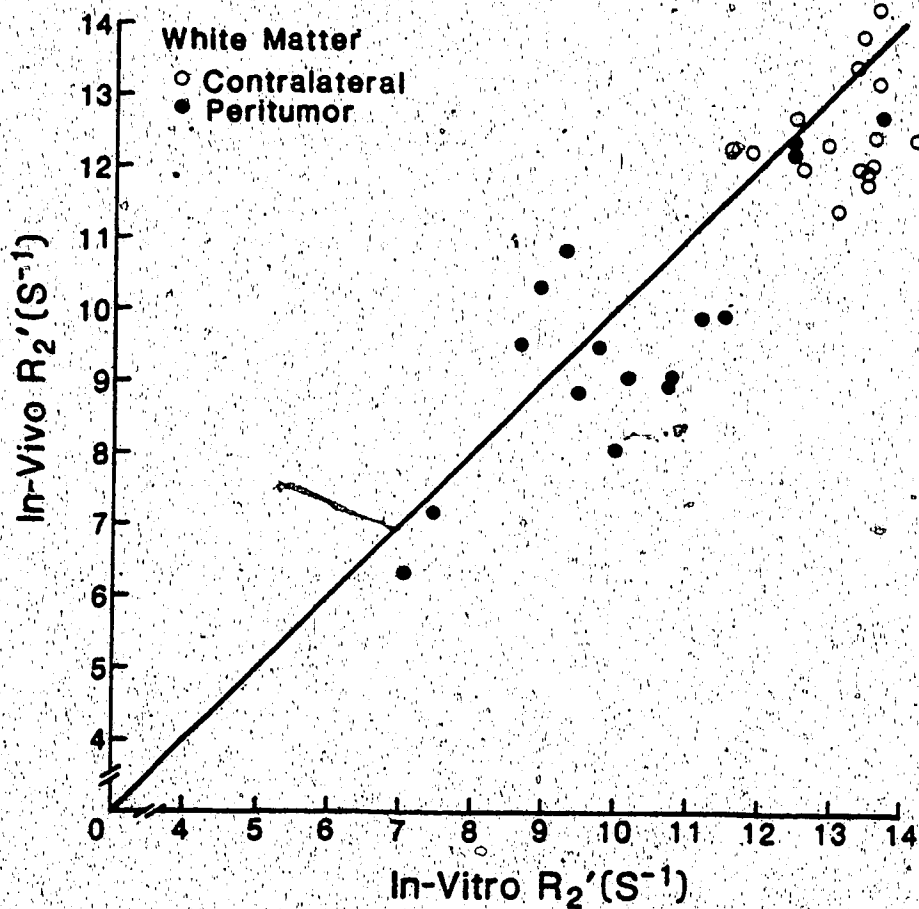
Figure 25. Comparison of transverse relaxation rates obtained
in vivo and in vitro in white matter of cats with brain tumors.
The solid line represents the line of identity and shows that
the in-vitro R_2' values are slightly greater than the in-vivo
ones. The difference, however, was only statistically
significant for R_2' values from peritumor white matter.

Figure 26. Comparison of transverse relaxation rates obtained
in vivo and in vitro in white matter of control and TET-
intoxicated cats. The solid line represents the line of
identity and shows much greater R_2' values in vitro than in vivo
for samples from TET-intoxicated animals but not from controls.

Table 11. Comparison of in-vitro and in-vivo components of biexponential transverse relaxation decay from edematous white matter of cats with TET intoxication.

	In-vitro white matter edema (n=12)	In-vivo white matter edema (n=12)	p
R_{2s} (slow component), s^{-1}	3.97±0.41	2.69±0.19	<0.001
R_{2f} (fast component), s^{-1}	14.03±1.35	16.76±1.63	<0.001
%f (amount of signal contributing to R_{2f})	72±5	66±5	<0.005
Weighted average of R_2, s^{-1}	11.32±1.46	11.88±1.10	n.s.

3f. __Effect__ __of__ __tissue__ __water__ __content__ __on__ __the__ __relaxation__ __rates__ __in__ __vitro__

Significant increases in water content of edematous white matter were observed. Also, a statistically significant decrease in water content of the white matter of the unaffected hemisphere of cats with implanted tumors was detected. There was a marginal decrease of water in the grey matter of cats with brain tumors and TET intoxication (Table 12).

The period elapsing during the __in-vitro__ determination of relaxation rates did not affect tissue water content as shown by the similarity in water content between tissue samples subjected to __in-__ __vitro__ NMR measurements and samples frozen immediately after weighing.

The biexponential relaxation data were transformed into a single value by obtaining a weighted average of the two rates of decay. The resultant R_2 of edematous white matter from groups II and III was plotted against the dry-tissue content (Figs 27 and 28). Linear regression analysis was performed giving the gradients of sensitivity of R_2 to water content in the two groups (G_2) that are shown in Table 13. Multiple linear regression analysis showed no significant difference in sensitivity of R_2 to dry-tissue content between the two types of edema.

Plotting R_1 against ratio of dry-tissue content showed a good correlation for all the samples of tissue studied. Its sensitivity, however, is about 14 times less than that of transverse relaxation. R_2 and $R_{1\rho}$ correlated with water only when a single type of tissue was employed (Figs 27 and 28).

Table 12. Water content of brain samples (in g H_2O /g dry wt) from the three groups of cats.

	Group					
	Control	(n)	Tumor		(n)	TET	(n)
WM	2.02+0.17	(28)	L 1.83+0.15	R 1.77-3.27	(17)[*] (17)‡	2.58+0.49 (36)[+]
GM	4.36+0.33	(18)	L 4.06+0.37	R 4.07+0.25	(6)[*] (6)★	4.13+0.27 (12)★
Caudate	4.11+0.20	(10)	L 4.03+0.15	R 4.01+0.17	(4) (4)	4.04+0.32 (12)

WM = white matter, GM = grey matter

* Signficiantly different from control, p<0.05

+ Significantly different from control, p<0.001

‡ The range is given instead of the mean because the data is skewed by variation in size of tumor.

★ Significantly different from control, p<0.025
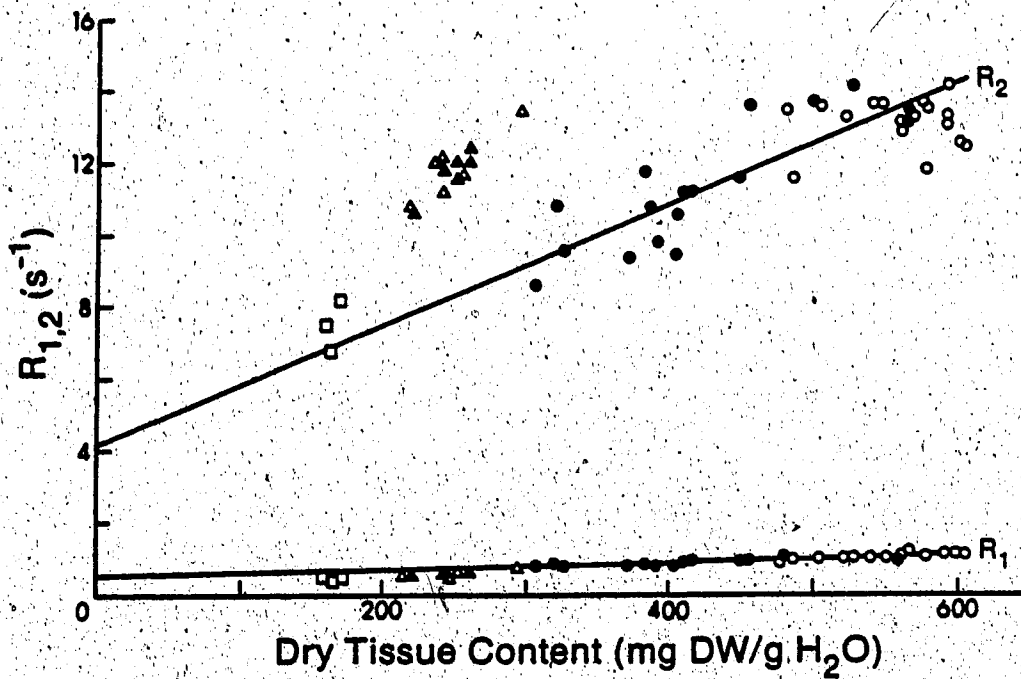
Figure 27. Relationship between longitudinal and transverse relaxation rates and dry tissue weight (DW) : water content ratio in brain samples of cats with implanted 9L glioma tumors. (For clarity not all points are shown.) The straight lines represent the least squares fit to peritumor white matter values only (●). Unaffected contralateral white matter (O), peritumor grey matter (▲), unaffected contralateral grey matter (△), and tumor (□).
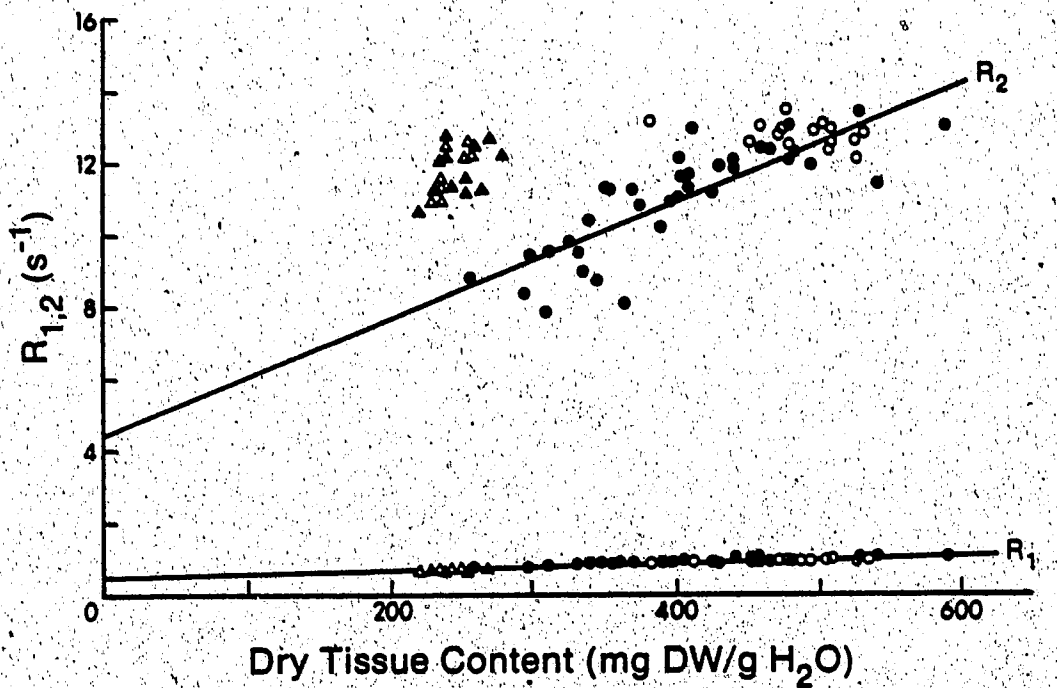
Figure 28. Relationship between longitudinal and transverse relaxation rates and dry tissue weight (DW) : water content ratio in brain samples of control and TET-intoxicated cats. (For clarity not all points are shown.) The straight lines represent the least squares fit to edematous white matter values only (●). Control white matter (○), grey matter of TET-intoxicated cats (▲), and grey matter of control cats (△).

Table 13. Gradients of sensitivity (G_2) of transverse relaxation to
tissue dry wt:water content ratio in areas of peritumor and
TET-induced white matter edema.

	Peritumor edema (n=12)	TET edema (n=36)	p
G_2, s^{-1}/gDW/gH$_2$O	17.00±3.13	16.27±2.01	n.s.
Intercept, s^{-1}	4.14±0.40	4.43±0.20	n.s.
r	0.814	0.812	----

3g. <u>Tissue protein content</u>

Total and soluble protein content in various regions of the brain (Table 14) showed no change from control in cats with TET-induced edema. In animals with peritumor edema, however, even with very small tumors, protein content was elevated in nearly all samples of edematous white matter. The difference in protein content of peritumor and contralateral grey matter displayed a tendency to increase especially in cats with larger tumors.

The total protein content from peritumor samples of white matter was transformed into units per fresh weight and plotted against the corresponding rates of transverse relaxation. No correlation was observed, which suggests that changes in tissue protein content of edematous white matter do not have an appreciable effect on the averaged transverse relaxation rate.

The SDS-PAGE gels demonstrated a very small amount of albumin in normal brains; i.e., approximately 4% and 3% of the total protein in grey and white matter respectively (Fig. 29). Similarly, in cats intoxicated with TET, there was no change in albumin content from control values (Fig. 30). In group II animals, however, there were marked increases in albumin in both peritumor grey and white matter (Figs. 31--33). The differences in protein and water content between peritumor and contralateral white matter were taken as the increase in protein and water induced by the edematous process. Linear regression analysis of these values showed good correlation (Figs. 34--36).

Table 14. Protein content in brains of the three groups of cats

	Total protein (mg/g DW)	(n)	Soluble protein (mg/g DW)	(n)
Normal WM	132 ± 25	(26)	29 ± 10	(25)
Peritumor WM*	101 – 268	(17)	26 – 83	(17)
Contralateral WM	126 ± 19	(17)	27 ± 8	(17)
TET WM	130 ± 19	(36)	39 ± 31	(30)
Normal GM	303 ± 57	(17)	116 ± 38	(17)
Peritumor GM*	281 – 380	(6)	110 – 147	(6)
Contralateral GM	279 ± 28	(6)	110 ± 21	(6)
TET GM	308 ± 40	(12)	115 ± 64	(11)
Normal caudate	315 ± 45	(9)	99 ± 30	(10)
Peritumor caudate*	271 – 374	(4)	134 – 145	(4)
Contralateral caudate	299 ± 19	(4)	120 ± 32	(3)
TET caudate	317 ± 45	(11)	146 ± 65	(11)

WM = white matter, GM = grey matter

* Ranges are given for peritumor tissue because data are skewed by variation in size of tumor
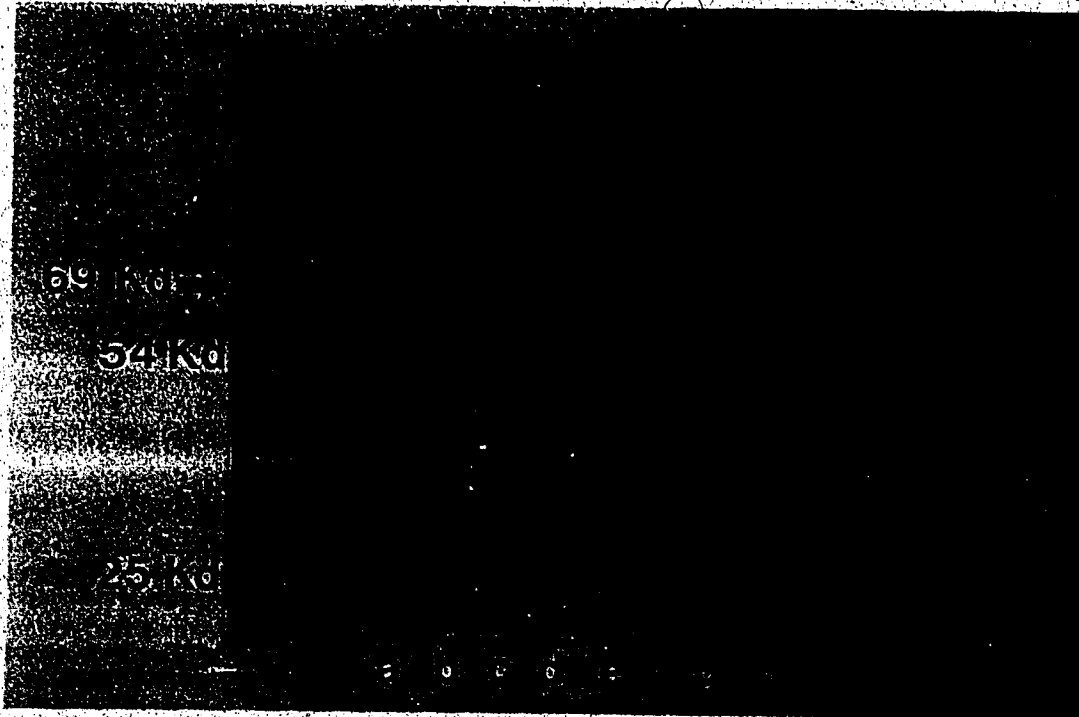
Figure 29. SDS—PAGE gel of tissue homogenates from a control cat.
Molecular weight is shown on the ordinate and each column
represents one sample. (a) Left caudate, (b) right caudate, (c)
left parietal grey matter, (d) right parietal grey matter, (e)
left occipital white matter, (f) right occipital white matter,
(g) left parietal white matter, (h) left parietal grey matter,
(i) left frontal white matter, (j) right frontal white matter.
The albumin band is indicated by the arrows. (kd=kilodaltons)
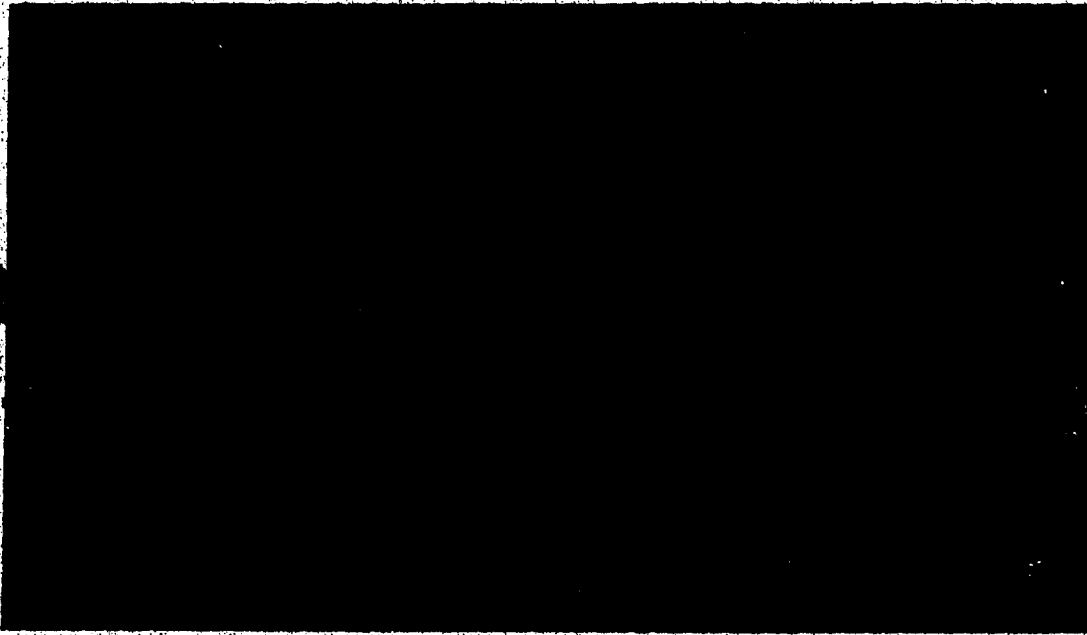
Figure 30. SDS--PAGE gel of tissue homogenates from TET-intoxicated
cats. Molecular weight is shown on the ordinate and each column
represents one sample. (a) Left caudate, (b) right caudate, (c)
left parietal grey matter, (d) right parietal grey matter, (e)
left occipital white matter, (f) right occipital white matter,
(g) left parietal white matter, (h) right parietal white matter,
(i) left frontal white matter, (j) right frontal white matter.
The albumin band is indicated by arrows and does not differ from
that of control animals. (kd=kilodaltons).
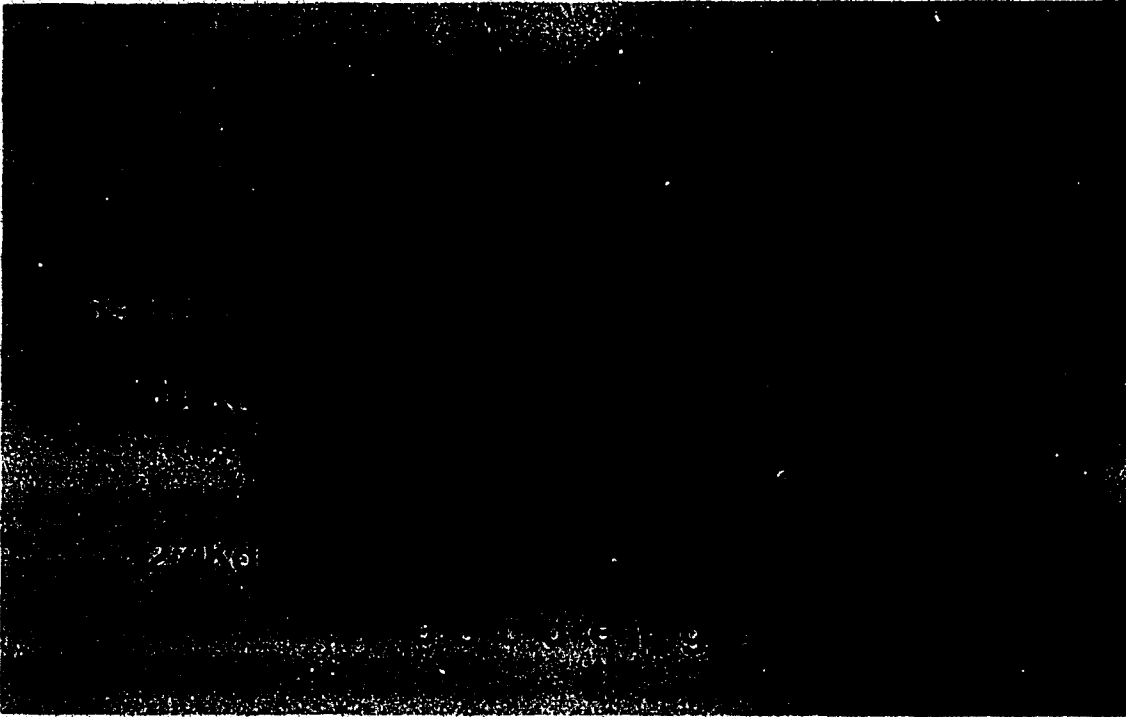
Figure 31. SDS--PAGE gel of tissue homogenates from cats with
implanted brain tumors. Molecular weight is shown on the
ordinate and each column represents one sample. (a) Left
caudate, (b) right caudate, (c) left parieto-occipital white
matter, (d) right parieto-occipital white matter, (e) left
parietal grey matter, (f) right parietal grey matter, (g) left
parietal white matter, (h) left frontal white matter, (i) right
parietal white matter, (j) right frontal white matter, (k)
tumor. Marked increases in albumin are observed in the
peritumor tissues (right side) relative to the unaffected side
(arrows). (kd=kilodaltons)
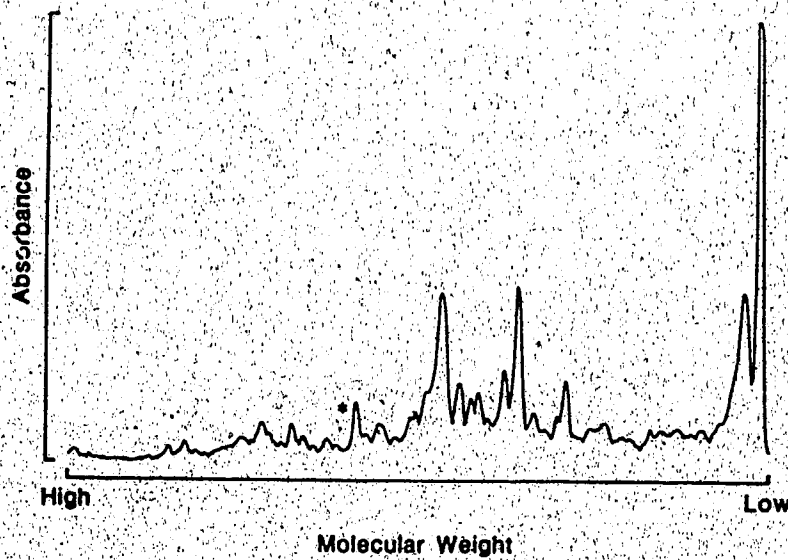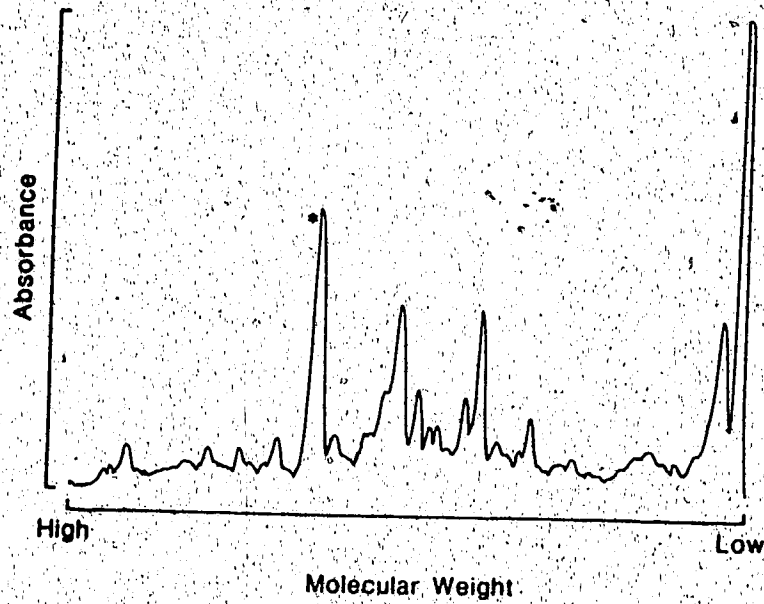
Figure 32. Laser densitometry scans of SDS--PAGE gels of parietal white matter show a marked increase in albumin (*) in the peritumor region (a), relative to the corresponding area of the opposite hemisphere (b).
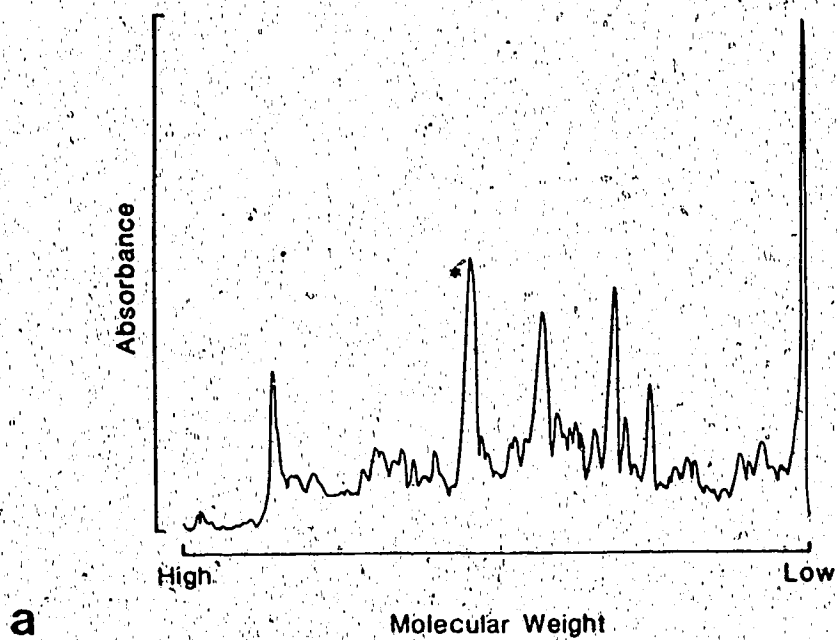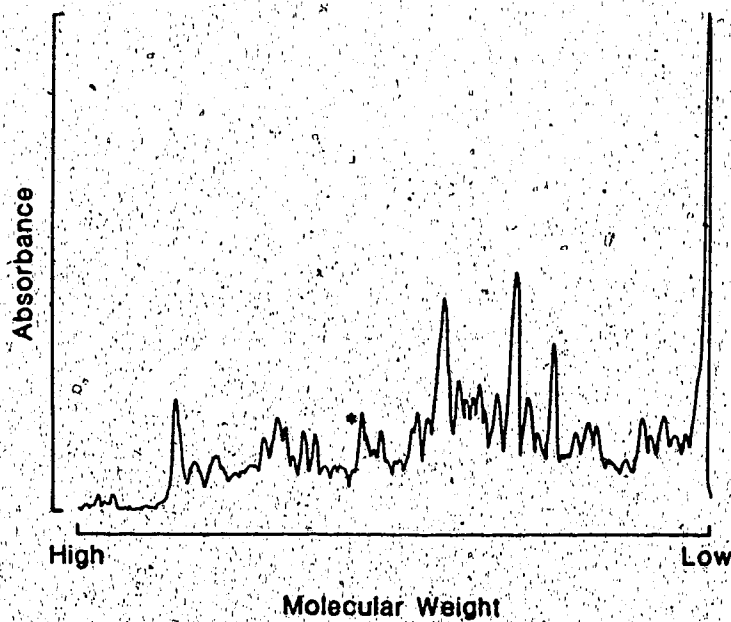
Figure 33. Laser densitometry scans of SDS—PAGE gels of parietal grey matter show a marked increase in albumin (*) in the peritumor region (a), relative to the corresponding area of the opposite hemisphere (b).
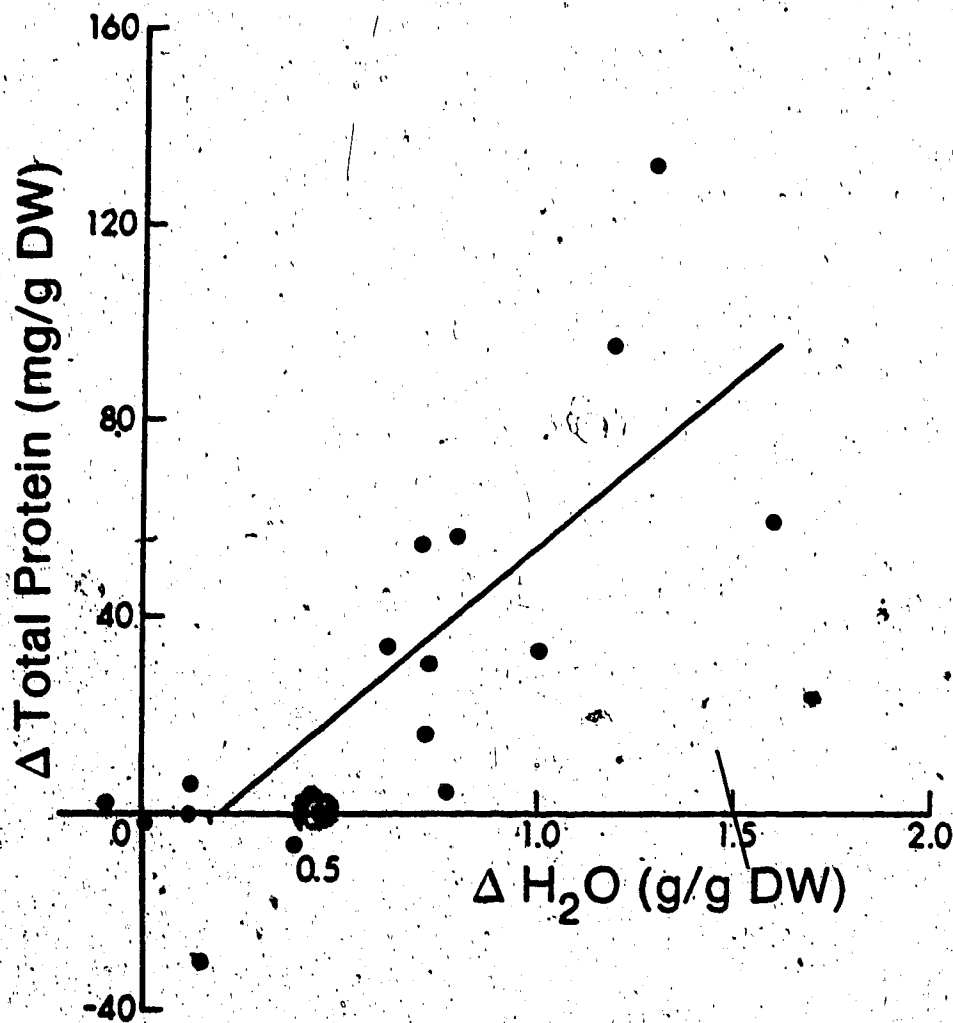
Figure 34. Relationship between the increase in total protein and the increase in water content in regions of peritumor white matter. The relationship is given by: $y = 64x - 14$, $r = 0.788$, $p < 0.01$.
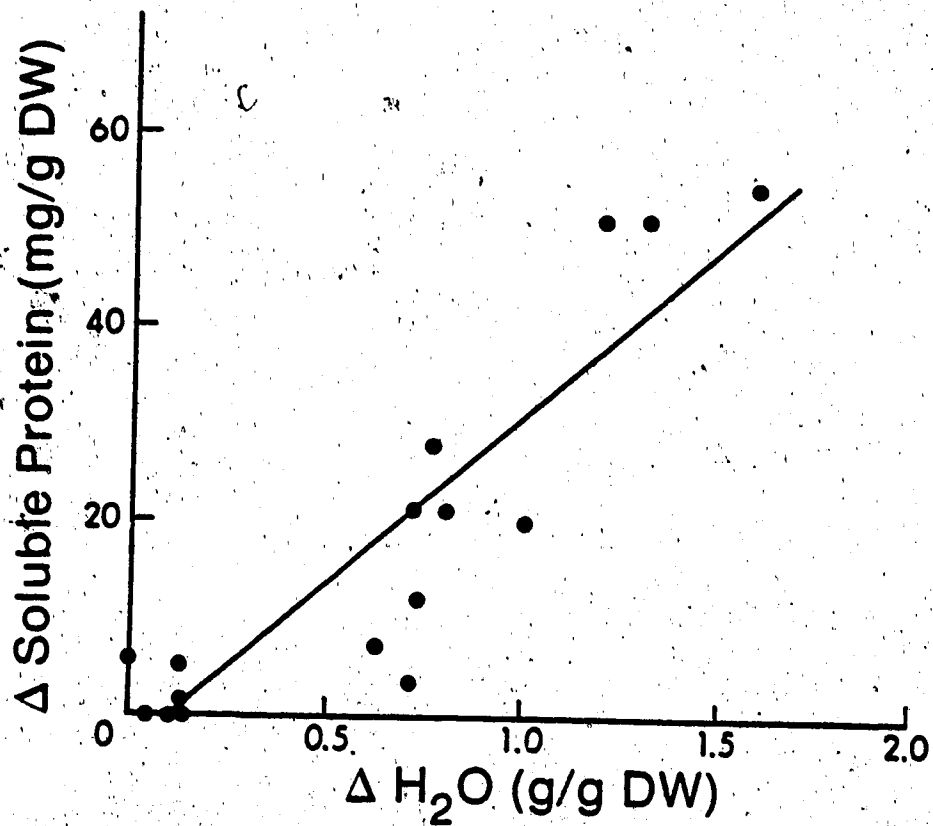
Figure 35. Relationship between the increase in soluble protein and the increase in water content in regions of peritumor white matter. The relationship is given by: $y = 34x - 3$, $r = 0.892$, $p < 0.01$.
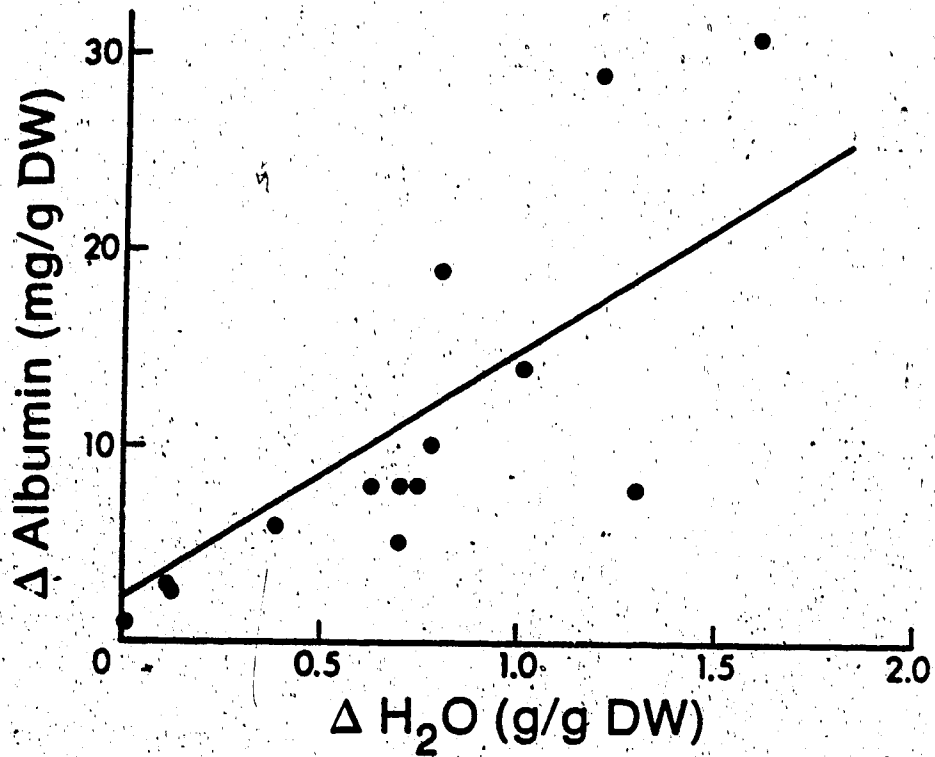
Figure 36. Relationship between the increase in albumin and the increase in water content in regions of peritumor wihte matter. The relationship is given by: $y = 12x + 2$, $r = 0.650$, $p < 0.02$.

In this section the animal models used in this study are evaluated and characteristics of the observed relaxation rates in normal and edematous tissues are discussed. The factors responsible for the similarities and discrepancies observed between in-vitro and in-vivo R_2 are then considered. Finally relationships between relaxation rates and tissue water content and between tissue protein content and tissue water are discussed.

4a. Adequacy for NMR studies of the models of brain edema used in this study .

As judged by the predictability of the tumor take the model of peritumor edema we employed for this study proved reliable. The variation in size of the neoplasms was difficult to predict, however, and several factors are known to contribute to this (Baker et al., 1973; Mennel and Groneck, 1977; Rama et al., 1986). The tumor was probably rejected in one cat. This event has also been observed by Hossmann et al. (1979) employing a similar model of peritumor edema. Partial or complete deposition of tumor cells in the grey matter also affected growth of the tumor with, more importantly, the production of very little edema. This is consistent with observations by Clasen et al. (1962) showing a marked resistance of grey matter to the spread of edema fluid. Another factor responsible for irregular growth of neoplasms is the deposition of varying volumes of cell suspension due to reflux along the needle tract during injection. This was minimized by slow injection of 50 μl over 1 min and use of a

growth observed with the 9L glioma clone may be due to biological change in the cell cultures over time (Baker et al., 1973).

To improve the reproducibility of edema production from implanted tumors, cells should be injected into a specific location by stereotactic techniques. It appears that the centrum semiovale is an appropriate area that allows frontal and occipital spread of the edema fluid, which can be easily detected in proton NMR images taken in the transverse plane.

The larger neoplasms were associated with more extensive edema, probably due to the more numerous abnormal capillaries and hence a larger area of altered permeability within the tumor, although differences in permeability characteristics of the BBB in experimental brain tumors of various sizes have been shown (Groothuis et al., 1982).

The finding of a decreased water content of white matter in the unaffected hemisphere suggests that compression by the tumor mass produces this effect. According to the Monro--Kellie doctrine (see chapter I), the increase in brain mass produced by the tumor must be accompanied by a decrease in volume of CSF, of blood, and possibly of tissue water content of normal structures. Studies by Schettini and Walsh (1973) have shown that when constant pressure is applied to the surface of the brain, its resistance to the applied pressure decreases with time. Because the rate of decrease of resistance was faster in normal than in edematous brain, they concluded that a mass lesion produces displacement of water. This is in accord with our

decrease in water content of unaffected white and grey matter.

More relevant to the present study is the fact that in this model the cerebral tumor is associated with vasogenic edema. The marked increases in protein and particularly in albumin confirm the origin of the edema fluid from plasma. It has been shown that the site of protein extravasation is within the tumor (Hossmann et al., 1979), although increased permeability of capillaries in the tissue adjacent to the tumor may also account for the production of edema (Yamada et al., 1983). Our findings are in agreement with those of Hossmann et al. who showed that the edema spread was limited to the white matter of the affected hemisphere and did not cross to the opposite side through the corpus callosum. The BBB in this type of lesion shows structural alterations due to the formation of new capillaries that lack tight junctions (Vick, 1980), resulting in continuous escape of plasma into the surrounding tissue. Such accumulation of fluid causes both compression of the microvasculature and increased inter-capillary distance leading to tissue hypoxia, which adds a component of cytotoxic edema to peritumor edema (Reulen et al., 1972). This complication might have precluded discrimination between cytotoxic and vasogenic edema employing quantitative proton NMR. As will be shown later, however, this technique may be able to provide enough information to allow differentiation between the two types of edema.

Intoxication with TET bromide resulted in a very reproducible and reliable induction of brain edema in cats. Injection of

matter in 48--72 hr. In the present study it was demonstrated that

TET edema is of the cytotoxic type as shown by the increase in water

in the absence of serum protein changes. This disagrees with the

findings of Kalsbeck and Cumings (1963) that showed an increase in

albumin content of white and grey matter in cats with TET edema.

Most investigators, however, have demonstrated that the permeability

of the BBB to tryphan blue (Aleu et al., 1963), or to ^{131}I-labeled

albumin (Bakay, 1965), or to FTIC-dextrans of molecular weights

ranging from 3000 to 70,000 (Hulstrom et al., 1984) remains unaltered

in this condition and that TET intoxication produces exclusively

cytotoxic edema.

A marked increase in tissue water content of white matter, but

not of the grey matter, has been reported previously (Aleu et al.,

1963). We found edema to be more severe in the subcortical U-fibers

of white matter, which confirms the findings of Aleu et al. and

Watanabe (1977). The fluid that accumulates is restricted to the

intraperiod line of myelin and is isolated from the rest of the

tissue (Hirano et al. 1968; Katzman et al., 1963). Kalsbeck and

Cumings (1963) reported that of six cats that they injected

repeatedly with TET at intervals of one week, two died after

injection without showing clinical signs. In the group of TET-

intoxicated cats of this study, the two animals that died showed

severe signs of neurological dysfunction such as quadriparesis,

urinary and fecal incontinence, a depressed state of consciousness,

and respiratory rhythm abnormalities. This form of edema is not

basis for differentiating vasogenic from cytotoxic edema. Clinical examples of cytotoxic edema with similar characteristics as those produced by TET intoxication are Reye's syndrome, Canavan's disease, and intoxications with isonicotinic acid hydrazide, cuprozine, or hexachlorophene. These findings indicate that the present model of cytotoxic edema is an appropriate one to use in proton NMR studies; however, it is important to note that the injection of cats with TET produces severe morbidity.

4b. <u>Proton NMR relaxation characteristics in tissues</u>

4b.1. <u>Normal tissues</u>

A single exponential recovery or decay process could characterize adequately all the normal brain tissue samples we studied. This finding has been reported by several researchers (Bakay <u>et al</u>., 1975; Go and Edzes, 1975; Naruse <u>et al</u>., 1982; Kamman <u>et al</u>., 1984; Moseley <u>et al</u>., 1984). In the case of white matter it might be expected that the lipids of myelin could give rise to a multiexponential type of relaxation. The very small lipid signal detected in the proton NMR spectra from white matter in this study suggests that the lipid contribution to the relaxation was probably overwhelmed by that of the water signal. A similar conclusion has been reported by Kamman <u>et al</u>. (1984).

The TEFE model of proton relaxation has been used to explain the characteristics of water in tissues by many researchers (Kirikuta

this model it can be predicted that the monoexponential relaxation is
due to rapid exchange of water molecules between those existing in a
free environment and those in an environment associated with
macromolecules. In tissues the associated environment must be highly
heterogeneous owing to the complexity of the cell constituents and,
due to the fast exchange condition, the relaxation rates should
provide information about the average molecular motion of all water
molecules in biological systems (see chapter III for a discussion on
relaxation rates in normal tissues).

4b.2. Pathologic tissues

Grey matter in animals with brain tumors or with TET
intoxication showed magnetization recovery and decay processes that
could be described by a monoexponential curve. In edematous white
matter, however, a biexponential curve described the transverse
magnetization decay more adequately. Several authors have observed a
biexponential decay of the transverse magnetization in studies of
animal models of white matter edema (Bakay et al., 1975; Go and
Edzes, 1975; Naruse et al., 1982). Studies by Moseley et al.
(1984), however, showed monoexponential behavior of the transverse
magnetization in samples of brain from rabbits 5 hr after being
subjected to cryo-injury. This is probably due to their employing a
limited observation time of 7—91 ms in the CPMG sequence. Our study
shows that the transverse magnetization decay in the first 100 ms can

be adequately described by a single exponential curve even when there

is severe edema present as in TET intoxication (Figs. 22,23, and 37).
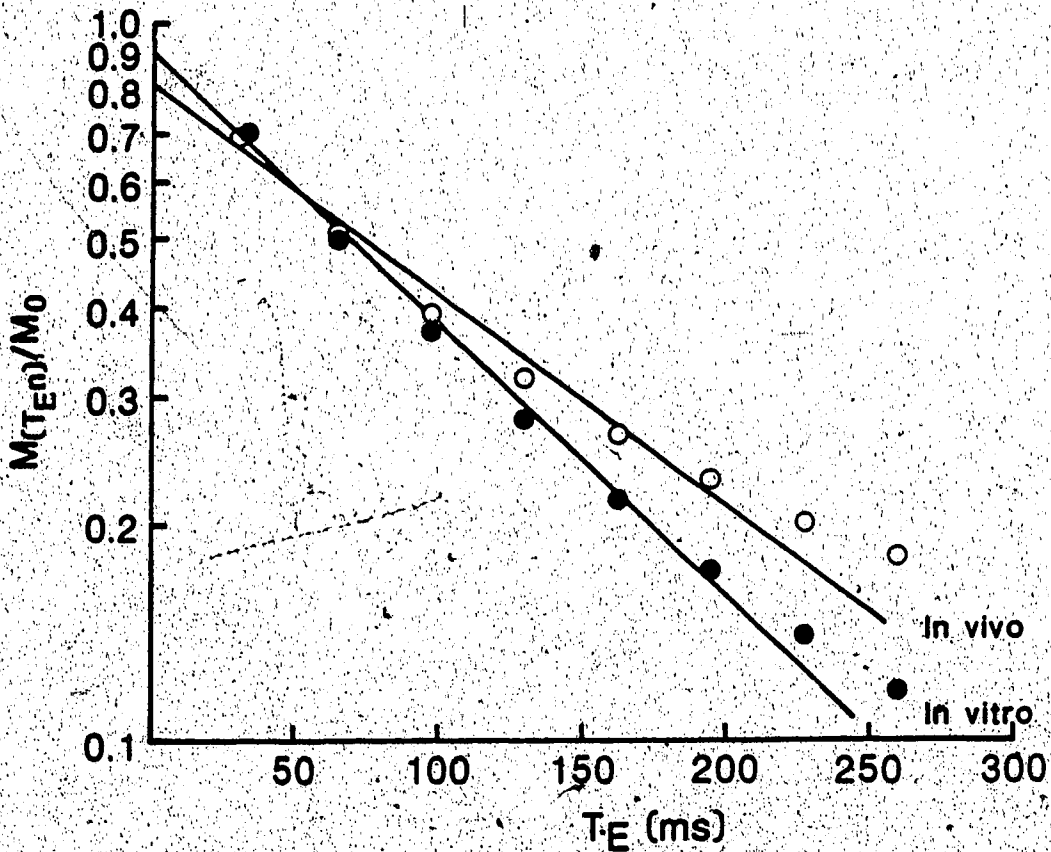
Figure 37. Normalized transverse magnetization decay in vivo (○) and in vitro (●) plotted against T_E for white matter of cats with TET intoxication. The lines represent the non-linear least squares fit to the data employing a single exponential term in the equation. The slopes of these lines represent R_2' and show that the marked difference between in-vivo and in-vitro R_2' values is due to postmortem effects on the rates and weightings of two components of the magnetization decay.

The biexponential behavior of the transverse, but not the longitudinal, relaxation in edematous white matter probably depends upon the following factors. First, the sensitivity of the transverse relaxation to very slow molecular motion suggests that diffusion of water may play an important role, as has been indicated by the studies of Belton et al. (1972), Diegel and Pintar (1975), and Rutsgi et al. (1978). Moreover, these investigators have tentatively assigned each of the component relaxation rates to proton NMR signal arising from intra- and extracellular spaces. The difference in rates from each compartment is determined by the relative proportion of associated water in the various compartments as suggested by Diegel and Pintar. Second, the much greater sensitivity of the transverse compared with the longitudinal relaxation (i.e., more than 10 times, see Figs. 27 and 28) implies that if there are contributions from more than one component each with different decay constants, they are more likely to be missed when R_1 rather than R_2 is measured.

Physiologically, the presence of two exponential components in edematous white matter may be due to: (1) a change in relative size or in rate of relaxation of a compartment that undergoes slow exchange of protons with the surrounding tissue allowing two components to be resolved with the NMR techniques employed for this study, (2) the creation of an additional compartment that undergoes slow exchange of protons with the rest of the tissue, (3) a decrease in the rate of water exchange between two compartments that normally

show a rapid exchange of water molecules, or (4) a combination of these.

It is possible that a change in the size and/or the rates of relaxation of a second component could not have been detected in normal tissues due to its small contribution or the similarity of its relaxation rate to that of the other component. Under the signal-to-noise conditions associated with the NMR technique, the R_2 of each component would have to differ by a factor of about 3 or more to be detectable (Koenig et al., 1984). If the contribution of one of the components is small (i.e., 5--10%) even though the rates of decay vary by a factor of about 3, then a single exponential decay curve will adequately describe the data.

An example of an additional compartment created in regions of white matter is that of edema induced by intoxication with TET. Here, there is vesicle formation in the intraperiod line of myelin which is physically separate from the surrounding tissue (Hirano et al., 1968, Katzman et al., 1963). Thus, to explain biexponential transverse relaxation, it is necessary to assume that this compartment is associated with a substantial restriction of the diffusion of water between the myelin vesicles and the rest of the brain.

Decrease in rate of water exchange between compartments is an interesting possibility because brain edema is recognized as a disturbance in fluid homeostasis due to disruption of the normal function of cell membranes. If the two components of relaxation arise from the intra- and extracellular spaces, then an alteration in

membrane characteristics may be responsible for changes in water transfer between these two compartments. A more detailed discussion of this topic is given in Chapter III, section 2.

Notwithstanding the complexity of the factors responsible for transverse relaxation decay in edematous white matter samples, vasogenic and cytotoxic edema could be differentiated, at least in these animals. We assume that the slow component, R_{2s}, corresponds to proton signal arising from the extracellular fluid in the peritumor white matter of Group II cats, or from myelin vesicles in cats with TET-induced edema. As macromolecules are the main determinants of relaxation in edema fluid (see Study A, Discussion), the protein-rich fluid in the peritumor white matter could be expected to have a more efficient relaxation than the protein-poor fluid in the white matter of cats intoxicated with TET. That this was indeed the case is shown by the markedly different R_{2s} in both groups of cats (Table 10). Hence, we suggest that R_{2s} can be used to discriminate between vasogenic and cytotoxic edema.

4c. Comparison of R_2 in vivo and in vitro

We observed that R_2 for normal white matter was similar when measured in vivo and in vitro. A single exponential curve was used to fit the transverse magnetization decay of edematous white matter. The resultant R_2 for in-vivo measurements differed from that obtained in vitro. Also, the R_2 measured in grey matter from control cats in vivo was different from that in vitro. In this subsection factors that might have been responsible for the similarities and

discrepancies between the R_2 measured in images and in tissue samples are discussed.

4c.1. <u>Factors affecting measurement of R_2 in vivo</u>

Partial volume artifacts, obtained when two or more types of tissue with different values of R_2 occur in the same ROI, may be a significant problem with measurements in white matter. Similarly, in grey matter the convoluted nature of the cortex contributed markedly to such artifacts. Due to the smaller R_2 of either CSF or edematous white matter that can occur within a ROI when the measurement of the R_2 of grey matter is attempted, a smaller value of R_2 would be expected <u>in vivo</u> than <u>in vitro</u>. Because the opposite case was observed, it appears that partial volume artifacts did not contribute significantly to the difference in R_2 of grey matter observed <u>in vivo</u> and <u>in vitro</u>.

Another difficulty which could arise with proton NMR imaging is the effect on the signal intensity of incomplete magnetization recovery. If the T_R is very short, the magnetization recovery will be incomplete and the measurement of R_2 <u>in vivo</u> will be affected by a low signal-to-noise ratio. For our imaging sequence we employed a T_R of 4.3 s which allows a magnetization recovery of >95% for normal grey and white matter, and for edematous white matter. As a result, the signal-to-noise ratio was maximized.

The MSE imaging sequence employed in Study B is a modification of the CPMG sequence used for measurement of R_2 <u>in vitro</u>. This modified sequence differs from the standard CPMG sequence in two

important respects. First, in the latter 'hard' RF pulses with a broad frequency band are employed, whereas in the MSE sequence an initial 90° 'soft' RF pulse of a narrow frequency band is used to define the slice for imaging. The 180° pulses subsequently used are hard RF pulses similar to those used in the CPMG sequence. A drawback with the 90° soft pulse is that it induces variations in the tip angle of proton magnetization from one edge of the imaging slice to the other (Rosen et al., 1984). Second, with the MSE sequence, in addition to the soft pulse a magnetic field gradient is also required to define an imaging slice. This gradient results in the molecular diffusion processes contributing more to the dephasing mechanism responsible for transverse magnetization than they do with the CPMG sequence. Because of these factors equation (6) must be modified to the following:

$$A(T_En) = \int_{z = -\infty}^{\infty} \{A(z)\ \sin[\delta(z)]dz\} \cdot \exp(-R_2 \cdot T_En) \cdot \exp[-(D/3)\ \gamma^2 G^2 (T_E/2)^2]\quad (13)$$

where z is the direction normal to the slice plane, δ is the tip angle of the soft pulse, D is the translational diffusion coefficient, and G is the gradient strength.

The term $\{A(z)\ \sin[\delta(z)]dz\}$ in equation (13) indicates that tip angle variations across the slice induced by the 90° soft pulse result in a reduced amplitude of the NMR signal compared to that obtained with 90° hard pulses, and that this amplitude is independent of both T_E and the echo index. Hence, the use of soft 90° pulses in conjunction with hard 180° refocusing pulses for imaging gives a

decay of the echo amplitude that is similar to that obtained with the CPMG sequence.

The diffusion term [$(D/3) \gamma^2 G^2 (T_E/2)^2$], however, might have a more important effect on R_2 measurements in NMR images. Fitting the echo amplitudes to an exponential decay curve would result in an apparent value for the relaxation rate, $R_2^\wedge$, (Abragham, 1983) given by

$$R_2^\wedge = R_2 + [(D/3) \gamma^2 G^2 (T_E/2)^2] \qquad (14)$$

where R_2 is the actual transverse relaxation rate of the sample.

Values for the translational diffusion coefficient, D, of solutions are of the order of 2.2 x 10^{-5} cm^2/s (Fung and Puon, 1981), whereas values measured in tissue (e.g., muscle) where diffusion is restricted, are of the order of 1.2 x 10^{-5} cm^2/s (Fung and Puon, 1981). Substituting the higher value of D, a typical gradient strength of 0.3 G/cm and a $T_E/2$ of 16.25 ms in equation (12) we obtain: $R_2 + 0.003$ s^{-1}. Thus, even allowing for an increase in diffusion rate with a higher temperature, this contribution is insignificant compared with error in the measurement of R_2. Therefore, the effects of using two techniques were ruled out as a significant cause in R_2 measured in vivo and in vitro.

4c.2. Factors affecting the measurement of R_2 in vitro

In the in vitro procedure, samples were kept on ice except for the 30--40 min of the NMR measurements, and relaxation was determined at 2 hr, and at approximately 11--12 hr, postmortem. As the R_2 did

not vary during this period we considered the effect of storage on water--macromolecule interaction to be negligible. Changes in water content during this period were assessed by freezing a number of samples from control animals immediately after extracting the brain. As no difference was observed between these and the samples subjected to NMR measurements we concluded that the NMR procedure does not cause alterations in water content. On the other hand, the smaller R_2 in vitro than in vivo obtained at day 0 for grey matter and caudate nuclei (Fig. 24) may be due to an uptake of fluid by these tissues during preparation of the samples. It is known that when cortical blood flow decreases to below 10--15 ml/100g/min, a rapid increase in water content of the cortex occurs (Schuier and Hossmann, 1980). In our study, perfusion of the brain at hydrostatic pressures above normal may have contributed to water uptake by the grey matter. White matter appears not to be markedly affected by the preparation of samples (Fig. 24).

A likely explanation for the difference between the in-vitro and in-vivo R_2' rates may be the changes that result from death of the animal. These include shifts of water from the extracellular to the intracellular space, which affect the rates and weightings of the observed biexponential decay of the transverse relaxation. A fuller discussion of this is given in Chapter III, section 2.

4d. <u>Relationship between relaxation rates and water content of</u> <u>tissues</u>

Hazlewood (1979), after a comprehensive review of the literature on measurements of proton relaxation rates in tissues, concluded that the TEFE model describes adequately the NMR relaxation of protons in tissues (see Chapter III, section 2). Moreover, he pointed out that the environment of associated water molecules are the main determinants of proton relaxation in tissues, and that the amount of water in this environment is proportional to the dry-weight content of a tissue sample. Thus, we employed the reciprocal values of water content per unit of dry weight (dry-tissue content) in determining the effect of changes in water content of edematous white matter on the relaxation rates.

The variation of relaxation rates with dry-tissue content showed a very good correlation. The longitudinal relaxation rate could be used as an index of dry-tissue content irrespective of the type of brain tissue employed (similarly, the relaxation rates can be used as an index of water content within the range observed in white matter edema when this is expressed as water weight per unit of fresh tissue, i.e. percent water content). Although the sensitivity of R_1 to small changes in water is very low, it still provides for reliable discrimination between normal white matter and moderate to severe edema. The application of <u>in-vivo</u> R_1 measurements to the clinical situation is, however, limited by several factors, one of the more important being the excessively long acquisition time required to generate the number of images used in calculating R_1 (Pykett <u>et al.</u>,

1983). Measurement of $R_{1\rho}$ from images is subjected to the same limitations as that of R_1; furthermore, the possible effect of depositing in subjects large amounts of RF energy required to obtain an $R_{1\rho}$ image have yet to be determined.

Correlations of the averaged values of R_2 and $R_{1\rho}$ with dry-tissue content were only observed when a specific type of tissue was used (Figs. 27 and 28). Correlations of these parameters emplying different tissues was unsatisfactory. For example, the dry-tissue content of normal grey matter was 46% of that of normal white matter, whereas its averaged R_2 was 87% of that of white matter. By comparison, the dry tissue content of edematous white matter was 78% of that of normal white matter and its R_2 was 86% of normal (Tables 8 and 12). If water content was the only factor responsible for the observed relaxation rates, it would be expected that the marked difference in water content between normal grey and white matter would result in a greater difference in their relaxation rates when compared to those differences between normal and edematous white matter. Therefore, other factors that affect R_2 and $R_{1\rho}$ but not R_1, such as slow diffusion of water or the effect of certain paramagnetic agents such as manganese (Tingey, 1937; Koenig and Brown, 1984) probably account for such differences.

Studies performed on a variety of biological tissues from different species suggest that relaxation parameters depend primarily upon the total water content of tissues (Kirikuta and Simplaceanu, 1975; Inch et al., 1974; Saryan et al., 1974; Eggleston et al, 1975; Fung, 1977; Baker and Vriend, 1983). Others, however, have not found

such a relationship (Ranade et al., 1976; Hazelwood et al., 1974).
Studies of cerebral edema in experimental animals show that the
relaxation rates correlate closely with tissue water content (Bakay
et al., 1975; Go and Edzes, 1975; Naruse et al., 1982). Our studies
support the latter finding if the relaxation rates are plotted
against g of water per 100 g of fresh tissue or, as shown in Figures
27 and 28, if relaxation rates are plotted against dry-tissue
content.

An unexpected but important finding was the similarity in the
sensitivity of the averaged transverse relaxation rate to dry-tissue
content of the samples of edematous white matter in both groups of
experimental animals (Table 13). The increase in water and serum
proteins that occur in peritumor edema have opposite effects on the
relaxation rates, i.e., an increase in water decreases the relaxation
rates, whereas an accumulation of proteins increases them. The
effect of an increase in water, however, predominates, resulting in a
net reduction of relaxation rates in peritumor white matter. In the
edematous white matter of cats with TET intoxication, no alterations
in protein content occur, so a greater reduction in relaxation rates
was expected. The transverse relaxation data from peritumor white
matter showed that the slow component of the relaxation, which
probably corresponds to proton signal arising from the extracellular
fluid, is significantly more efficient than that observed for TET
edema. This suggests that a larger number of macromolecular
surfaces, i.e. proteins, were present in the extracellular fluid of
peritumor white matter edema, which is expected to contribute to the

averaged R_2 plotted against dry tissue content. Therefore, these results suggest that the scatter in the weighted average of R_2 prevents detection of a difference between vasogenic and cytotoxic edema.

Naruse et al. (1982) concluded that the composition of vasogenic edema fluid may result in different rates of relaxation from those observed with accumulation of protein-poor fluid, which occurs in the early phase of edema due to cold injury. This difference is associated with a change in rate of decrease of transverse relaxation rates 4 hr after the lesion is induced. These workers also observed that the transverse relaxation becomes biexponential after 4 hr. However, in plotting R_2 against water content of edematous white matter, they compared the rate of decay of a monoexponential fit to the data for the first four hours, to the slow component only of a biexponential fit to their data for the subsequent period. Hence, we belive their conclusions are unfounded. As the results of Study B show, the fast component of the decay accounts for more than half the proton signal and its presence cannot be neglected.

Bartkowski et al. (1985) also reported different values of R_1 and R_2 in brains with different types of edema but similar water content. As they did not provide a detailed account of their methodology, we are unable to suggest a possible explanation for the apparent discrepancy between their results and ours.

4e. Relationship between increased protein and water in tissue

The measurement of tissue proteins in brain is subject to errors due to the complex molecular associations of proteins in this organ (Bogoch, 1969). The large number of proteins embedded in the extensive membranes of the brain cells accounts in part for the variability in protein content due to the insolubility in aqueous buffers of proteins associated with membranes. Also, the use of albumin as a standard may introduce errors in measurement due to the different dye-binding capacities of tissue proteins. This is especially true for the cats with peritumor edema, in which protein content and structure is expected to change. Measurements of total and soluble protein in samples from four cats with brain tumors had to be repeated after being stored at -20°C for several months, due to inconsistent binding of dye in one batch of albumin used for determination of standard curves. Storage for such a long period may have affected the protein structure, which in turn may be a source of error.

Despite such limitations, some general observations on the role of proteins in brain edema can be made. The increase in total protein in peritumor tissue was higher than the increase in soluble protein. As the former is composed of both structural and soluble proteins, this suggests that there is a net increase in structural protein in areas of vasogenic edema. Such an increase may be due, in part, to increased production of astrocyte-derived proteins, such as glial-fibrillary acidic protein, which have been shown to accumulate in regions of peritumor edema (Szymas et al., 1984).

The good correlation between the increase in protein and in water suggests that osmotic pressure plays a role in the development of vasogenic edema. Such a finding has been reported by Kuroiwa et al. (1985) and Bothe et al. (1984). Kuroiwa and co-workers used a model of pure vasogenic edema in rabbits, in which a short hypertensive period is employed to open the BBB temporarily. Their findings showed a linear relationship between the increases in serum proteins and in water content of the tissues during the time the BBB was open. Bothe and co-workers, employing cats with brain tumors, abscesses, or cryoinjury, also observed a linear relationship between increases in protein and in water in the edematous white matter. Such a relationship suggests that the protein content of edema fluid is relatively constant; however, as Bothe et al. demonstrated, the concentration of protein is much less than in plasma. They concluded that the osmotic pressure generated by proteins was insufficient to account completely for the increase in water occurring in vasogenic edema. Our findings are in agreement with theirs; however, the protein content of edema fluid calculated in this study is probably higher than that reported by Bothe et al. (see Chapter I, Part II, section 2 and Figs. 34--36).

An interesting finding was the marked increase of albumin in the peritumor grey matter (Fig. 33), which was not associated with changes in water content or relaxation rates. Hossmann et al. (1983) using immunochemical methods, and Klatzo et al. (1960), using albumin labeled with fluorescein compounds, found a similar increase in albumin and traced it to the perikarya of neurons. They suggested

regrograde axonal transport from the areas of edema as a possible
mechanism for this increase. The lack of change in water content we
noted suggests that albumin may be taken up against an osmotic
gradient by an active concentration mechanism. The absence of change
in R_1 or R_2 would support this suggestion if protein accumulation
affected the relaxation rates as indicated by the results of Study A.
Thus, if protein accumulates in a compartment with a low water
content and undergoes slow exchange of water with the surrounding
medium, the R_2 observed in this compartment would be very high. This
'fast' component would likely be missed with the technique employed
to measure R_2 in this study. Alternatively, the increase in albumin
may not be sufficient to induce a detectable change in the observed
relaxation rates.

4f. Summary

In conclusion, the results of this study have shown that (1)
the models of TET and peritumor edema are associated with cytotoxic
and vasogenic edema respectively. The latter may have an additional
component of cytotoxic edema, which is more representative of the
clinical situation. (2) For normal brain tissues monoexponential
recovery or decay processes describe well the relaxation rates within
the time frame of their measurement. For edematous white matter,
however, a biexponential curve described more accurately the decay of
both the transverse and the longitudinal relaxation in the rotating
frame. This may be due to decreased diffusion of water between the
intracellular and the extracellular compartments. (3) The value of

R_2' from normal white matter measured _in vivo_ is similar to that

observed _in-vitro_ using corresponding samples. Such values from

edematous white matter, however, demonstrated that the _in-vitro_ R_2'

values were significantly greater than the _in-vivo_ ones due to

changes in the rates and proportions of the two components of the

transverse relaxation that occurred with death of the animal. (4) It

is possible to differentiate cytotoxic from vasogenic edema on the

basis of the slow component of transverse relaxation; a large R_{2s}

points to vasogenic edema. (5) When cats with peritumor and TET-

induced edema were compared, no difference was observed in the

sensitivity of the averaged R_2, derived from samples of edematous

white matter, to the ratio of dry tissue weight to weight of water.

(6) The increase in serum proteins may contribute to the accumulation

of water in vasogenic edema.

CHAPTER III

MODELS DEVELOPED FROM THE PRESENT STUDIES

In this section two models are described in an attempt to explain the observed relaxation behavior in edematous white matter. The first is an extension of the two-environment fast-exchange model presented in Chapter II and is used to establish the role of changes in water content on the observed relaxation rates. The second model attempts to explain the observed changes from monoexponential transverse relaxation in normal white matter to biexponential relaxation in edematous white matter. As the arguments we employ mainly have to do with physiology rather than biophysics, details of the molecular dynamics contributing to proton relaxation are omitted. The model is, therefore, only a first approximation to the events that occur during brain edema.

1. Two-environment Fast-exchange Model of Proton Relaxation in Tissues

In Study A we determined that the two-environment fast-exchange (TEFE) model of proton relaxation adequately described the relaxation characteristics of protein solutions. Moreover, the main factors responsible for relaxation were the type and amount of protein and, possibly, their organization in the solution.

The application of this model to biological tissues should provide information on the molecular dynamics of water. When related to physiologic changes, the role of water in tissue function can be

physiology of brain edema.

The fact that relaxation rates correlate directly with the dry-tissue content (Figs. 27, 28), suggests that the TEFE model of proton relaxation may be applicable to brain tissues in a way similar to that used for the CSF-protein solutions. Studies of the longitudinal relaxation rate in muscle (Belton and Packer, 1974; Fung, 1977; Pocsik et al., 1986) and brain (Fung, 1977) subjected to progressive dehydration have given results that agree adequately with this model. The technique of progressive dehydration of tissues provides information on the rates and relative proportions of water molecules in each of the two environments, associated or free. A similar situation is observed with cerebral edema induced by TET intoxication; however, in this case the relaxation rates are studied as a function of increasing water content, which does not provide direct information on the characteristics of associated water. An advantage of the model of TET intoxication is that the increase in water is iso-osmotic, whereas in dehydration studies the decrease in water occurs together with a progressive increase in ionic concentration.

Fullerton et al. (1984) has developed an equation that enables calculation of the longitudinal relaxation time of water protons in the associated environment at different magnetic field strengths. For the resonant frequency used in this study (100 MHz), the expected R_1 of the associated environment is 4.8 s^{-1}. Because the TEFE model

respectively, are constants under conditions of constant temperature and magnetic field strength, the relative proportions of the water molecules in each environment are responsible for alterations in the observed relaxation rate R_{1obs}, which for normal white matter is 1.06 ± 0.04 s^{-1}. The relaxation rates of pure water, R_{1b}, at 37°C are: $R_1 = 0.26$ s^{-1}, $R_2 = 0.38$ s^{-1}, and $R_{1\rho} = 0.27$ s^{-1}.

The proportion of associated water molecules f_a can be calculated from the following:

$$f_a = (R_{iobs} - R_{ib}) / (R_{ia} - R_{ib}) \quad ; \quad i=1,2,1\rho \qquad (15)$$

The R_1 of distilled, deionized water at 37°C is 0.26 s^{-1} and represents R_{1b}. Thus, when these values are substituted in eq. (15) the proportion of water in the associated environment equals 0.176. Assuming these predictions to be correct, R_{2a} and $R_{1 a}$, are calculated as 70.2 s^{-1} and 49.9 s^{-1} respectively. The value of $R_{1\rho}$ is that calculated when the magnetic field strength corresponds to a Larmor frequency of 5 kHz, as employed in study B.

To determine whether the TEFE model predicts the relaxation of protons in brain edema, the previous data can be used to predict the relaxation rates for various values of dry-tissue content. In TET-induced edema there is an increase in total water and no increase in macromolecules from plasma, and we assume that no major conformational changes occur in the tissue. Thus we expect that only an increase in free water content occurs, which modifies eq. (3a) to:

above the normal. In white matter from control cats, the water content is 2.02 g H_2O/g DW and this value is subtracted from that of the water content for each sample of edematous white matter. The difference is expressed as the proportional change in water over the normal and this is multiplied by the proportion of free water in normal white matter already calculated from equation (3a), to give the value of f_b'. Because

$$f_a + f_b + f_b' = 1$$

new values of f_a and f_b can be calculated from

$$f_a = f_a/(f_a + f_b + f_b') \qquad (17)$$

and

$$f_b = (f_b + f_b')/(f_a + f_b + f_b') \qquad (18)$$

and used in equation (3a) to provide the predicted values of the relaxation rates. Linear regression analysis of these values plotted against the dry-tissue content gives a slope that is equivalent to G_i. A comparison between observed and calculated values of the various G_i is presented in Table 15. The calculated values clearly show a greater sensitivity than the observed values of G_i. Such a discrepancy can be explained by the relaxation rate of free water in tissues, as will now be shown.

It is known that the amount of associated water is proportional to the relative dry-tissue content (Hazelwood, 1979). The intercepts, which are calculated from the relationship between

relaxation rate of 'free' water in tissues. Substituting these values of free water in equations (3a and 15) and repeating the calculations results in much closer agreement between the observed and the predicted $\bar{G}_i$ (Table 16).

There may be several reasons why the relaxation rates of free water in tissues were higher than those of pure water and these are presented below.

Table 15. Comparison between observed gradients of sensitivity (G_i) of relaxation rates to changes in ratio of dry tissue wt:water content wt of edematous white matter of TET-intoxicated cats and similar values predicted from the TEFE model of proton relaxation. Relaxation rates for free water are those of pure water at 37°C.

	Intercept (s^{-1})	G_i $(s^{-1}/mg$ DW/g $H_2O)$
Observed		
R_1	0.50 ± 0.01	1.01 ± 0.11
R_2	4.43 ± 0.20	16.27 ± 2.00
$R_{1\rho}^{*}$	4.31 ± 0.24	8.79 ± 2.27
Predicted		
R_1	0.36 ± 0.001	1.42 ± 0.01
R_2	1.92 ± 0.01	21.74 ± 0.13
$R_{1\rho}^{*}$	1.38 ± 0.01	15.40 ± 0.11

*$R_{1\rho}$ measured at 5 kHz

Table 16. Comparison between observed gradients of sensitivity (G_1) of relaxation rates to changes in ratio of dry tissue wt:water content wt of edematous white matter of TET-intoxicated cats and similar values predicted from the TEFE model of proton relaxation. Relaxation rates for free water are those calculated for zero dry weight content (i.e., intercepts).

	Intercept (s^{-1})	G_1 (s^{-1}/mg DW/g H_2O)
Observed		
R_1	0.50 ± 0.01	1.01 ± 0.11
R_2	4.43 ± 0.20	16.27 ± 2.00
$R_{1\rho}^{*}$	4.31 ± 0.24	8.79 ± 2.27
Predicted		
R_1	0.55 ± 0.001	1.02 ± 0.01
R_2	5.19 ± 0.01	15.35 ± 0.07
$R_{1\rho}^{*}$	4.76 ± 0.01	8.78 ± 0.05

$^{*}R_{1\rho}$ measured at 5 kHz

Two hypotheses of the behavior of water in tissues other than the TEFE model will be considered. Ling (1970) has proposed that most, if not all, water molecules within the cell are ordered through preferential orientation in polarized multilayers. Such multilayers arise from fixed charges on extended protein surfaces and exclude ions and other solutes to varying degrees. The binding of ATP at cardinal sites on the protein surface leads to cooperative interactions between proteins that results in selective accumulation of K^+ over Na^+, and to the generation of polarized multilayers of water. This would cause decreased mobility of water molecules within the cell and account for the greater relaxation rates in tissues than in pure water. The TEFE model in this case would not apply. Evidence for the actual existence for polarized multilayers, however, is not definitive (for a review see Hazelwood, 1979).

Horowitz et al. (1979) proposed another hypothesis to explain the state of water in tissues. They used reference-phase analysis to measure concentrations of free and bound solutes in salamander oocytes and showed that only one third of the cytoplasmic water acts as a solvent (free aqueous phase), the rest (ordered phase) having a slow exchange of ions such as Na^+ and K^+ and, therefore, lower solubility. Horowitz and Paine (1979), using the same methodology, concluded that this behavior of water could be generalized to other cells and proposed a model in which the ordered phase is in equilibrium with the free aqueous phase, the composition of which is controlled by the plasma membrane. These findings suggest that a

water; however, the characteristics of such a model would have to be very different from those proposed by Belton and Packer (1974) and Fung (1977) and applied in the present work. Reference-phase analysis has the advantage over NMR that no models of cell water are required for the interpretation of results. On the other hand, it has the disadvantage of being applicable only to large cells and generalizations about its applicability to other cells may be subject to error. It remains to be proven whether this hypothesis is correct.

1b. Application of the TEFE model to proton NMR relaxation in brain edema

Another explanation for the larger relaxation rates of free water in tissues compared with pure water retains the TEFE model, but assumes that the free water environment behaves differently from pure water. Several studies using different techniques suggest that free water in cytoplasm may have a reduced rate of molecular motion. For example, the fact that water within cells freezes only when the temperature has reached -6 C°or less suggests that water has some degree of ordering (Peemoeller and Pintar, 1979; Fung and McGaughy, 1974; Belton et al., 1973). This is also supported by studies by Escayne et al. (1982) who showed that R_1 for the free-water environment in mouse muscle was about 0.57 s^{-1} and by Fung (1977), who, using the same tissue, demonstrated an R_1 of free water of 0.6 $\pm$ 0.1 s^{-1}. Additional evidence for reduced molecular motion of

cells. It is well established that the diffusion coefficient of water in tissues is slower by a factor of 2 than that of pure water (for a review see Hazlewood, 1979). It has been shown that when $R_2/R_1 \geqslant 9$, slow molecular motion is the dominant relaxation mechanism (Allen et al., in press). In our study R_2/R_1 was 8.9 (observed relaxation rates at zero dry-tissue content, Table 15), therefore, a slower molecular motion of the free water, may account for the large R_1 and R_2 values of free water. Thus it appears that reduced molecular motion of water within cells could account for the difference in relaxation rates between water in the free environment and pure water.

In this discussion the rate of exchange between populations of water molecules has not been considered thus far. However, as shown in Chapter II, Study A, subsection 4a.1., the presence of a magnetization recovery or decay describing a monoexponential curve would point towards the existence of fast exchange between environments of water. This was the case for the recovery of longitudinal magnetization; however, a biexponential decay of the magnetization (i.e., for both R_2 and $R_{1\rho}$) was observed in samples of edematous white matter. Such behavior is probably due to anatomical compartmentalization of water with an associated slow to intermediate exchange of protons between two compartments, rather than a decrease in the exchange rate of water protons between the associated and free environments of water molecules. Evidence in favor of this is going to be shown in the following section.

for the free-water environment are valid, then the TEFE model of proton relaxation describes adequately the observed dependence of R_1, R_2, and $R_{1\rho}$ on tissue water content of edematous white matter. In turn, this would mean that the averaged R_2 derived from biexponential decay data and obtained from a multiple-spin-echo image sequence using 16 echoes, could provide a useful index of water content in cerebral edema.

Transverse Relaxation in Edematous White Matter

2a. Background

It was shown in Study B that areas of white matter with
moderate to severe edema show a transverse magnetization decay that
can be described by a biexponential decay curve. This has been
observed by others (Bakay et al., 1975; Go and Edzes, 1975; Naruse et
al., 1982), but, no explanation was given. In this section we
attempt to demonstrate that the biexponential transverse relaxation
is due to an alteration in the rate of transfer of water across cell
membranes.

Proton NMR studies in normal tissues show that more than one
exponential term is often needed to describe the transverse
relaxation decay. For example, up to five components have been used
by Peemoeller et al. (1980). With the present technique we could, at
most, distinguish only the two slowest of the components of
relaxation decay observed by others. There is debate as to the
origin of these two components. Several authors have proposed that
the 'fast' R_{2f} and the 'slow' R_{2s} components correspond to the proton
signal originating from water in the intracellular and extracellular
spaces respectively (Cooke and Kuntz, 1974; Belton et al., 1972;
Diegel and Pintar, 1975; Foster, 1976). Most of these studies have
been performed on muscle from various species, but others have been
done on sciatic nerve from rabbits (Fritz and Swift, 1967; Dea et
al., 1972), or on human red blood-cell suspensions (Conlon and

results.

Assuming that anatomical compartments are responsible for the occurrence of two exponential components of the transverse magnetization decay, its presence may be explained providing that at least three conditions are fulfilled. First, the diffusion of water between two tissue compartments must be slow relative to the rates of decay of each compartment; second, these rates of decay should differ by at least a factor of 3 to be separable with an acceptable degree of uncertainty; and third, the compartments must be large enough to be detectable with proton NMR. For example, in suspensions of normal red blood cells, the transverse relaxation decay is monoexponential because the R_2 in each compartment is smaller than the rate of water diffusion between compartments, even though the rates of decay for both are sufficiently different and their compartments are relatively large. As a result, the observed relaxation rate is a weighted average of the R_2 from each compartment. After greatly increasing the R_2 in both intra- and extracellular spaces by adding a paramagnetic agent to the suspensions, it is possible to observe a biexponential decay of the transverse magnetization because the diffusion of water is now slow relative to the rates of decay in each compartment (Conlon and Outhred, 1972). That the cell membrane restricts diffusion of water between tissue compartments is suggested by the studies of Benga et al. (1983) using erytrocyte suspensions. They showed that agents that affect the permeability of membranes

extracellular spaces

Controversy arises with the work of Fung (1977) and Peemoeller et al. (1980) whose studies suggest that multiexponentiality is not due to slow exchange of water between the intracellular and the extracellular spaces. Based on substitution of deuterium for the water in muscle samples, Peemoeller and his collaborators suggested that the slow component could correspond to NMR signal coming from the protons of macromolecules. However, deuterium does not completely substitute for water molecules, and its very small magnetic moment, which would be associated with an extremely small R_1 of water protons (i.e., 0.01—0.02 s^{-1}), may explain why these workers did not observe any signal from water in muscle (Fung and Puon, 1981). Fung (1977) reported changes in the R_2 of muscle with time after death. Immediately after killing the animal he observed a single relaxation decay, but after 40 minutes the decay was better described by a biexponential curve. Because the extracellular space is known to decrease with cell death (see below), he concluded that the appearance of a slow component could not be due to an increase in the extracellular space as the muscle cells died. When in subsequent experiments Fung and Puon (1981) used a preparation of glycerinated muscle to disrupt the cell membranes, their results still showed multiexponential decay of the transverse relaxation. Finding an extracellular space accounting for 76% of the total tissue water, as compared to about 12% observed in normal muscle, they concluded that most cells were disrupted and that factors other than slow exchange

of water between the intra- and extracellular spaces were responsible for the observed multiexponential behavior. However, they also report that the water content of the muscle preparation was 82.8%, which contrasts with the normal value of 75%. Because it is the change in volume of water that is of importance, this parameter should be expressed as weight of water per unit dry weight. The proportion of intracellular volume in the glycerinated muscle preparation was 24%, corresponding to 1.16 g H_2O/g·DW, which is about 44% of that of normal muscle. Therefore, a very large proportion of cells remained intact and thus a slow excange of water between the intracellular and extracellular spaces could still have accounted for the observed biexponentiality. Therefore, present evidence suggests that the fast and slow components of the transverse relaxation decay, as observed in study B, correspond to proton signal arising from the intracellular and extracellular compartments respectively.

The present study provides indirect evidence that the two components of the transverse relaxation decay arise from the intra- and extracellular spaces. Table 11 clearly shows that the rates of magnetization decay and the respective proportions of the two components, R_{2f} and R_{2s}, are different before and after death. With death of the animal there is a decrease in the volume of the extracellular space because water moves into cells (see Chapter I, Part I). The resultant increase in intracellular volume is suggested by the increase in weighting of R_{2f} and a decrease in its efficiency of relaxation (i.e., a smaller value of R_{2f}). In addition, the values of R_{2s} in peritumor white matter are significantly different

of accummulation of protein-rich fluid in the extracellular space, which supports that anatomical compartments give rise to biexponential magnetization decay.

2b. Present model

A different interpretation for the change from mono- to biexponential transverse relaxation decay, observed by Fung (1977) suggests that alterations in the rate of water transfer between the extracellular and intracellular spaces occur. They can be accounted for by the double-Donnan steady state (see Chapter I) whereby in normal conditions the cell utilizes some of its energy reserves to maintain a steady state of ionic fluxes across the membrane by activation of Na^+-K^+-ATPase. It is generally assumed that water movement across membranes is passive and coupled to active ionic transport (MacKnight and Leaf, 1977). Hence, active 'pumping' of ions by the Na^+-K^+-ATPase is associated with transfer of water between the intracellular and extracellular compartments. In addition, transport of other ions such as chloride and bicarbonate, and of glucose and aminoacids, is thought to be associated with transfer of water between compartments (Finkelstein, 1984).

The present hypothesis assumes that intercompartmental water transfer in normal white matter is fast relative to the R_2 of the populations of water molecules in the intracellular and extracellular spaces. When water exchange between these spaces is fast relative to

water molecule within the cell is about 8 ms (Conlon and Outhred, 1972; Andrasko, 1976), and its reciprocal value (i.e., the rate of transfer of water from the intracellular to the extracellular space) is much greater than the relaxation rates for each compartment. In other tissues this rate of transfer is about one order of magnitude smaller than for erythrocytes (Finkelstein, 1984). This rate of water transfer is in the 'intermediate' exchange limit (see below), which may be associated with biexponential magnetization decay of both R_2 and $R_{1\rho}$ but not R_1. With the progressive decrease in energy compounds that occurs after death, Na^+-K^+-ATPase is inactivated and transport of ions and concomitant transfer of water across the cell membrane slows down. Other transport processes are also expected to decrease as well. Thus a two-exponential decay may be observed providing the rates of decay differ sufficiently and the compartments are large enough. Hence, Fung's observation (1977) of a single relaxation decay immediately after death suggests that in this case the Na^+-K^+-ATPase was still active. At 40 min, however, the muscle cells had consumed all the energy reserves causing inactivation of the Na^+-K^+-ATPase; the resultant slow exchange of water across the cell membranes would probably account for the observed biexponential decay. This hypothesis may explain not only our findings but also those of others who observed biexponential transverse relaxation in brain edema (Bakay et al., 1975; Go and Edzes, 1975; Naruse et al., 1982).

the proportionately small decreases in energy compounds that may occur in cerebral edema, would be expected to produce marked alterations in ionic transport and water transfer across them. This may explain the biexponential,transverse relaxation of white matter edema in vivo.

Studies by Averet et al. (1984) have shown that vasogenic edema induced by cold injury is associated with an inhibition of the Na^+-K^+-ATPase pump, and studies by Hossmann et al. (1986) showed that regions of peritumor edema have a reduced glucose utilization and, therefore, decreased energy production. Such alterations in peritumor vasogenic edema may be expected to result in a decrease of water transfer between the intracellular and the extracellular spaces and account for our observation of biexponential decay in edematous white matter surrounding tumors (Fig. 38).

With TET intoxication, water accumulates in the intraperiod line of myelin forming large vesicles that are physically separate from the surrounding tissue (Hirano et al., 1968; Katzman et al., 1963). A slow exchange of Na^+ has been demonstrated between these vesicles and the rest of the tissue (Katzman et al., 1963), probably as a result of the indirect inhibition of Na^+-K^+-ATPase by TET (Sone and Hagihara, 1964). Therefore, we would expect a slow exchange between the myelin vesicles and the brain, which may explain the biexponential transverse relaxation behavior in TET-induced edema (Fig. 39).

molecules associated with macromolecules with each compartment.

Figure 38. Diagram showing the postulated mechanism for the behavior
of transverse relaxation in white matter of cats with brain
tumors. (a) In normal conditions there is active transport of
ions between intracellular and extracellular spaces as shown by
the arrows ( ). (Dark area represents intracellular space,
empty area extracellular space.) This movement of ions is
associated with fast transfer of water, which results in an
observed single exponential decay of the transverse
magnetization. (b) The presence of edema leads to enlargement of
the extracellular space due to accumulation of protein-rich
fluid and also to metabolic alterations of the cell. Loss of a
indicates reduction in active transport which is
associated with a slow diffusion of water across membranes
(bidirectional arrows). This accounts for the observed
biexponential transverse relaxation decay. (c) With death there
is complete inactivation of ionic transport and water moves into
the intracellular space according to the Gibbs—Donnan
equilibrium (arrows). This results in dilution of intracellular
nonpermeant solutes and concentration of extracellular
nonpermeant solutes. (d) After death there is slow diffusion of
water across cells and the shift of water into cells accounts
for the observed decrease in intracellular R_2, increase in
extracellular R_2, and an increase in the weighting of the
intracellular component. (Changes in shading representing the
changing composition of the intracellular and extracellular
spaces are exaggerated for clarity.(
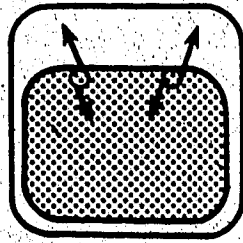
Normal   In vivo (Tumor)
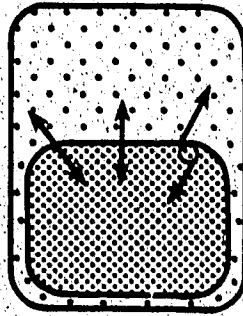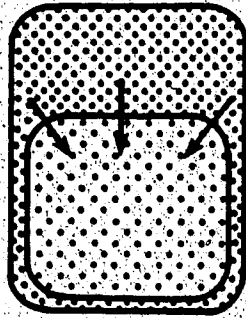
Death (Tumor)   In vitro (Tumor)
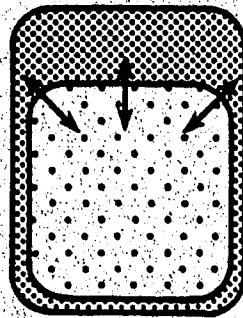
Figure 39. Diagram showing the postulated mechanism for the behavior of the transverse relaxation in white matter of cats with TET intoxication. (a) In normal conditions the extracellular (empty area) and the intracellular spaces (dark area) show apparent monoexponential decay of transverse relaxation due to fast transfer of water across cell membranes associated with active ion transport (⇌). (b) With TET intoxication the creation of a new space in the myelin sheath, which allows slow exchange of water with the rest of the parenchyma (⟷), accounts for biexponential transverse relaxation. It is assumed that ionic transport in other regions is not severely affected. (c) With death, ionic transport ceases and water moves into cells (unidirectional arrows) as a consequence of differences in osmotic pressure as suggested by the Gibbs–Donnan equilibrium. (d) This produces an increase in volume of the intracellular space and a decrease in volume of both myelin vesicles and extracellular space. Cessation of ionic transport is associated with slow exchange of water between spaces. Dilution of the intracellular space reduces the observed R_{2f} and concentration of solutes (probably represented by membranes and their proteins) in the myelin vesicles leads to an increase in its R_{2s}. Increase in volume of the intracellular space results in greater weighting of the corresponding relaxation rate (see Table 11; changes in shading representing the changing composition of the intracellular and extracellular spaces are exaggerated for clarity).

Normal   In vivo
(TET)
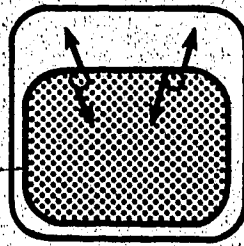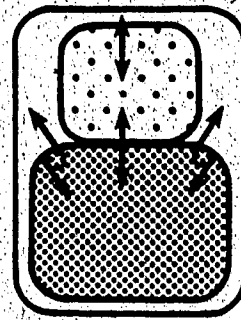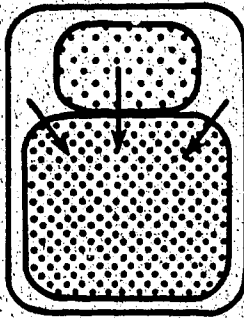
Death   In vitro
(TET)   (TET)
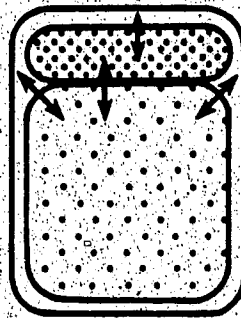
intracellular and extracellular spaces we obtain:

$$M(T_E n) = p_f'' \exp(-T_E \cdot R_{2f}'') + p_s'' \exp(-T_E \cdot R_{2s}'') \tag{19}$$

and because fast exchange occurs between the associated and free

environments of water, the exponential term in eq. (19) become:

$$\exp[-T_E(p_a \cdot R_{2a} + p_b \cdot R_{2b})] \tag{20}$$

The biprime notations represent the observed values of the

proportions and rates of relaxation of the water in each compartment,

which are different from the real values of p_f, p_s, R_{2f}, and R_{2s} due

to transfer of nuclear magnetization that results from the proton

exchange between compartments.

As an approximation we assume that $p_f \approx p_s$ and $\tau_f \approx \tau_s$, in

which τ_f and τ_s correspond to the residence times of water in each

compartment. Under these conditions $\tau_{ex} \approx \tau_f/2$ and a value of τ_f of

about 100 ms is assumed from measurements of water permeability in

tissues (Finkelstein, 1984). The τ_{ex} of 50 ms would probably be

associated with a monoexponential decay of transverse magnetization;

however, this is probably in the limiting value for intermediate

exchange (i.e., $\tau_{ex} \cdot R_2 \approx 1$), which may be associated with

biexponential decay of the magnetization. Therefore, any small

decreases in the permeability of membranes in white matter may be

responsible for the observed biexponential decay. On the other hand,

the value of τ_{ex} observed in normal conditions may be responsible for

the monoexponential decay of transverse magnetization.

It has been concluded by Finkelstein (1984) that glucose and

aminoacid membrane carriers, together with ionic channels, may

superimposed on the permeability to water of the lipid bilayer, which allows transfer of water. Thus it is to be expected that a distribution of τ_{ex} values exists between intracellular and extracellular spaces. That this may be the case is shown by preliminary studies in our laboratory in which measurements of $R_{1\rho}$ at different field strengths of H_1 demonstrated a marked field-dependence of $R_{1\rho f}$, $R_{1\rho s}$, and the weighting of their relative contributions consistent with different rates of water exchange between compartments.

In accounting for the apparent single exponential decay of the transverse magnetization in normal brain after death, it should be recalled that a biexponential decay curve with rate components that differ by a factor of less than 3 can be represented by a single exponential decay with an acceptable degree of uncertainty (Koenig et al., 1984). Moreover, component decays with a weighting of less than 10% and with smaller differences in rates of decay are still likely to be represented adequately by a monoexponential decay. When there is brain ischemia, as in death, the extracellular space of the cortex decreases from 18.9% to 8.5% of the tissue volume (Hossmann, 1976), due to a shift of water into the intracellular space as predicted by the Gibbs—Donnan hypothesis. Such an alteration reduces the weighting of the signal originating from the extracellular space and reduces the difference in the rates from both compartments by reducing R_{2f} and increasing R_{2s}. Thus, in our study, we would expect, postmortem, the slow component to contribute less than 10% of

of three between the fast and slow rates of decay. These data can be easily represented by a single exponential decay, which is a weighted average of the two components (Koenig et al., 1984). Support for this assumption comes from the work of Kato et al. (1986) who showed that a single exponential decay could adequately describe the transverse relaxation of brain samples from rats with cerebral ischemia of 4 hr or less in duration. Although in ischemia there is an increase in tissue water content, during the first 4 hr this remains within the intracellular space and the volume of the extracellular space remains small (Schuier and Hossmann, 1980). Therefore a decrease in relaxation rates is observed, but the transverse relaxation can be described by a single exponential curve.

Based on these considerations we may explain the difference between the in-vitro and in-vivo R_2'. In regions of cerebral edema the in-vitro R_2' is significantly greater than the in-vivo R_2'. From Table 11 it is possible to see that the rates of decay for the two components of transverse relaxation, R_{2f} and R_{2s}, and the respective proportions of such components are different before and after death. These changes are compatible with shifts of water from the extracellular (R_{2s}) to the intracellular (R_{2f}) compartments in a way predicted by the Gibbs--Donnan theory. The decrease in the proportion of the signal from the extracellular protons and the increase in their R_2 with death, will result in a greater rate of decay postmortem when a single exponential is fitted to only eight data points (Fig. 37; Table 11). The similarity of the averaged R_2

water content before and after death.

In normal white matter we observed $\underline{in}$ $\underline{vitro}$ a weighted average of R_2 after death due to the small contribution of the extracellular space. $\underline{In}$ $\underline{vivo}$ we also measured a weighted average of R_2 due to relatively fast exchange of water between the extracellular and the intracellular spaces. As a result their values were approximately the same because the total water content did not change before and after death. The tendency for the R_2 values obtained $\underline{in}$ $\underline{vitro}$ to be higher than those $\underline{in}$ $\underline{vivo}$ may be due to a shift of water into the cells with death. Thus, even though there is a decrease in the relaxation rate of the intracellular space, the change is relatively small and taken together with the increase in weighting of the signal originating from the intracellular space, results in a net increase in the observed R_2. Therefore, this model suggests that the R_2 of white matter measured $\underline{in}$ $\underline{vivo}$ should be greater than that measured $\underline{in}$ $\underline{vitro}$. It is unclear at present why we did not observe a difference in these values. On the other hand, the greater susceptibility of grey matter than of white matter to metabolic alterations leading to uptake of water by cells, could result in larger differences in R_2 before and after death. That this was the case is clearly shown in Figure 24.

Comparing Figures 25 and 26 it is possible to see that the difference between the calculated R_2' $\underline{in}$ $\underline{vivo}$ and $\underline{in}$ $\underline{vitro}$ is less for peritumor edema than for TET edema. This is attributed to less fluid shift after death and to a greater R_{2s} in peritumor white

relaxation respectively, resulting from the increased protein content
of peritumor edema fluid.

It can be concluded that transverse relaxation measurements of
tissues may provide information on changes in the distribution of
water between intracellular and extracellular compartments. This,
together with the fact that the weighted average of R_2 gives an
adequate index of water content in edematous white matter
irrespective of the type of edema present, can be directly applied to
the clinical setting for objective monitoring of patients with this
condition.

CHAPTER IV

CONCLUSIONS AND RECOMMENDATIONS

1. Conclusions

The main objective of the present studies was to develop criteria that would permit vasogenic and cytotoxic edema to be distinguished in vivo using proton NMR. These criteria are based on the following findings. 1) The type, amount, and, possibly, the degree of aggregation of the proteins in vasogenic edema fluid increase the rates of relaxation. Electrolyte concentration and pH probably play a minimal role. 2) Biexponential transverse relaxation decay was observed in areas of moderate to severe peritumor white matter edema and in edematous white matter resulting from TET intoxication. The two components, R_{2f} and R_{2s}, probably correspond to NMR signal arising from intra- and extracellular spaces respectively, as judged by changes in their rates and weightings after death, which follow those predicted by the Gibbs—Donnan equilibrium. 3) The slow component of the transverse relaxation decay, R_{2s}, can be used to differentiate vasogenic from cytotoxic edema. In vasogenic edema, R_{2s} is greater due to the presence of serum proteins in the extracellular fluid. 4) The weighted average of both components of transverse relaxation cannot be used to differentiate between vasogenic and cytotoxic edema. We conclude that discrimination between these two conditions is possible in vivo by using a multiple-spin-echo image sequence generating at least 12,

212

relaxation rates obtained _in vivo_ using MSE images with those obtained _in vitro_ from excised tissue samples using the Carr—Purcell—Meiboom—Gill sequence. The results showed that in normal white matter both values were similar. In grey matter, however, _in-vitro_ R_2 values were lower than those obtained _in vivo_. The difference in values is probably the result of the greater susceptibility of the grey matter to changes in tissue water content with death. The transverse relaxation of normal grey and white matter could be described by a single exponential decay. In most samples of edematous white matter, however, a biexponential decay curve could be used to describe the transverse relaxation. Because a limited time-frame was available for observation of the magnetization decay _in vivo_, a monoexponential curve with decay rate R_2' was fitted to the data. Comparison of these with corresponding _in-vitro_ R_2' values showed that the latter were larger, probably due to transfer of water from extracellular to intracellular spaces at the time of death. We conclude that the measurement of transverse relaxation rates _in vivo_ provides more accurate relaxation values than _in vitro_ if the observations span a sufficiently large number of images (i.e., about 16) to allow reliable separation of the component rates, as the severe changes in water homeostasis that occur with death are avoided. It is important to note, however, that detailed calibration

imaging could provide an index of water content in tissues. The results showed that in-vitro measurements of relaxation rates on excised tissue provide an adequate index of water content in edematous white matter, with the transverse relaxation being the most sensitive. Measurements of R_2 in vivo, however, were limited by the short time-frame used for the observation of the magnetization decay. Values of R_2' obtained from these data do not give an index of tissue water content in white matter edema because of different rates and weightings of the two components of decay in different types of brain edema. Therefore, to quantify properly the water content in areas of edema it is necessary to obtain enough data points to separate the two rates of decay that are commonly observed.

Although the measurements of tissue protein showed low sensitivity, good correlation with tissue water content was obtained, suggesting that proteins play a role in the accumulation of water in peritumor white matter. Moreover, tissue-protein content clearly established the nature of the edema present, i.e., vasogenic in peritumor white matter and cytotoxic in white matter from TET-intoxicated cats.

2a. Formation of brain edema

The typical feature of the formation phase of brain edema is an impairment in the normal homeostasis of water in brain cells due to changes in the normal characteristics of cell membranes. It is well established that alterations in metabolism disrupt membrane function (see Chapter I, Part I, section 6). Thus, it appears that a brain lesion from any cause may be associated with some degree of metabolic alteration in the surrounding brain, which, in turn, produces cytotoxic edema. If this is the case, the widely held view that vasogenic edema is the most common form of cerebral edema is not valid. Vasogenic edema probably always occurs together with cytotoxic edema, whereas the cytotoxic type may occur alone. This is supported by the finding of a cytotoxic component in experimental models of vasogenic edema such as cryo-injury, cerebral tumor, or abscess. Testing of the hypothesis that slow exchange of water across cells is responsible for biexponential relaxation observed in these experiments, would clarify whether metabolic changes occur in both types of edema.

Discrimination between vasogenic and cytotoxic edema appears feasible because of the different rates of transverse relaxation of the slow component between peritumor or TET-induced edema of the white matter. The larger R_{2s} in peritumor than in cytotoxic edema suggests that a higher protein content was present in the compartment

2b. Spread of brain edema

The direct relationship between the average transverse relaxation rate obtained from the transverse magnetization decay and the dry-tissue content of the edematous white matter regardless of type of edema, points to the usefulness of the average R_2 for quantifying the physiologic changes of water in cerebral edema. This is based on the direct relationship between dry-tissue content and water content expressed as grams per gram of wet weight that exists within the range of water content values observed in edema of the white matter. For example, measurements of R_2' with distance from the lesion in the cats with brain tumors provided an indication of the spread of edema fluid. Values of R_2' in peritumor white matter were subtracted from those of the contralateral hemisphere. This change in R_2', plotted against distance normalized for tumor size, showed a similar behavior in all cats except that in which the tumor developed in grey matter and that showed signs of rejection of the tumor (Fig. 39). The fitted curve from this figure denotes an empirical equation that is based on the relationship between R_2 and water content and has two major components. First, it has been reported that water content decreases linearly from the site of a lesion that does not occupy space, such as a cold injury (Marmarou et al., 1976; Reulen et al., 1977), and arises from the opposing forces

component that probably results from the compressive effects of the

tumor on the surrounding tissues with an increase in tissue

resistance and a decrease in tissue compliance (Fig. 40). The

results of our experiments showed that the effect of electrolytes, or

even serum proteins in edematous regions, do not have a detectable

effect on the observed relaxation rates. The relationship between R_2

and distance from the tumor suggests that NMR may be employed as an

adjunct for the study of the biomechanics of the brain's response to

edema. In the present studies this was not possible because an MSE

sequence with 16 echoes was not available at the time, and an R_2'

only could be calculated from 8 echoes (Figs. 21 and 36). This is

not an adequate index of tissue water content because it

overestimates water content and varies from animal to animal.

The great advantage of proton NMR over other techniques

employed for the study of brain edema is its non-invasive

nature; therefore, experiments can be carried out serially on

the same animal to follow the progression of edema. With this

technique it is possible to evaluate objectively the

pathophysiology of edema, and more importantly, new forms of

treatment. In addition, the measurement of R_2 in vivo has the

advantage over that performed in vitro in that it does not

alter the homeostasis of the brain and thus permits more

accurate assessment of water distribution in tissues.
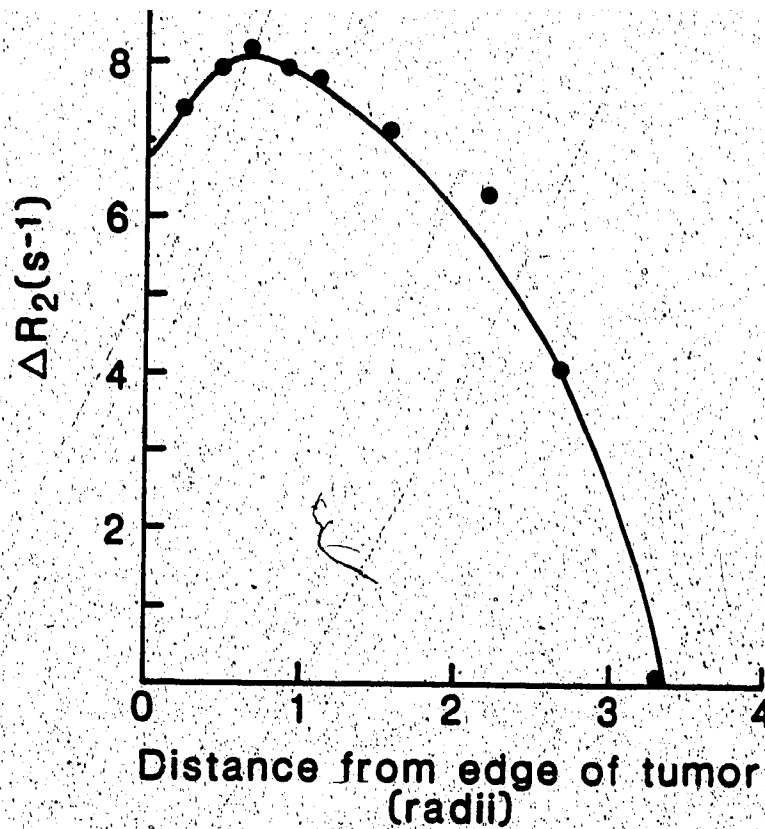
Figure 40. Plot of the difference in R_2' between affected (right) and unaffected (left) white matter of cats with implanted tumors and distance from the latter, normalized to the radius of the neoplasm. It shows that in the immediate vicinity of the tumor the change in R_2' is not as severe as it is at about 0.8 radii, presumably because the compression of the tumor forces fluid away from the region. From this maximum, it decreases steadily to zero. The solid line represents a least squares fit to the data points (see text).
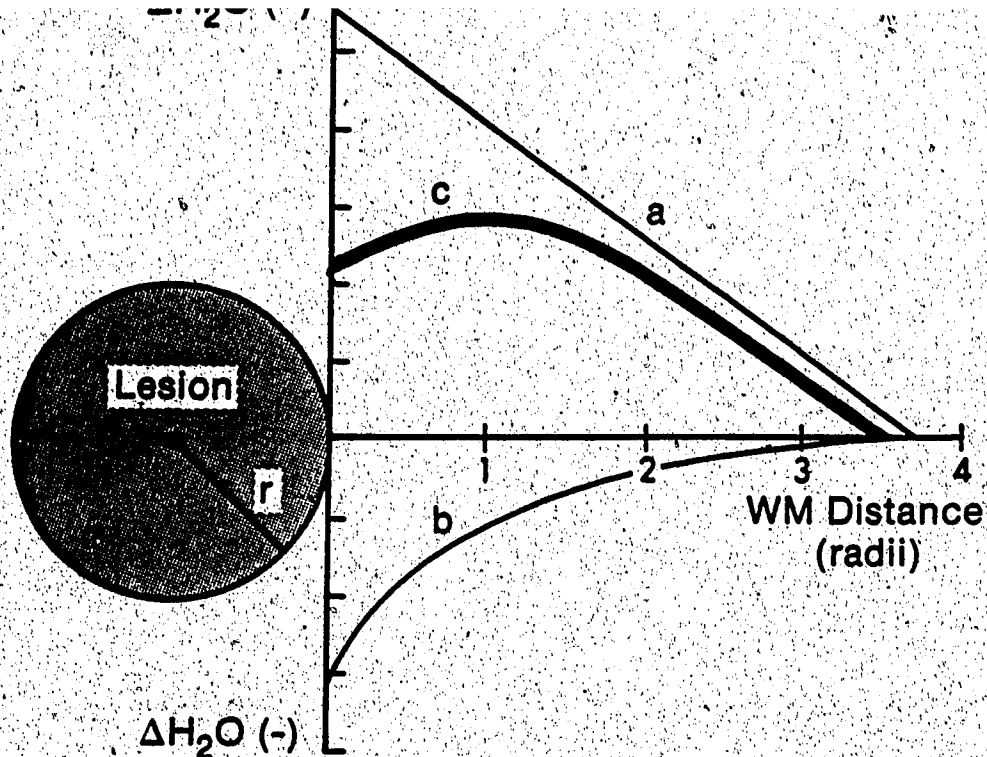
Figure 41. Diagram showing the effects of a tumor on the surrounding white matter (WM). The ordinate represents the change in tissue water content. Line (a) shows the decrease in water content with distance from a lesion in which no compression effects occur and is given by the opposing effects of direct transmission of blood pressure to the parenchyma and tissue resistance and tissue compliance. Line (b) results when a lesion of radius r produces some degree of compression on the surrounding tissue increasing the tissue resistance and decreasing tissue compliance. The net water content in the vicinity of the lesion is shown by line (c), which is the result of adding lines (a) and (b) and is inferred from the direct relationship between tissue water content and R_2.

As contrast in NMR images improves diagnosis, it is important to select machine parameters to optimize contrast in accordance with factors such as relaxation rates, and proton densities, of different tissues. The results of the MSE sequence show that the R_2 of normal grey and white matter are similar. This means that obtaining contrast between these tissues relies on their different proton densities because the images were generated with a T_R of 4.3 s which minimizes the contribution of R_1 to contrast between grey and white matter. In this case a short T_E and a long T_R provide the best contrast between the two tissues. In the case of edematous white matter, its very different R_2 and proton density from normal white matter suggest that contrast is best achieved with a long T_E and a long T_R. Preliminary trials in these studies and the findings of others support this conclusion (Brandt-Zawadzki et al., 1984; Smith et al., 1985).

The transverse magnetization decay measured in regions of moderate to severe edema is described by more than one exponential within the echo times, T_E, commonly employed for clinical imaging. Therefore, present methods of measuring R_2 in clinical practice using two data points could result in marked inaccuracies, the nature of which will depend upon the T_E used for the measurement, as has been observed by Mills et al. (1984).

The application of high field NMR imaging using the MSE sequence to patients with cerebral edema seems to provide information

points to a possible disturbance in membrane transfer of water across cells, which characterizes cytotoxic edema. Also, the larger R_{2s} in peritumor edema than in TET-induced edema suggests that the fluid responsible for this component is protein-rich in the former indicating its vasogenic origin. Such information may prove of diagnostic and therapeutic value, especially in evaluating the response to treatment of individual patients.

Peritumor edema, however, is a pathologic manifestation that occurs late in the natural history of brain tumors. It is generally detected when the mass effects of both tumor and edema have overwhelmed the compensatory mechanisms that mantain intracranial pressure within normal limits. At this point decompensation occurs and the patient follows a rapid worsening that leads to death if left untreated. The edema around tumors responds dramatically to steroids but this response is usually transient if the drug is discontinued because the tumor, which is responsible for the production of edema, is largely unaffected by steroids. These drugs affect one or several factors responsible for the production, spread, or resolution of brain edema. Thus, an understanding of the basic factors involved provides a rationale for developing alternative treatment regimens.

The role of NMR in the management of edema associated with brain tumors remains to be determined. At present, it is the expectation of radiologists that NMR imaging will allow an improvement in diagnosis of brain edema over present diagnostic

cerebral alterations. It is well established, however, that large ovelap occurs in the values of relaxation rates obtained from different brain lesions. An alternative that may be of some benefit is the measurement of more than one index of relaxation, i.e. R_1 and R_2 in the same region. As shown in the present studies, R_2 is specific for different brain tissues irrespective of their dry-tissue content. The longitudinal relaxation rate, on the contrary, gives an index of dry-tissue content irrespective of the type of brain tissue. The combination of these indices may increase the specificity of diagnosis in pathologic conditions.

It is important to note that peritumor brain edema should be treated as early as possible in the natural history of a cerebral neoplasm. Because none or few and unspecific symptoms are usually produced by this pathology, its early detection is uncommon. NMR imaging, due to its high sensitivity to dry-tissue content, may provide earlier detection of peritumor edema; however, this is a very expensive modality for diagnosis and it is unlikely that it will find wide application as a screening procedure. On the other hand, when edema is present, quantitative measurements of relaxation may provide a good index of dry-tissue content that allows accurate assessment of the severity and extent of peritumor edema. This index, therefore, may prove very useful to determine the response of brain edema to different treatment modalities. Its clinical application may be limited to the research setting mainly because of time and economic

calculation of relaxation rates from images. Other limitations are
the very large memory space required to temporarily store a large
number of images, such as a MSE sequence with 16 echoes or more;
furthermore, obtaining a series of images and calculation of
relaxation rates may require dedicated personnel with special
training in the interpretation of NMR images and the associated
relaxation rates.

It is more difficult to detect cytotoxic edema in its early
stage because it occurs most commonly with cerebrovascular disorders,
which follow a very rapid course with associated vasogenic edema a
few hours after the ictus. The brain edema following an ischemic
event, however, is not uniform. It is known that in the periphery of
an infarct viable tissue with associated cytotoxic edema may be
found. Thus, treatment modalities can be directed at preserving the
viable tissue in these regions. Quantitative NMR imaging may help
detect non-invasively the affected tissue and differentiate between
areas of reversible and irreversible ischemia. This may be
accomplished on the basis of the relationship between cerebral blood
flow and tissue-water content, and the relationship between
relaxation rates and the reciprocal values of tissue-water content.
Thus, NMR imaging may provide an indirect index of tissue perfusion
in the brain. In addition, it is to be expected that brain tissue
with irreversible ischemia has a combination of cytotoxic and
vasogenic edema; whereas reversibly damaged cerebral tissue has only

reversible and irreversible ischemic damage to brain tissues. Its

application to the clinical situation, however, may be limited to

specialized centers dedicated to the sudy of these disorders.

University Press, New York

Allen PS (1984) In vivo applications of NMR to medicine. Radiat Phys Chem 24:419-435

Aleu FP, Edelman FL, Katzman R, Scheinber LC (1964) Ultrastructural and biochemical analysis in cerebral edema associated with experimental mouse gliomas. J Neuropathol Exp Neurol 23:253-263

Aleu FR, Katzman R, Terry RD (1963) Fine structure and electrolyte analysis of cerebral edema induced by alkyltin intoxication. J Neuropath Exp Neurol 22:403-413

Andrasko J (1976) Water diffusion permeability of human erythrocytes studied by a pulsed gradient NMR technique. Biochim Biophys Acta 428:304-311

Andrew ER (1984) A historical review of NMR and its clinical applications. Br Med Bull 40:115-119

Andrew ER, Bottomley PA, Hinshaw WS, Holland GN, Moore WS, Simaroj C (1977) NMR images by the multiple sensitive point method: application to larger biological samples. Phys Med Biol 22:971-974

Aprison MH, Lukenbill A, Segar WE (1960) Sodium, potassium, chloride and water content of six discrete parts of the mammalian brain. J Neurochem 5:150-158

Asato K, Handa H, Hashi T, Hatta J, Komoike M, Yazaki T (1983) Chronological sequences and blood-brain barrier permeability changes in local injury as assessed by nuclear magnetic resonance (NMR) images from sliced rat brain. Stroke 14:191-197

Astrup J, Sorensen M, Sorensen HR (1981) Oxygen and glucose consumption related to Na^+-K^+ transport in canine brain. Stroke 12:726-730

Averet N, Rigoulet M, Cochandon F (1984) Modifications of synaptosomal Na^+-K^+-ATPase activity during vasogenic brain edema in the rabbit. J Neurochem 42:275-277

Bakay L (1965) Morphological and chemical studies in cerebral edema: Triethyltin-induced edema. J Neurol Sci 2:52-61

Bakay L, Kurland RJ, Parrish RG, Lee JC, Peng RJ, Bartkowski HM (1975) Nuclear magnetic resonance studies in normal and edematous brain tissue. Exp Brain Res 23:241-248

225

Baker M, Hoshino T, Guray O, Wilson CB, Nielsen SL, Downie R, Eliason J (1973) Development of an animal brain tumor model and its response to therapy with 1,3-Bis(2-chloroethyl)-1-nitrosourea. Cancer Res 33:976-986

Barbour HG, Hamilton WF (1926) The falling drop method for determining specific gravity. J Biol Chem 69:625-640

Bartkowski HM, Bederson J, Nishimura M, Brant-Zawadzki M, Moon K, Longar S, Pitts L (1985) Nuclear magnetic resonance (NMR) imaging and spectroscopy in experimental brain edema in the rat. In: Hartmann A, Hoyer S (eds) Cerebral Blood Flow and Metabolism Measurement. Springer, New York, pp 540-545

Beall PT, Hazlewood CF, Rao PN (1976) Nuclear magnetic resonance patterns of intracellular water as a function of HeLa cell cycle. Science 192:904-907

Beaney RP, Brooks DJ, Leenders KL, Thomas DGT, Jones T, Halman KE (1985) Blood flow and oxygen utilization in the contralateral cerebral cortex of patients with untreated intracranial tumors as studied by positron emission tomography, with observations on the effect of decompressive surgery. J Neurol Neurosurg Psychiatry 48:310-319

Bell BA (1983) A history of the study of cerebral edema. Neurosurgery 13:724-728

Belton PS, Jackson RR, Packer KJ (1972) Pulsed NMR studies of water in striated muscle. I. Transverse nuclear spin relaxation times and freezing effect. Biochim Biophys Acta 286:16-25

Belton PS, Packer KJ (1974) Pulsed NMR studies of water in striated muscle. III. The effects of water content. Biochim Biophys Acta 354:305-314

Belton PS, Packer KJ, Sellwood TC (1973) Pulsed NMR studies of water in striated muscle. II. Spin-lattice relaxation times and the dynamics of non-freezing fraction of water. Biochim Biophys Acta 304:56-64

Benga G, Pop VI, Popescu O, Ionescu M, Mihele V (1983) Water exchange through erythrocyte membranes: nuclear magnetic resonance studies on the effects of inhibitors and of chemical modification of human membranes. J Membr Biol 76:129-137

Investigation of protein hydration by proton spin-relaxation time measurements. Biochim Biophys Acta 207:381-389

Bloch F, Hansen WW, Packard M (1946) The nuclear induction experiment. Phys Rev 69:127

Bodsch W, Mies G, Paschen W, Hossmann KA (1984) Regional quantitative biochemistry and autoradiography of protein synthesis and serum extravasation in brain edema. In Go KG, Baethmann A (eds) Recent Progress in the Study and Therapy of Brain Edema. Plenum, New York, pp 27-35

Bodsch W, Hossmann KA (1983) 125I-antibody autoradiography and peptide fragments of albumin in cerebral edema. J Neurochem 41:239-243

Bodsch W, Hurter T, Hossmann KA (1982) Immunochemical method for quantitative evaluation of vasogenic edema following cold injury of rat brain. Brain Res 249:111-121

Bogoch S (1969) Proteins. In: Lajtha A (ed) Handbook of Neurochemistry. Plenum, New York, Vol 1, pp 75-92

Bothe HW, Bodsch W, Hossmann KA (1984) Relationship between specific gravity, water content, and serum protein extravasation in varous types of vasogenic edema. Acta Neuropathol 64:37-42

Bottomley PA, Foster TH, Argersinger RE, Pfeifer LM (1984a) A review of normal tissue hydrogen NMR relaxation times and relaxation mechanisms from 1--100MHz: dependence on tissue type, NMR frequency, temperature, species, excision, and age. Med Phys 11:425-448

Bottomley PA, Hart HR, Edelstein WA, Schenck JF, Smith LS, Leve WM, Mueller OM, Redington RW (1984b) Anatomy and metabolism of the normal human brain studied by magnetic resonance at 1.5 tesla. Radiology 150:441-446

Bourke RS, Greenberg ES, Tower DB (1965) Variations of cerebral cortex fluid spaces as a function of species brain size. Am J Physiol 208:689-692

Bourke RS, Kimelberg HK, Nelson LR, Barron KD, Auen EL, Popp AJ, Waldman JB (1980) Biology of glial swelling in experimental brain edema. Adv Neurol 28:99-109

York

Bradbury MWB (1984) The structure and function of the blood-brain barrier. Fed Proc 43:186-190

Bradbury MWB, Cserr HF, Westrop RJ (1981) Drainage of cerebral interstitial fluid into deep cervical lymph of the rabbit. Am J Physiol 240:F329-F336

Bradford MM (1976) A rapid and sensitive method for the quantitation of microgram quantities of protein utilizing the principle of protein dye binding. Anal Biochem 72:248-254

Brady TJ, Buonanno FS, Pykett IL, New PFJ, Davis KR, Pohost GM, Kistler JP (1983) Preliminary clinical results of proton (^{1}H) imaging of cranial neoplasms: in-vivo measurements of T_1 and mobile proton density. Am J Neuroradiol 4:225-228

Brant-Zawadzki M, Bartkowski HM, Pitts LH, Hylton NM, Mills CM, Nishimura MC, Orthendahl DA (1984) NMR imaging of experimental and clinical cerebral edema. Noninv Med Imag 1:43-47

Bratton CB, Hopkins AL, Weinberg JW (1965) Nuclear magnetic resonance studies of living muscle. Science 147:738-739

Brightman MW (1965) The distribution within the brain of ferritin injected into cerebrospinal fluid compartments. II. Parenchymal distribution. Am J Anat 117:193-220

Brightman MW, Hori M, Rapoport SI, Reese T, Westergaard E (1973) Osmotic opening of tight junciton in cerebral endothelium. J Comp Neurol 152:317-326

Britt RH, Enzmann DR, Yeager AS (1981) Neuropathological and computerized tomographic findings in experimental brain abscess. J Neurosurg 55:590-603

Brody TM, Akera T, Baskin ST, Gubitz R, Lee CY (1974) Interaction of Na, K-ATPase with chlorpromazine free radical and related compounds. Ann NY Acad Sci 242:527-542

Bryant RG, Halle B (1982) NMR relaxation of water in heterogeneous systems — consensus views? In: Franks F, Mathias SF (eds) Biophysics of water. Wiley, New York, pp 389-393

Bull JWD (1961) History of neuroradiology. Br J Radiol 34:69-84

~~Carr DH, Brown J, Bydder GM, Weinmann HJ, Speck U, Thomas DJ, Young~~ IR (1984) Clinical use of intravenous gadolinium-DTPA as a contrast agent in NMR imaging of cerebral tumors. Lancet 1:484-486

Cervos-Navarro J,Ferzst R (1973) Connective tissue in pericapillary spaces of the human spinal cord. Acta Neuropathol (Berl) 24:178-183

Chan PH, Fishman RA, Caronna J, Schmidley JW, Piroleau G, Lee J (1983a) Induction of cerebral edema following intracerebral injection of arachidonic acid. Ann Neurol 13:625-632

Chan PH, Fishman RA, Lee JL, Candelise L (1979) Effects of excitatory neurotransmitter aminoacids on swelling of rat brain cortical slices. J Neurochem 33:1309-1315.

Chan PH, Kerlan R, Rishman RA (1983b) Reductions of -aminobutiric acid and glutamate uptake and (Na^+-K^+)-ATPase activity in brain slices and synaptosomes by arachidonic acid. J Neurochem 40:309-316

Chan PH, Yurko M, Fishman RA (1981) Phospholipid degradation and cellular edema induced by free radicals in brain cortical slices. J Neurochem 38:525-531

Civian MM, Shporer M (1975) Pulsed nuclear magnetic resonance study of ^{17}O, ^2D, and ^1H of water in frog striated muscle. Biophys J 15:299-306

Clasen M, Bezkorovainy A, Pandolfi S (1982) Protein and electrolyte changes in experimental cerebral edema. J Neuropathol Exp Neurol 41:113-128

Clasen RA, Cooke PM, Pandolfi S, Boyd D, Raimondi AJ (1962) Experimental cerebral edema produced by focal freezing. 1. An anatomic study using vital dye techniques. J Neuropathol Exp Neurol 21:579-596

Clasen RA, Huckman MS, Von Roenn KA, Pandolfi S, Laing I, Lobick J (1981) A correlative study of computed tomography and histology in human and experimental vasogenic edema. J Comput Assist Tomogr 5:313-327

Clifford J, Sheard B (1966) Nuclear magnetic resonance investigation of the state of water in human hair. Biopolymers 4:1057-1065

....
288:354-361

Cooke R, Kuntz ID (1974) The properties of water in biological
systems. Ann Rev Biophys Bioeng 3:95-126

Cooke R, Wien R, (1971) The state of water in muscle tissue as
determined by proton nuclear magnetic resonance. Biophys J
11:1002-1017

Crooks LE, Arakawa M, Hoenninger J, Watts J, McRee R, Kaufman L,
Davis PL, Margulis AR, DeGroot J (1982) Nuclear magnetic
resonance whole-body imager operating at 3.5 K gauss. Radiology
143:169-174

Cserr HF, Cooper DN, Milhorat TH (1977) Flow of cerebral interstitial
fluid as indicated by the removal of extracellular markers from
rat caudate nucleus. Exp Eye Res 25(suppl.):461-473

Cumings JN (1961) Soluble cerebral proteins in normal and oedematous
brain. J Clin Pathol 14:289-294

Cushing H (1901) Concerning a definite regulatory mechanism of the
vaso-motor centre which controls blood pressure during cerebral
compression. Bull Johns Hopkins Hosp 12:290-292

Damadian R (1971) Tumor detection by nuclear magnetic resonance.
Science 171:1151-1153

Damadian R, Minkoff L, Goldsmith M, Stanford M, Koutcher J (1976)
Field focusing nuclear magnetic resonance (FONAR) visualization
of a tumor in a live animal. Science 194:1430-1432

Dandy WE (1918) Ventriculography following the injection of air into
the cerebral ventricles. Ann Surg 68:5-11

Dandy WE (1919) Rontgenography of the brain after the injection of
air into the spinal canal. Ann Surg 70: 397-403

Daszkiewicz OK, Hennel JW, Lubas B, Szczepkowski TW (1963) Proton
magnetic relaxation and protein hydration. Nature 200:1006-1007

Davson H (1976) The blood--brain barrier. J Physiol (Lond) 255:1-28

Dea P, Chan SI, Dea FJ (1972) High resolution proton magnetic
resonance spectra of a rabbit sciatic nerve. Science 175:206-
209

Decker RV, Foster JF (1967) Amphoteric behavior of bovine plasma albumin and its detergent complexes. J Biol Chem 242:1526–1532

De La Paz RL, Patronas NJ, Brooks RA, Smith BH, Kornblith PL, Milam H, Di Chiro G (1983) A PET study of suppression of glucose utilization in cerebral grey matter associated with brain tumor. J Cereb Blood Flow Metab, Suppl 1, 3:21–22

Demopoulos HB, Flamm ES, Pietronigro DD, Seligman ML (1980) The free radical pathology and the microcirculation in the major central nervous system disorders. Acta Physiol Scand Suppl 492:91–119

Di Chiro G, Brooks RA, Dubal L, Chew E (1978) The apical artifact: elevated attenuation values observed toward the apex of the skull. J Comput Assist Tomogr 2:65–70

Diegel JG, Pintar MM (1975) Origin of the nonexponentiality of the water proton spin relaxation in tissues. Biophys J 15:855–860

Eggleston JC, Saryan LA, Hollis DF (1975) Nuclear magnetic resonance investigations of human neoplastic and abnormal non-neoplastic tissues. Cancer Res 35:1326–1332

Elliot KAC, Jasper H (1949) Measurement of experimentally induced brain swelling and shrinkage. Am J Physiol 157:122–129

Ericson K, Lilja A, Bergstrom M, Collins VP, Eriksson L, Ehrin E, von Holst H, Lundqvist H, Langstrom, Mosskin M (1985) Positron emission tomography with ([11C] methyl)-L-methionine, [11c]-D-glucose, and [68Ga]EDTA in supratentorial tumors. J Comput Assist Tomogr 9:683–689

Escayne JM, Canet D, Robert J (1982) Frequency dependence of water proton longitudinal nuclear magnetic relaxation times in mouse muscle tissues at 20 C. Biochim Biophys Acta 721:305–311

Farrell CL, Shivers RR (1984) Capillary junctions of the rat are not affected by osmotic opening of the blood-brain barrier. Acta Neuropathol (Berl) 63:179–189

Farrar TC, Becker FD (1971) Pulse and Fourier Transform NMR. Academic, New York

Fenstermacher JD (1975) Mechanism of ion distribution between blood and brain. In: Tower DB (ed) The Nervous System. Vol 1: The Basic Neurosciences. Raven, New York, pp 299–311

in the brain of mammals. In: Pappius HM, Feindel W (eds) Dynamics of Brain Edema. Springer, New York, pp 87-94

Ferszt R, Hahm H, Cervos-Navarro J (1980) Measurement of the specific gravity of the brain as a tool in brain edema research. Ann Neurol 28:15-26

Fishman RA (1975) Brain edema. N Engl J Med 293:706-711

Finkelstein A (1984) Water movement through membrane channels. Curr Top Membr Transp 21:295-308

Flamm ES, Demopoulos HB, Seligman ML, Poser RG, Ransohoff J (1978) Free radicals in cerebral ischemia. Stroke 9:445-447

Folkman J (1971) Tumor angiogenesis: therapeutic implications. New Engl J Med 285:1182-1186

Foster KR, Resing HA, Garroway AN (1976) Bounds on "bound water": transverse nuclear magnetic resonance relaxation in barnacle muscle. Science 194:324-326

Foster MA (1984) Magnetic Resonance in Medicine and Biology. Pergamon, New York.

Fritz OG JR, Swift TJ (1967) The state of water in polarized and depolarized frog nerves. A proton magnetic resonance study. Biophys J 7:675-687

Fujiwara K, Nitsch C, Suzuki R, Klatzo I (1981) Factors in the reproducibility of the gravimetric method for evaluation of edematous changes in the brain. Neurol Res 3:345-361

Fullerton GD, Cameron IL, Ord VA (1984) Frequency dependence of magnetic resonance spin-lattice relaxation of protons in biological materials. Radiology 151:135-138

Fullerton GD, Potter JL, Dornbluth NC (1982) NMR relaxation of protons in tissues and other macromolecular water solutions. Mag Res Imag 1:209-228

Fung BM (1974) Non-freezable water and spin-lattice relaxation time in muscle containing a growing tumor. Biochim Biophys Acta 362:209-214

Fung BM (1977) Correlation of relaxation time with water content in muscle and brain tissues. Biochim Biophys Acta 497:317-322

relaxation in muscle water. Biophys J 33:27-38

Gaab MR, Heissler HE (1984) ICP monitoring. Crit Rev Biomed Eng
11:189-250

Garrison FH (1929) An Introduction to the History of Medicine.
Saunders, Philadelphia, pp 92-105

Gazendam J, Go KG, van Zanten AK (1979) composition of isolated edema
fluid in cold-induced brain edema. J Neurosurg 51:70-77

Go KG, Edzes HT (1975) Water in brain edema. Observations by the
pulsed nuclear magnetic resonance technique. Arch Neurol
32:462-465

Go KG, Houthoff HJ, Hartsuiker J, van der Molen-Woldendorp D,
Zuiderveen F, Teelken AW (1985) Exudation of plasma protein
fractions in vasogenic brain edemq. In: Inaba Y, Klatzo I,
Spatz M (eds) Brain Edema. Springer, New York, pp 76-87

Go KG, Patberg WR, Teelken AW, Gazendam J (1976) The Starling
hypothesis of capillary fluid exchange in relation to brain
edema. In: Pappius HM, Feindel W (eds) Dynamics of Brain Edema.
Springer, New York, pp 63-67

Go KG, Pratt JJ (1975) The dependence of the blood to brain passage
of radioactive sodium on blood pressure and temperature. Brain
Res 93:329-336.

Greenfield JG (1939) The history of cerebral edema associated with
intracranial tumors. Brain 62:129-152

Groothuis DR, Fischer JM, Lapin G, Biogner DD, Vick NA (1982)
Permeability of different experimental brain tumor models to
horseradish peroxidase. J Neuropathol Exp Neurol 41:164-185

Grosch L, Noack F (1976) NMR relaxation investigation of water
mobility in aqueous bovine serum albumin solutions. Biochim
Biophys Acta 453:218-232

Halle B, Anderson T, Forsen S, Lindman B (1981) Protein hydration
from water oxygen-17 magnetic relaxation. J Am Chem Soc
103:500-508

Hallenga K, Koenig SH (1976) Protein rotational relaxation as studied
by solvent 1H and 2H magnetic relaxation. Biochemistry 15:4255-
4263

its behaviour in acid solution. Biochem J 62:569–582

Harris RJ, Symon L, Branston NM, Bayhan M (1981) Changes in
    extracellular calcium activity in cerebral ischemia. J Cereb
    Blood Flow Metab 1:203–209

Hatam A, Yu Z-Y, Bergstrom M, Berggren B-M, Greitz T (1982) Effect of
    dexamethasone treatment of peritumoral brain edema: evaluation
    by computed tomography. J Comput Assist Tomogr 6:586–592

Hawkes RC, Holland GN, Moore WS, Worthington BS (1980) Nuclear
    magnetic resonance (NMR) tomography of the brain: a preliminary
    clinical assessment with demonstration of pathology. J Comput
    Assist Tomogr 4:577–586

Hazelwood CF (1979) A review of the significance and understanding of
    the physical properties of cell-associated water. In: Drost-
    Hansen W, Clegg J (eds) Cell-Associated Water. Academic, New
    York, pp 165–259

Hazelwood CF, Chang DC, Nichols BL, Woessner DE (1974) Nuclear
    magnetic resonance transverse relaxation times of water protons
    in skeletal muscle. Biophys J 14:583–606

Herzog I, Levy WA, Scheiberg LC (1965) Biochemical and morphological
    studies of cerebral edema associated with intracerebral tumors
    in rabbits. J Neuropathol Exp Neurol 24:244–255

Hinshaw WS (1974) Spin mapping: the application of moving gradients
    to NMR. Phys Lett 48A:87–88

Hirano A (1980) Fine structure of edematous encephalopathy. Adv
    Neurol 28:83–97

Hirano A, Zimmerman HM, Levine S (1968) Intramyelinic and
    extracellular spaces in triethyltin intoxication. J Neuropathol
    Exp Neurol 27:571–580

Hochwald GM, Sahar A (1971) The effect of spinal fluid pressure on
    cerebrospinal fluid formation. Exp Neurol 32:30–40

Hollis DP, Economou JS, Parks LC, Eggleston JC, Saryan LA, Czeisler
    JL (1973) Nuclear magnetic resonance studies of several
    experimental and human malignant tumors. Cancer Res 33:2156–
    2160

Horowitz SB, Paine PL, Tluczek L, Reynhout JK (1979) Reference phase
    analysis of free and bound intracellular solutes. I. Sodium and
    potassium in amphibian oocytes. Biophys J 25:33-44

Hossmann KA (1976) Development and resolution of ischemic brain
    swelling. In: Pappius HM, Feindel W (eds) Dynamics of Brain
    Edema. Springer, New York, pp 218-227

Hossmann KA (1982) Treatment of experimental cerebral ischemia. J
    Cereb Blood Flow Metab 2:275-297

Hossmann KA, Bothe HW, Bodsch W, Paschen W (1983a).
    Pathophysiological aspects of blood--brain barrier disturbances
    in experimental brain tumors and brain abscesses. Acta
    Neuropathol, Suppl 8:89-102

Hossman KA, Hurter T, Oschlies V (1983b) The effect of dexamethasone
    on serum protein extravasation and edema development in
    experimental brain tumors of cats. Acta Neuropathol (Berl)
    60:223-231

Hossman KA, Mies G, Paschen W, Szabo L, Dolan E, Wechsler W (1986)
    Regional metabolism of experimental brain tumors. Acta
    Neuropathol (Berl) 69:139-147

Hossman KA, Takagi S (1976) Osmolality of brain in cerebral ischemia.
    Exp Neurol 51:124-131

Hossmann KA, Wechsler W, Wilmes F (1979) Experimental peritumorous
    edema. Morphological and pathophysiological observations. Acta
    Neuropathol (Berl) 45:195-203

Hounsfield GN (1973) Computerized transverse axial scanning
    (tomography): part I. Description of system. Br J Radiol
    46:1016-1022

Houthoff HJ, Go KG, Gerrits PO (1982) The mechanisms of blood--brain
    barrier impairment by hyperosmolar perfusion. An electron
    cytochemical study comparing exogenous HRP and endogenous
    antibody to HRP as tracers. Acta Neuropathol (Berl) 56:99-112

Hulstrom D, Forssen M, Patterson A, Tengvar C, Jarild M, Olsson Y
    (1984) Vascular permeability in acute triethyltin-induced brain
    edema studied with FTIC-dextrans, sodium fluorescein and
    horseradish peroxidase as tracers. Acta Neurol Scand 69:255-263

Inch WR, McCredie JA, Knispel RR, Thompson RT, Pintar MM (1974) Water
content and proton spin relaxation time for neoplastic and non-
neoplastic tissues from mice and humans. J Natl Cancer Inst
52:353–356

Ito I, Tomita H, Yamazaki S, Takada Y, Inaba Y (1986) Brain swelling
and brain oedema in acute head injury. Acta Neurochir 79:120–
124

James TL, Gillen KT (1972) Nuclear magnetic resonance relaxation time
and self-diffusion constant of water in hen egg white and yolk.
Biochim Biophys Acta 286:10–15

Jahde E, Rajewsky MF (1982) Tumor-selective modification of cellular
microenvironment in vivo: effect of glucose infusion on the pH
in normal and malignant rat tissues. Cancer Res 42:1505–1512

Jones JM, Creeth JM, Kekwick RA (1972) Thiol reduction of human
$_2$-macroglobulin. The subunit structure. Biochem J 127:187–197

Joo F (1972) Effect on N^6O^2-dibutyryl cyclic 3':5'-adenosine
monophosphate on the pinocytosis of brain capillaries of mice.
Experientia 28:1470–1471

Kalsbeck JE, Cumings JN (1963) Experimental edema in the rat and cat
brain. J Neuropathol Exp Neurol 22:237–247

Kamijyo Y, Garcia J, Cooper J (1977) Temporary regional cerebral
ischemia in the cat. A model of hemorrhagic and subcortical
infarction. J Neuropathol Exp Neurol 36:338–350

Kamman RL, Go KG, Muskiet FAJ, Stomp GP, Van Dijk P, Berendsen HJC
(1984) Proton spin relaxation studies of fatty tissue and
cerebral white matter. Mag Res Imag 2:221–22

Karcher D, Lowenthal A (1967) Hydrosoluble proteins of edematous
human nervous tissue. In: Klatzo I, Seitelberger F (eds) Brain
Edema. Springer, New York, pp 195–201

Kato H, Kogure K, Ohtomo H, Izumiyama M, Tobita M, Matusi S, Yamamoto
E, Kohno H, Ikebe Y, Watanabe T (1986) Characterization of
experimental ischemic brain edema utilizing proton nuclear
magnetic resonance imaging. J Cereb Blood Flow Metab 6:212–221

Katzman R (1961) Electrolyte distribution in mammalian central
nervous system. Are glia high-sodium cells? Neurology 11:27–
36

Katzman R, Clasen R, Klatzo I, Meyer JS, Pappius HM, Waltz AG (1977)
Study group on brain edema in stroke. Stroke 8:512-540

Katzman R, Pappius HM (1973) Brain Electrolytes and Fluid Metabolism.
Williams and Wilkins, Baltimore, pp 33-48

Kimelberg HK, Bourke RS (1982) Anion transport in the nervous system.
In: Lajtha A (ed) Handbook of Neurochemistry, Vol 1. Plenum,
New York, pp 31-45

Kiricuta IC Jr, Simplaceanu V (1975) Tissue water content and nuclear
magnetic resonance in normal and tumor tissues. Cancer Res
35:1164-1167

Klatzo I (1967) Neuropathological aspects of brain edema. J
Neuropathol Exp Neurol 26:1-14

Klatzo I (1983) Disturbances of the blood--brain barrier in
cerebrovascular disorders. Acta Neuropathol (Berl) Suppl 8:81-
83

Klatzo I, Chui E, Fujiwara K, Spatz M (1980) Resolution of vasogenic
brain edema. Adv Neurol 28:359-373

Klatzo I, Miquel J, Otenasek R (1960) The application of fluorescein
labelled serum proteins (FLSP) to the study of vascular
permeability in the brain. Acta Neuropathol (Berl) 2:144-160

Klatzo I, Pirax A, Laskowski EJ (1958) The relationship between
edema, blood--brain barrier and tissue elements in a local
brain injury. J Neuropath Exp Neurol 17:548-561

Klatzo I, Suzuki R, Orzi F, Schuier F, Nitsch C (1984)
Pathomechanisms of ischemic brain edema. In: Go KG, Baethmann
A (eds) Recent Progress in the Study and Therapy of Brain
Edema. Plenum, New York, pp 1-10

Klatzo I, Wisniewski H, Steinwall O, Streicher (1967) Dynamics of
cold injury edema. In: Klatzo I, Seitelberger F (eds) Brain
Edema. Springer, New York, pp 554-563

Koenig SH, Brown RD (1985) The importance of the motion of water for
magnetic resonance imaging. Invest Radiol 20:297-305

Koenig SH, Brown RD (1984) Relaxation of solvent protons by
paramagnetic ions and its dependence on magnetic field and
chemical environments. Implications for NMR imaging. Mag Res
Med 1:478-495

Koenig SH, Hallenga K, Shporer M (1975) Protein-water interaction studied by solvent ^1H, ^2H, and ^{17}O magnetic relaxation. Proc Natl Acad Sci USA 72:2667-2671

Koenig SH, Schillinger WE (1969) Nuclear magnetic relaxation dispersion in protein solutions. I. Apotransferrin. J Biol Chem 244:3282-3289

Kramer DM, Schnedier JS, Rudin AM, Lauterbur PC (1981) True three-dimensional nuclear magnetic resonance zeugmatographic images of a human brain. Neuroradiology 21:239-244

Krogh A (1946) The active and passive exchanges of inorganic ions through the surfaces of living cells and through living membranes generally. Proc R Soc Lond (B) 133:140-200

Kuntz ID (1971) Hydration of macromolecules. III. Hydration of polypeptides. J Am Chem Soc 93:514-516

Kuntz ID, Brassfield TS, Law GD, Purcell GV (1969) Hydration of macromolecules. Science 163:1329-1331

Kuroiwa T, Cahn R, Juhler M, Goping G, Campbell G, Klatzo I (1985) Role of extracellular proteins in the dynamics of vasogenic brain edema. Acta Neuropathol (Berl) 66:3-11

Kuroiwa T, Ting P, Suzuki R, Fenton I, Klatzo I (1982) The relationship of the blood--brain barrier (BBB) opening to the thresholds of regional blood flow (rCBF) in cerebral ischemia. J Neuropathol Exp Neurol 41:352

Kyota K (1959) Electrophoretic protein fractions and hydrophilic property of brain tissue. The proteins of brain with oedema. J Neurochem 4:209-219

Laemmli UK (1970) Cleavage of structural proteins during the assembly of the head bacteriophage T4. Nature 227:680-685

Landau WM, Freygang WH, Rowland LP, Sokoloff L, Kety SS (1955) The local circulation of the living brain; values in unanesthetized and anesthetized cats. Trans Am Neurol Assn 80:125-129

Langfitt TW, Kassell NF (1966) Acute brain swelling in neurosurgical patients. J Neurosurg 24:975-983

Lassen NA (1968) On the regulation of cerebral blood flow in diseases
    of the brain with regasrd to the "luxury perfusion syndrome" of
    brain tissue, i.e., a syndrome characterized by relative
    hyperemia or absolute hyperemia in brain tissue. Prog Brain Res
    30:121-124

Lassen NA (1974) Control of cerebral circulation in health and
    disease. Circ Res 34:749-760

Lauterbur PC (1973) Image formation by induced local interactions:
    examples employing nuclear magnetic resonance. Nature 242:190-
    191

Le Bas JF, Leviel JL, Decorps M, Benabid AL (1984) NMR relaxation
    times from serial stereotactic biopsies in human brain tumors.
    J Comput Assist Tomogr 8:1048-1057

Lee JC (1971) Evolution in the concept of the blood-brain barrier
    phenomenon. Prog Neuropathol 1:84-145

Lee JC, Bakay L (1966) Ultrastructural changes in the edematous
    central nervous system. II. Cold-induced edema. Arch Neurol
    14:36-49

Lehman EP, Parker WH (1935) The unsolved problems of brain injury. A
    critical review of the literature. Int Clin 3:180-226

Levin VA, Freeman-Dove M, Landahl HD (1975) Permeability
    characteristics of brain adjacent to tumors in rats. Arch
    Neurol 32:785-791

Ling GN (1970) The physical state of water in living cells and its
    physiological significance. Int J Neurosci 1:129-152

Long DM (1970) Capillary ultrastructure and the blood-brain barrier
    in human malignant tumors. J Neurosurg 32:127-144

Long DM (1985) New therapies for brain edema. In: Inaba Y, Klatzo I,
    Spatz M (eds) Brain Edema. Springer, New York, pp 565-577

Long DM, Hartmann F, French LA (1966) The ultrastructure of human
    cerebral edema. J Neuropathol Exp Neurol 25:373-395

Lossinsky AS, Garcia JH, Iwanowski L, Lightfoote WE Jr (1979) New
    ultrastructural evidence for a protein transport system in
    endothelial cells of gerbil brains. Acta Neuropathol (Berl)
    47:105-110

Lynch LJ (1983) Water relaxation in heterogeneous and biological systems. In: Cohen JS (ed) Magnetic Resonance in Biology. Wiley, New York, pp 248-304

Macknight ADC, Leaf A (1977) Regulation of cellular volume. Physiol Rev 57:510-573

Magee PN, Storner HB, Barnes JM (1957) The experimental production of edema in the central nervous system of the rat by triethyl tin compounds. J Pathol Bacteriol 73:107-124

Maier-Hauff K, Lange, M, Schurer L, Guggenbichler C, Vogt W, Jacob K, Baethmann A (1984) Glutamate and free fatty acid concentration in extracellular vasogenic edema fluid. In: Go KG, Baethmann A (eds) Recent Progress in the Study and Therapy of Brain Edema. Plenum, New York, pp 183-192

Mansfield P, Maudsley AA (1977) Medical imaging by NMR. Br J Radiol 50:188-194

Mansfield P, Morris PG (1982) NMR Imaging in Biomedicine. Academic, New York

Manz HJ (1974) The pathology of cerebral edema. Hum Pathol 5:291-313

Marmarou A, Nakamura T, Tanaka K, Hochwald GM (1984) The time course and distribution of water in the resoltuion phase of infusion edema. In: Go KG, Baethmann A (eds) Recent Progress in the Study and Therapy of Brain Edema. Plenum, New York, pp 37-44

Marmarmou A, Shulman K, LaMorgese J (1975) Compartmental analysis of compliance and outflow resistance of the cerebrospinal fluid system. J Neurosurg 43:523-534

Marmarou A, Shulman K, Shapiro K, Poll W (1976) The time course of brain-tissue pressure and local CSF in vasogenic edema. In: Pappius HM, Feindel W (eds) Dynamics of Brain Edema. Springer, New York, pp 113-121

Marmarou A, Takagi H, Shulman K (1980) Biomechanics of brain edema and effects on local cerebral blood flow. Adv Neurol 28:345-358

Marmarou A, Tanaka K, Schulman K (1982a) The brain response to infusion edema: dynamics of fluid resolution. In: Hartmann A, Brock M (eds) Treatment of Cerebral Edema. Springer, New York, pp 11-18

Mathur-De Vre R (1979) The NMR studies of water in biological systems. Prog Biophys Molec Biol 35:103-134

Maynard EA, Schultz RL, Pease DC (1957) Electron microscopy of the vascular bed of the rat cerebral cortex. Am J Anat 100:409-433.

McQueen JD, Jelsma LF, Morooney K (1966) Determination of brain water using distillation with xylene. Confin Neurol 27:409-419

Meiboom S, Gill D (1958) Modified spin-echo method for measuring nuclear relaxation times. Rev Sci Inst 29:688-691

Mennel HD, Groneck P (1977) Quantitative aspects of transplantation of experimentally induced tumors of the nervous system. Acta Neuropathol (Berl.) 40:145-150

Mettler FA, Williams AG, Christie JH, Moseley RD, Kelsey CA (1985) Trends and utilization of nuclear medicine in the United States: 1972-1982. J Nucl Med 26:201-205

Milhorat TH (1975) The third circulation revisited. J Neurosurg 42:628-645

Milhorat TH, Clark RG, Hammock MK, McGrath PP (1970) Structural, ultrastructural and permeability changes in the ependyma and surrounding brain favoring equilibration in progressive hydrocephalus. Arch Neurol 22:397-407

Milhorat TH, Davis DA, Lloyd BJ (1973) Two morphologically distinct blood--brain barriers preventing entry of cytochrome C into cerebrospinal fluid. Science 180:76-78

Mills CM, Crooks LE, Kauffman L, Brant-Zawadzki M (1984) Cerebral abnormalities: use of calculated T_1 and T_2 magnetic resonance images for diagnosis. Radiology 150:87-94

Moore GE (1948) Use of radioactive diiodofluorescein in the diagnosis and localization of brain tumors. Science 197:569-571

Moseley ME, Nishimura MC, Pitts LH, Bartkowski HM, James TL (1984) Proton-nuclear magentic resonance spectroscopy of normal and edematous brain tissue in vitro: changes in relaxation during tissue storage. Mag Res Imag 2:205-209

Nag S, Robertson DM, Dinsdale HB (1979) Quantitative estimate of pinocytosis in experimental acute hypertension. Acta Neuropathol (Berl) 46:107-116

edema. J Neurosurg 30:747-752

Nelson SR, Mantz ML, Maxwell JA (1971) Use of specific gravity
    measurements of cerebral edema. J Appl Physiol 30:268-271

Nishio S, Ohta M, Abe M, Kitamura K (1983) Microvascular
    abnormalities in ethylnitrosourea (ENU)-induced rat brain
    tumors: structural basis for altered blood--brain barrier
    function. Acta Neuropathol (Berl) 59:1-10

Nichols D, Ackerman K (1982) Mitochondrial calcium transport. Biochim
    Biophys Acta 683:57-88

Oakes J (1976) Protein hydration. Nuclear magnetic resonance
    relaxation studies of the state of water in native bovine serum
    albumin solutions. JCS Faraday ser. I 72:216-227

O'Brien MD (1979) Ischaemic cerebral oedema - a review. Stroke
    10:623-628

O'Brien MD, Waltz AG, Jordan MM (1974) Ischemic cerebral edema.
    Distribution of water in brains of cats after occlusion of the
    middle cerebral artery. Arch Neurol 30:456-460

Odeblad E, Lindstrom G (1955) Some preliminary observations on the
    proton magnetic resonance in biological samples. Acta Radiol
    43:469-476

Oldendorf WH (1973) Carrier mediated blood--brain barrier transport
    of short chain monocarboxylic organic acids. Am J Physiol
    224:1450-1453

Oldendorf WH, Cornford ME, Brown WJ (1977) The large apparent work
    capability of the blood-brain barrier: a study of the
    mitochondrial content of capillary endothelial cells in brain
    and other tissues of the rat. Ann Neurol 1:409-417

Olsson Y, Crowell RM, Klatzo I (1971) The blood-brain barrier to
    protein tracers in focal cerebral ischemia and infarction
    caused by occlusion of the middle cerebral artery. Acta
    Neuropathol (Berl) 18:89-102

Pappius HM (1980) Mapping of cerebral functional activity with
    radioactive deoxyglucose: application in studies of
    traumatized brain. Adv Neurol 28:271-279

Pappius HM (1982) Dexamethasone and local cerebral glucose
    utilization in freeze-traumatized rat brain. Ann Neurol 12:157-
    162

Neuropathol 2:451-460

Pappius HM, McCann WP (1969) Effects of steroids on cerebral edema in cats. Arch Neurol 20:207-216

Pappius HM, Wolfe LS (1984) Effects of drugs on local cerebral glucose utilization in traumatized brain: mechanisms of action of steroids revisited. In: Go KG and Baethmann A (eds) Recent Progress in the Study and Therapy of Brain Edema. Plenum, New York, pp 11-26

Patek PR (1944) The perivascular spaces of the mammalian brain. Anat Rec 88:1-24

Peemoeller H, Pintar MM (1979) Nuclear magnetic resonance multiwindow analysis of proton local fields and magnetization distribution in natural and deuterated mouse muscle. Biophys J 28:339-356

Peemoeller H, Pintar MM, Kydon DW (1980) Nuclear magnetic resonance analysis of water in natural and deuterated mouse muscle above and below freezing. Biophys J 29:427-436

Peemoeller H, Schreiner LJ, Pintar MM, Inch WR, McCredie JA (1979) Proton T_1 study of coverage parameter changes in tissues from tumor-bearing mice. Biophys J 25:203-208

Penn RD (1980) Cerebral edema and neurological function: CT, evoked responses, and clinical examination. Adv Neurol 28:383-394

Pessen H, Purcell JM, Farrell HM Jr (1985) Proton relaxation rates of water in dilute solutions of -lactoglobulin. Determination of cross relaxation and correlation with structural changes by the use of two genetic variants of a self-associating globular protein. Biochim Biophys Acta 828:1-12

Petito CK (1979) Early and late mechanisms of increased vascular permeability following experimental cerebral infarction. J Neuropathol Exp Neurol 38:222-234

Petito CK, Schaefer JA, Plum F (1977) Ultrastructural characteristics of the brain and the blood-brain barrier in experimental seizures. Brain Res 127:251-267

Pocsik I, Furo I, Tompa K, Neumark T, Takacs J (1986) Combined ^{1}H-NMR and vacuum dehydration study of rat muscles. Biochim Biophys Acta 880:1-9

Pollay M, Curl F (1967) Secretion of cerebrospinal fluid by the ventricular ependyma of the rabbit. Am J Physiol 213:1031-1038

...., ..., ... (eds) Dynamic Properties of Glia
Cells: Pergamon, New York, pp 13-20

Purcell EM, Torrey HC, Pound RV (1946) Resonance absorption by
nuclear magnetic moments in a solid. Phys Rev 69:37-43

Pykett IL, Rosen BR, Buoano FS, Brady TJ (1983) Measurement of spin-
lattice relaxation times in nuclear magnetic resonance imaging.
Phys Med Biol 28:723-729

Raichle ME (1980) Brain edema: evaluation in vivo with positron
emission tomography. Adv Neurol 28:423-427.

Raichle ME, Eichling JO, Straatmann MG, Welsh MJ, Larson KB, Ter-
Pogossian MM (1976) Blood-brain barrier permeability of ^{11}C-
labeled alcohols and ^{15}O-labeled water. Am J Physiol 230:543-
552

Rama B, Spoerri O, Holzgraefe M, Mennel HD (1986) Current brain tumor
models with particular consideration of the transplantation
techniques. Outline of the literature and personal preliminary
results. Acta Neurochir 79:35-41

Ranade SS, Shah S, Korgaonkar KS, Kasturi SR, Chaughule RS,
Vijayaraghavan R (1976) Absence of correlation between spin-
lattice relaxation times and water content in human tumor
tissues. Physiol Chem Phys 8:131-134

Rapoport SI (1976) Blood-Brain Barrier in Physiology and Medicine.
Raven, New York

Rapoport SI, Ohne K, Pettigrew KD (1979) Drug entry into brain. Brain
Res 172:354-359

Reed DJ, Woodbury DM (1963) Kinetics of movement of iodine, sucrose,
inulin, and radio-iodinated serum albumin in the central
nervous system and cerebrospinal fluid of the rat. J Physiol
(Lond) 169:816-850

Reese TS, Feder N, Brightman MW (1971) Electron microscopic study of
the blood-brain and blood-cerebrospinal barriers with
microperoxidase. J Neuropathol Exp Neurol 30:137-138

Reese TS, Karnovsky MJ (1967) Fine structural localization of a
blood-brain barrier to exogenous peroxidase. J Cell Biol
34:207-217

Reivich M, Jehle J, Sokoloff L, Kety SS (1969) Measurement of
regional cerebral blood flow with antipyrine-^{14}C in awake cats.
J Appl Physiol 27:296-300

gradients and bulk flow in dynamics of vasogenic edema. J
Neurosurg 46:24-35

Reulen HJ, Hadjidimos A, Schurmann K (1972) The effect of
dexamethasone on water and electrolyte content and on rCBF in
perifocal brain edema in man. In: Reulen HJ, Schurmann K (eds)
Steroids and Brain Edema. Springer, New York, pp 239-252

Reulen HJ, Medzinradsky F, Enzenbach R, Margoth F, Brendel W (1969)
Electrolytes, fluids, and energy metabolism in human cerebral
edema. Arch Neurol 21:517-525

Reulen HJ, Tsuyumu M, Tack A, Fenske AR, Piroleau GR (1978) Clearance
of edema fluid into cerebrospinal fluid. A mechanism for
resolution of vasogenic brain edema. J Neurosurg 48:754-764

Rosen BR, Pykett IL, Brady TJ (1984) Spin-lattice relaxation time
measurements in two-dimensional nuclear magnetic resonance
imaging: corrections for plane selection and pulse sequence. J
Comput Assist Tomogr 8:195-199

Rubinstein LJ, Klatzo I, Miguel J (1962) Histochemical observations
on oxidative enzyme activity of glial cells in local brain
injury. J Neuropath Exp Neurol 21:116-136

Rutherford RA, Ullan BR, Isherwood I (1976) Calibration and response
of EMI scanner. Neuroradiology 11:7-13

Rutsgi SN, Peemoeller H, Thompson RT, Kydon DW, Pintar MM (1978) A
study of molecular dynamics and freezing phase transition in
tissues by proton spin relaxation. Biophys J 22:439-452

Saryan LA, Hollis DP, Economou JS, Eggleston JC (1974) Nuclear
magnetic resonance studies of cancer. IV. Correlation of water
content with tissue relaxation times. J Natl Cancer Inst
52:599-602

Schaul N, Ball G, Gloor P, Pappius HM (1976) The EEG in cerebral
edema. In: Pappius HM, Feindel W (eds) Dynamics of Brain Edema.
Springer, New York, pp 144-149

Schettini A, Walsh EK (1973) Pressure relaxation of the intracranial
system in vivo. Am J Physiol 225:513-520

Schuier FJ, Hossmann KA (1980) Experimental brain infarcts in cats.
II. Ischemic brain edema. Stroke 11:593-600

Shigeno T, Brock M, Shigeno S, Fritschka E, Cervos-Navarro J (1982)
The determination of brain water content: microgravimetry
versus drying-weighing method. J Neurosurg 57:99-107

resonance imaging of experimental brain edema in cats. Neurosurgery 17:557-563

Shivers R (1979) The blood-brain barrier of a reptile, Anolis carolinensis. A freeze-fracture study. Brain Res 169:221-230

Siesjo BK (1985) Membrane events leading to glial swelling and brain edema. In: Inaba Y, Klatzo I, Spatz M (eds) Brain Edema. Springer, New York, pp 200-209

Siesjo BK, Wieloch T (1985) Cerebral metabolism in ischemia: neurochemical basis for therapy. Br J Anaesth 57:47-62

Simionescu N, Simionescu M, Palade GE (1978) Structural basis of permeability in sequential segments of the microvasculature of the diaphragm. II. Pathways followed by microperoxidase across the endothelium. Microvasc Res 15:17-36

Smith AS, Weinstein MA, Modic MT, Pavlicek W, Rogers LR, Budd TG, Bukowski RW, Purvis JD, Weick JK, Duchesneau PM (1985) Magnetic resonance with marked T_2-weighted images: improved demonstration of brain lesions, tumor, and edema. Am J Radiol 145:949-955

Sokoloff L, Reivich M, Kennedy C, Des Rosiers MH, Patlak CS, Pettigrew KD, Sakurada O, Shinohara M (1977) The [^{14}C]deoxyglucose method for the measurement of local cerebral glucose utilization: theory, procedure, and normal values in the conscious and anesthetized albino rat. J Neurochem 28:807-916

Sone N, Hagihara B (1964) Inhibitory action of trialkyltin compounds on oxidative phosphorylation in mitochondria. J Biochem 56:151-156

Starling E (1896) On the absorption of fluids from the connective-tissue spaces. J Physiol (Lond) 9:312-326

Stewart-Wallace AM (1939) A biochemical study of cerebral tissue and of changes in cerebral oedema. Brain 62:426-438

Streicher E, Ferris PJ, Prokop JD, Klatzo I (1964) Brain volume and thiocyanate space in local cold injury. Arch Neurol 11:444-448

Sullivan HG, Miller JD, Griffith RL, Engr D, Carter W, Rucker S (1979) Bolus versus steady-state infusion for determination of CSF outflow resistance. Ann Neurol 5:228-238

Sutton LN, Bruce DA, Welsch FA, Jaggi JL (1980) Metabolic and electrophysiologic consequences of vasogenic edema. Adv Neurol 28:241-254

Szumanska G, Palkama A, Lehtosalo JI, Usitalo H (1984) Adenylate
cyclase in the microvessels of rat brain. A histochemical study
with light and electron microscopy. Acta Neuropathol (Berl.)
62:219-224

Szymas J, Hossmann KA (1984) Effect of dexamethasone on glial
fibrillary acidic protein in peritumorous edema of cats: a
morphometric study. Acta Neuropathol (Berl) 62:309-315

Tanford C (1962) The interpretation of hydrogen ion titration curves
of proteins. Adv Prot Chem 17:69-165

Tarlov IM, Giacontti A, Rapisarda A (1959) Acute intracranial
hypertension. Experimental-clinical correlations. Arch Neurol
1:3-18

Tingey AH (1937) The iron, copper, and manganese content of the human
brain. J Ment Sci 83:452-460

Timiras PS, Koch A, Ballard A (1956) Distribution of radiochloride,
radiosulfate, and inulin in brain of rats. Fed Proc 15:501-502

Torack RM, Terry RD, Zimmerman HM (1960) The fine structure of
cerebral fluid accumulation. II. Swelling produced by triethyl
tin poisoning and its comparison with that in the human brain.
Am J Pathol 36:273-387

Tschirgi RD (1950) Protein complexes in the permeability of the
blood-brain barrier to dyes. Am J Physiol 163:756-757

Van Harreveld A (1962) Water and electrolyte distribution in central
nervous tissue. Fed Proc 21:659-664

Van Harreveld A, Crowel J, Malhotra SK (1965) A study of
extracellular space in central nervous tissue by freeze
substitution. J Cell Biol 25:117-137

Van Harreveld A, Malhotra SK (1966) Demonstration of extracellular
space by freeze-drying in the cerebellar molecular layer. J
Cell Sci 1:223-228

Van Harreveld A, Ochs S (1956) Cerebral impedance changes after
circulatory arrest. Am J Physiol 187:180-192

Vick NA (1980) Brain tumor microvasculature. In: Weiss L, Gilbert
HA, Posner JB (eds) Brain Metastasis. Hall, Boston, pp 115-133

Vorbrodt AW, Lossinsky AS, Wisniewski HM, Suzuki R, Yamaguchi T,
Masaoka H, Klatzo I (1985) Ultrastructural observations on the
transvascular route of protein removal in vasogenic edema. Acta
Neuropathol (Berl) 66:265-273

Wagner HJ, Pilgrim C, Brandl J (1974) Penetration and removal of horseradish peroxidase injected into the cerebrospinal fluid: role of cerebral perivascular spaces, endothelium, and microglia. Acta Neuropathol (Berl) 27:299-315

Wald A, Hochwald GM, Gandhi M (1978) Evidence for the movement of fluid, macromolecules, and ions from the brain extracellular space to the CSF. Brain Res 151:283-290

Watanabe I (1977) Effect of triethyltin on the developing brain of the mouse. In: Roizin L, Shiraki H, Grcevic N (eds) Neurotoxicology, Raven, New York.

Weiss MH, Wertman N (1978) Modulation of CSF production by alterations in cerebral perfusion pressure. Arch Neurol 35:527-529

Westergaard E (1977) The blood brain barrier to horseradish peroxidase under normal and experimental conditions. Acta Neuropathol (Berl) 39:181-187

Westergaard E, Brightman MW (1973) Transport of proteins across normal cerebral arterioles. J Comp Neurol 152:17-44

Westergaard E, van Devrs B, Brondsted HE (1977) Increased vesicular transfer of horseradish peroxidase across cerebral endothelium, evoked by acute hypertension. Acta Neuropathol (Berl) 37:141-152

Wolff HG, Blumgart HL (1929) The cerebral circulation. VI. The effect of normal and of increased cerebrospinal fluid pressure on the velocity of intracranial blood flow. Arch Neurol Psychiatry 21:795-807

Wolman M, Klatzo I, Chui E, Wilmes F, Nishimoto K, Fujiwara K, Spatz M (1981) Evaluation of dye-protein tracers in pathophysiology of blood-brain barrier. Acta Neuropathol (Berl) 54:55-61.

Woodbury DM (1958) Effects of carbon dioxide on brain excitability and electrolytes. Am J Physiol 192:79-90

Yamada K, Ushio Y, Hayakawa T, Arita N, Yamada N, Mogami H (1983) Effects of methylprednisolone on peritumoral brain edema. A quantitative autoradiographic study. J Neurosurg 59:612-619

Yamada K, Ushio Y, Hayakawa T, Kato A, Yamada N, Magami H (1982) Quantitative autoradiographic measurements of blood-brain barrier permeability in the rat glioma model. J Neurosurg 57:394-398

Zimmerman JR, Brittin WE (1957) Nuclear magnetic resonance studies in
    multiple phase systems: lifetime of a water molecule in an
    adsorbing phase on silica gel. J Phys Chem 61:1328-1333

Zulch KJ (1967) Neuropathological aspects and histopathological
    criteria of brain edema and brain swelling. In: Klatzo I,
    Seitelberger F (eds) Brain Edema, Springer, New York, pp 95-116